OLD DOMINION UNIVERSITY RESEARCH FOUNDATION

DEPARTMENT OF PHYSICS
SCHOOL OF SCIENCES AND HEALTH PROFESSIONS
OLD DOMINION UNIVERSITY
NORFOLK, VIRGINIA

Technical Report PTR-82-8

RADIATION EFFECTS STUDIES FOR THE HIGH-RESOLUTION SPECTROGRAPH

By

L.C. Smith

and

Jacob Becher, Principal Investigator

Progress Report
For the period ending July 1, 1982

Prepared for the
National Aeronautics and Space Administration
Goddard Space Flight Center
Greenbelt, Maryland

Under
Research Grant NSG 5289
Walter J. Fowler, Technical Monitor
Laboratory for Astronomy and Solar Physics

August 1982

DEPARTMENT OF PHYSICS
SCHOOL OF SCIENCES AND HEALTH PROFESSIONS
OLD DOMINION UNIVERSITY
NORFOLK, VIRGINIA

Technical Report PTR-82-8

RADIATION EFFECTS STUDIES FOR THE HIGH-RESOLUTION SPECTROGRAPH

By

L.C. Smith

and

Jacob Becher, Principal Investigator

Progress Report
For the period ending July 1, 1982

Prepared for the
National Aeronautics and Space Administration
Goddard Space Flight Center
Greenbelt, Maryland 20771

Under
Research Grant NSG 5289
Walter J. Fowler, Technical Monitor
Laboratory for Astronomy and Solar Physics

Submitted by the
Old Dominion University Research Foundation
P.O. Box 6369
Norfolk, Virginia 23508-0369

August 1982

TABLE OF CONTENTS

TABLE OF CONTENTS - CONCLUDED

LIST OF FIGURES

LIST OF FIGURES - CONTINUED

LIST OF FIGURES - CONCLUDED

MODELING CHARGE DIFFUSION FROM PROTON-INDUCED IONIZATION TRACKS IN SILICON PHOTODIODE ARRAYS

By

L. Cole Smith[1] and Jacob Becher[2]

ABSTRACT

We are modeling the combined problem of generation and collection of charge carriers created during passage of energetic protons through a silicon photodiode array. We have also experimentally obtained pulse-height distributions of noise charge collected during exposure of a digicon-type diode array to 21 and 75 MeV protons. It is shown that the magnitude of charge collected by a diode from each proton event is determined not only by diffusion, but by statistical considerations involving the ionization process itself. Utilizing analytical solutions to the diffusion equation for transport of minority carriers, together with the Vavilov theory of energy-loss fluctuations in thin absorbers, we present simulations of the pulse-height spectra which follow the experimental distributions fairly well, and provide us with an estimate for the minority carrier diffusion length L_d.

INTRODUCTION

The introduction of LSI microcircuit technology has made possible the construction of planar arrays of small p-n junctions on the surface of a single thin chip of silicon. Since the depletion zone of each junction can behave either as a tiny capacitor, or as a potential well, these arrays can be used to store patterns of charge which can be retrieved quickly and, if necessary, repeatedly. These devices are conveniently divided among two categories: (1) analogue, including image sensors (such as linear photodiode arrays (LPDA) and charge coupled devices (CCD's), and (2) digital, the

[1] Graduate Research Assistant, Department of Physics, Old Dominion University, Norfolk, Virginia 23508.

[2] Associate Professor, Department of Physics, Old Dominion University, Norfolk, Virginia 23508.

prime example being semiconductor memory chips (e.g. MOS dynamic RAM's (random access memory). Advances in LSI and VLSI techniques have increased the number of diode elements that can be arranged on a chip, by decreasing the size of each element, so that 64-kbit dynamic RAM's are now found with individual memory cells of only a few square microns in area. Although smaller device dimensions are likely to be forthcoming as the technology improves, it has been demonstrated in recent years that as downscaling continues, most of these microelectronic devices become critically sensitive to energetic particle radiation, such as found in cosmic ray showers and natural radioactaivity on earth and the Van Allen radiation belts and primary cosmic ray particles above the atmosphere. This consideration represents a very serious operational problem associated with the use of state-of-the-art VLSI technology in both analogue (imaging) and digital (memory) circuits, for either ground or space applications.

Radiation Effects on Digital Devices

Considerable attention has been paid recently to the problem of soft error generation in high-density dynamic RAM chips (refs. 1-5). (By soft error we mean random, nonrecurring, single bit errors in memory devices. The errors are not permanent). May and Woods (ref. 1) and Yaney, Nelson and Vanskike (ref. 3) demonstrated that alpha particles emitted during the spontaneous fission of U 238 and Th 230, (present in parts-per million levels in the ceramic packaging materials typically used for IC's), are capable of generating enough electron-hole pairs in the depletion region and silicon bulk to discharge a single cell on an LSI chip. Their results showed, predictably, that the alpha-particle-induced error rate depends upon the cell size, the energy of the alpha particle, the charge collection efficiency of each cell, and the critical charge Q_{crit}, i.e., the number of stored electrons which differentiates between a "1" and "0" (ref. 3). The critical charge for the 16 K RAM's used in the experiments was estimated to be about 200 fC, which required an alpha particle having an energy of at least 4.5 MeV to cause an upset. Other experiments have shown that CCD memory arrays are even more sensitive to ionizing radiation because, due to the increased levels of integration accompanied by a reduction in storage cell size, they possess a smaller value for Q_{crit} (ref. 6). Beta and gamma sources produce

negligible soft errors in dynamic memories because of their relatively lower ionization loss rate. Energetic ions may interact through a (p, alpha) or similar nuclear reaction to produce soft errors, but this effect decreases rapidly with decreasing particle kinetic energy (refs. 7, 8). Cosmic-ray-induced latch-up in CMOS logic and memory modules appear to remain a serious operational problem since its discovery onboard Air Force satellites in 1975 (ref. 9).

Radiation Effects on Analog Devices

The effects of particle radiation on image sensors has received a less exhaustive treatment, possibly due to the more widspread use of the ubiquitous memory chip. Multidiode image arrays are still fairly expensive, and users of these devices are perhaps unwilling to subject them to radiation levels that could be potentially destructive. Actually, tests have shown image sensors to be equally sensitive to extremely low fluences of particle radiation (refs. 6, 10, 11). Also, unlike a memory cell, which experiences only a change of state, each diode element is, by design, sensitive to a wide range of charge levels, down to about 0.5 fC. As a result, its sensitivity to charge noise is not limited to the effects of alpha particles, but extends to nearly any charged particle losing sufficient kinetic energy to produce ionization in the silicon.

Models of Charge Collection in Integrated Circuits

All of these considerations have inspired several authors to propose various charge diffusion models to explain the various effects resulting from ionizing radiation passing through silicon microelectronic devices (refs. 12-15). Techniques range from simple analytical solutions to the diffusion equations (12-15) to full-scale Monte Carlo simulations (refs. 13, 14), and so far results appear encouraging for predicting the soft error rate due to alpha-particle penetration of the chip.

To our knowledge no previous theoretical work has treated the problem of charge collection from proton-created ionization tracks in integrated circuits designed for analogue charge detection. Part of the problem is that generally little is known experimentally about charge collection from

particle tracks in these structures. Consequently several approximations commonly used in alpha particle work have gone untested. For example, many authors assume minority carrier recombination plays little part in determining the amount of charge reaching a diode element from the path of a charged particle. Kirkpatrick (ref. 12) assumes recombination lifetimes of several milliseconds, although experiments with 4.2 MeV alpha particles bombarding CCD arrays have indicated minority carrier lifetimes τ of less than a microsecond (ref. 6). This corresponds to a diffusion length of 26 μ, using $L_d = \sqrt{D\tau}$, which still exceeds the range of most alpha particles in silicon. Protons, however, can produce tracks equaling the thickness of the silicon wafer (100-400 μ) since they essentially penetrate the chip with little energy loss. This possibility of charge diffusing to the surface from very large distances necessitates the inclusion of recombination effects in charge collection models involving protons.

Another consideration related to proton-induced ionization in silicon involves energy-loss fluctuations along the ionization track. This effect is significant only for particles which deposit a small fraction of their kinetic energy in the medium, and hence has not been treated in alpha-particle models. However, energy-loss straggling plays a major role in determining the maximum amount of charge collected by a diode from proton-induced ionization tracks.

Experimental Work with the Digicon Diode Array

Both CCD arrays and LPD arrays are used as photoelectron targets in many image tube camera systems developed over the past few years. Some of these cameras, such as the Digicon, are to be flown on space astronomy satellites in the middle 1980's. This will expose the imaging components (including the diode arrays) to energetic particle radiation potentially capable of causing an interfering noise background. So far no arrays have flown in space, so little in situ data are available. Therefore, this information has to be obtained on the ground, using man-made particle beams of appropriate energy to simulate the radiation environment.

We performed these tests for NASA/Goddard in 1979-80, when three different 512 element linear photodiode array were irradiated with proton

beams at the University of Maryland 100 MeV Isochronous Cyclotron. Two of those arrays were the targets of engineering model Digicon tubes, similar to flight models to be flown on the Space Telescope. The other array was part of a breadboard circuit but was similar to the other two. The purpose of the experimental work was to evaluate the effect of South Atlantic Anomaly levels of proton radiation on the performance of the tube. This paper, which includes data from exposures to protons at 31.5 and 75.4 MeV, uses the essential results of those tests as a basis for the evaluation of a diffusion model that includes the effect of the shape and pattern of the diodes on the array, minority carrier recombination, and finite recombination velocities at the backside of the silicon wafer. Three-dimensional simulations are used to shown the necessity of including the effects of energy-loss straggling in accounting for the experimetal results. The intent of this model is twofold: first, to provide a solid theoretical framework within which to evaluate particle radiation effects in multi-diode structures, and second, to use this framework to investigate the dependence of experimentally measurable quantities on physical parameters in silicon.

We have emphasized the negative aspects of the charge sensitivity of analog silicon devices. It should be pointed out that the charge sensitive nature of the diode array coupled with the precise geometrical arrangement of diode elements could prove useful in nuclear and solid state experiments, with the possibilities of position sensitive detection of high energy particles and studies of carrier transport phenomena in silicon. Considerable attention has been devoted recently to the study of the determination of transport parameters of minority carriers in single p-n junctions by employing scanning electron beam excitation. Calculations have appeared in recent years in association with electron beam induced current (EBIC) experiments designed for quantitative determination of diffusion lengths, bulk lifetime and surface recombination velocity of minority carriers in silicon (refs. 28, 29, 30). However, none of these results have been applied to understanding charge diffusion and collection in microelectronic chips involving many diode elements. The extension of this work to multi-diode arrays appears promising. As recent tests utilizing cosmic-ray showers have indicated, the CCD array, because of its charge imaging property, appears to be especially suitable for experiments measuring carrier diffusion lengths and surface recombination effects (ref. 7).

Hence, both a theoretical and experimental void needs to be filled in order to understand the effects of ionizing radiation on these devices.

THE SILICON DIODE ARRAY TARGET

Introduction

Before we proceed with an assessment of the response of photodiode arrays to particle radiation, a brief description of the fabrication and structure of these devices is given. Particular emphasis is placed on arrays similar to those used in our experimental work.

Diode Array Fabrication

The employment of silicon-diode-array targets in various electron-imaging modes of operation, particularly low-light level applications, has been discussed in the published literature (refs. 16, 17, 18). Most multi-diode structures utilize a one- or two-dimensional array of sensing elements in which (for the case of a solid state image sensor) incident photons or photoelectrons are absorbed and converted to electric charge. The sensors or storage elements may be diffused photodiodes or MOS capacitors (surface depletion layers induced by a voltage applied to semi-transparent electrodes of a material such as polycrystalline silicon). The latter corresponds to the conventional CCD sensor array. These sensing elements are created on substrates made from thin slices of either n or p type silicon, usually homogeneous, (although epitaxial wafers are nowadays not uncommon). Bulk resistivity is usually low, around 10 ohm-cm. Since we are considering only photodiode arrays, we shall limit our discussion to their fabrication.

In preparation for forming diodes, the wafer surface is thermally oxidized (~1,000° C). Diode elements are formed using standard photolithographic and planar processing techniques employed in the manufacture of integrated circuits. This includes etching away the oxide layer according to the desired array pattern and forming p + n junctions by the diffusion of boron into the n-type silicon through the open windows. The shallowness of these diffusions (typically 1 μ), coupled with the low resistivity of the substrate creates very thin depletion layers when reverse bias is applied to the substrate. For photoelectron detection, only a few microns of sensitive volume is necessary so these thin junctions (typically 3-4 μ) are adequate. The remainder of the substrate serves as a rigid support for the

array and as a surface on which to bond the diode signal leads. Substrate thickness can vary from 10 μ to nearly 500 μ, depending on the application. A cross-section of a typical diode array is shown in Figure 1.

Detection of Charge Signal

Methods for detecting the charge collected at each diode are almost as numerous as the different types of sensors. Analogue and digital shift register scanning of the diode elements are used in both CCD and photodiode arrays; current generation LPD arrays use serial multiplexing whereby each diode is sensed sequentially. Charge injection and charge transfer techniques are usually associated with devices using MOS capacitors as sensing elements, and will not be discussed here. In photodiode arrays, conversion of the charge into a measurable signal in the external circuit is accomplished in one of two ways: charge-storage and charge-integration.

Charge-storage operation is based on the fact that if a p-n junction is reverse biased, then open circuited while illuminated with a light source, the charge initially stored on the depletion-layer capacitance decays at a rate proportional to the incident illumination level. Thus, by monitoring the charge required periodically to re-establish the initial-voltage condition, one will obtain a single proportional to the incident illumination. This method is not suitable for extremely low levels of illumination, when only single photons are incident, as the photon-induced diffusion currents are so small as to be insufficient to discharge the charge stored in each diode's potential well. In this case some intermediate gain stage is necessary, usually in the form of a photocathode and an accelerating potential of around 20,000 V.

In the latter case, a photon-ejected electron replaces the photon as the means of creating diffusion currents in the silicon, and the charge integration method is used to detect the signal. In this method charge sensitive preamplifiers connected to each diode are used to integrate the brief current pulse resulting from a single impinging photoelectron. The resulting voltage signal is thus proportional to the total charge either released in or eventually reaching the diode depletion layer. Using conventional pulse shaping and counting techniques, the incident illumination

level at the photocathode can be determined assuming knowledge of such factors as quantum efficiency, diode area, etc.

Radiation Sensitivity

Although usually designed to absorb photoelectrons having energies around 20-50 kiloelectron volts (keV), (depending on the accelerating voltage at the photocathode), each diode in the array will obviously detect any; charged particle losing enough energy in the silicon to produce a signal exceeding the electronic noise level (typically 4 keV equivalent noise charge). In fact, each diode can collect charge from two regions: (1) inside the diode's depletion layer, where large electric fields (10^6 V/m) cause rapid collection (10 nsec) of charge created there, and (2) outside the depletion layer, where there are no electric fields, and charge collection occurs through the relatively slow process of minority carrier diffusion in the homogeneous n (or p) substrate (see Figure 1). As a result, not only is an individual diode cell's noise sensitivity enhanced, but on an array containing many diode elements spaced closely together, the deeper an ionizing particle penetrates into the silicon wafer, the greater the potential for activating many diodes simultaneously. That this indeed takes place has received little attention in the literature. The author is aware of only two papers that experimentally document the effects of particle radiation on image sensors. Ko (ref. 6) and Marcus (ref. 11) briefly describe the effects of alpha particles and secondary cosmic ray partaicles on CCD sensor arrays. Marcus' work with the Fairchild CCD-211 shows vivid detail of charge diffusing over dozens of pixels resulting from the ionization tracks of secondary charged particles as they penetrate the wafer during the course of a 75-min exposure. Marcus presents no quantitative analysis, but Ko uses the results of similar experiments with alpha particles to estimate the minority carrier diffusion length of the substrate of his CCD array. It appears at present that our work, described next in "Experimental Work," represents the only data available on the effects of monoenergetic protons on imaging photodiode arrays.

EXPERIMENTAL WORK

Introduction

The silicon diode has been used for many years by nuclear physicists and others to detect electrons, protons and heavier particles from radioactive sources and accelerators. Fast, low-noise pre-amplifiers have been developed to permit energy determination with high resolution. However, surprisingly few data are available on the response to particle radiation of semiconductor devices intended for other purposes e.g. silicon photodiode arrays, CCD's, etc. This despite the ready availability of many of these devices as well as their potential usefulness as an experimental tool for the solid state physicist.

The response of a 512 element linear photodiode array to medium energy proton radiation has been described elsewhere by the author (refs. 19, 20, 21). The array was the photoelectron target of a Digicon tube similar to one being flown on the Space Telescope in 1985. In our test setup, the array was irradiated in situ by a focused monoenergetic proton beam while selected diodes on the array were monitored. Signals induced by the protons penetrating the diode array were measured, digitized and counted using pulse height and coincidence techniques described in (ref. 19), (see test set-up in Figure 3).

Description of Digicon Camera

Although the Digicon has been described in review articles elsewhere (refs. 22, 23, 24), a brief description here is in order. Essentially a digital imaging device, the Digicon is a multichannel parallel-output photon detector which uses a thin silicon diode array target to detect accelerated photoelectrons from a UV or visible sensitive photocathode. The photocathode is deposited on the inside surface of a transparent window, in this instance, magnesium flouride (MgF_2). In normal operation a spectrum image is focused onto the transmission photocathode at the front end of the detector, (see Figure 2). Ejected photoelectrons are accelerated through a 20-22 kV potential and are magnetically focussed by a rare earth permanent magnet assembly onto a linear target array of 512 discrete photodiodes. (In our

test set-up, this magnet assembly was replaced by a solenoid). Each of these diodes consists of a thin p + n junction imbedded on the surface of a 400 μ thick, n-Si (ρ = 4.5 ohm-cm) homogeneous substrate to which a +5 V reverse biasing potential is applied. Each diode measures 40 μ wide by 250 μ long and is spaced at 50 μ intervals. The geometrical arrangement of the diodes on the array, as well as the shape of each diode, is shown in Figure 4. When biased, each diode forms a depletion layer having a depth of about 2.5 μ. Every photoelectron that is stopped in the depletion zone results in the creation of a charge pulse of several thousand electron hole pairs. The presence of large electric fields in this region results in rapid separation and collection of this charge onto the aluminum electrodes deposited over about a third of the surface of each diode. Each of the 512 diodes is connected to a separate channel containing a charge sensitive preamp, shaping and amplification circuits and signal-processing electronics which digitize the measured charge from each diode independently into a digital word for storage in memory.

Test Configuration

The test configuration is shown in Figure 3. Collimated proton beams of 1 cm^2 cross-section were directed onto the center of the faceplate at the front of the Digicon, which was located inside a scattering chamber and securely bolted onto a movable arm. The Digicon was free to rotate around an axis centered on the photocathode, allowing the rear of the tube to be swung out of the path of the proton beam. This allowed monitoring of the luminescence in the MgF_2 faceplate without the strong interference created by protons penetrating the window and striking the diode array. To monitor the direct proton bombardment of the array, the arm could be returned to zero degrees very quickly, and the high voltage removed. With the photoelectron background thus eliminated, data accumulation could be resumed. By choosing angles between 0.0 and 10.0 degrees, various portions of the diode array could be brought into the path of the beam. Proton flux was measured using an Ortec surface barrier detector (SBD) mounted a few centimeters in front of the faceplate. Sheets of Polaroid film were exposed to obtain beam area and flux density (particles/cm^2-sec).

Although intended to operate with 512 fully independent diode channels, the Digicon could be tested effectively with a small fraction of these diodes active. Ten of the 512 diodes available were monitored through the use of a charge-sensitive hybrid preamp connected to each diode through a multipin header at the base of the tube. Each preamp was followed by a chain of electronics containing a pulse shaper, amplifier, discrimator, rate limiter and 16-bit count accumulator. Pulse-height analysis from any diode channel was possible, using switchable analog channels placed just after the preamps. These were followed by spectroscopy amplifiers and several multichannel analyzers. As many as three diodes were monitored simultaneously, allowing measurements of coincidence rates between any pair or all three.

It should be noted that although the primary beam energies were 85 and 40 MeV, passage of the protons through a 10-mil tantalum window used to isolate the beam line, as well as 0.5 m of air, the surface barrier detector, and a few low-density light shields, reduced the energies of the protons entering the window to 80.7 and 34.2 MeV, respectively. Passage through the 3 mm MgF_2 window further reduced this to 75.4 and 21.5 MeV. All results will be referred to by these last values.

Calibration

Shown in Figure 5 is a pulse-height distribution of photoelectrons collected by a typical diode and produced by exposing the MgF_2/CsTe faceplate to a UV penlight located several centimeters away. The peak of the distribution falls around channel 90,with the FWHM around 30 channels. Although each photoelectron has a kinetic energy of 22 keV, some spreading of the collected charge is expected on the basis of surface backscattering, and photoelectrons striking diode boundaries, both of which result in less than the full energy being deposited inside the diode. All pulse-height distributions presented here have the horizontal axis calibrated with respect to the photoelectron peak, which is assigned the value of 0.972 fC (6077 electron-hole pairs), assuming 1 electron-hole pair/3.62 eV of energy deposited in the silicon.

Pulse Height Analysis

The differential pulse height distributions of signals obtained from a typical diode during direct proton bombardment of the Digicon diode array are indicated by curve A) in Figures 6 and 7, for 21.5 and 75.4 MeV, respectively. We have plotted the number of counts N(Q)dQ versus Q, where Q is the charge collected at a diode. Incident flux was low (10^4 - 10^5 p+/sec-cm^2, measured in real time with a Ortec surface barrier detector) and beam energy was sufficient (>8 MeV) to allow the protons to penetrate and completely pass through the 400 μ silicon wafer with little energy loss (1 MeV). No radiation damage was expected at these low fluences. The shape of the differential pulse height distribution is typical of the response seen in all the diodes, and has been observed previously by us during proton bombardment of a similar diode array at other energies (ref. 19) and by others using low energy electrons and CCD's (ref. 10).

A more useful representation can be obtained by plotting these data in integral form, indicated by curve B) in Figures 6 and 7. Here we show the total number of events in which the collected charge was greater than Q, versus Q. Two immediate conclusions can be drawn from these spectra. Using the 21.5 MeV result as an example, we see that the largest value of charge occuring in the spectrum (11 fC) is more than an order of magnitude larger than the amount of ionization that would be produced by a 21.5 MeV proton passing through the 2.5 μ depletion layer. This result suggests that a substantial amount of charge released in the substrate beneath a diode reaches the diode depletion zone. A similar effect has been observed using low energy electron bombardment of thinned CCD arrays (ref. 10), and users of surface barrier detectors have observed pronounced diffusion collection from depths as great as 500 μ when these devices were irradiated with electrons (ref. 25).

Second, by recording the value of the integral spectrum at the noise threshold (0.5 fC), one obtains the total number of protons detected by the diode for the duration of the experiment. We have found this number to be larger than the number of protons incident on the area of the diode by almost an order of magnitude (for 21.5 MeV). This suggests that the ionizing particle does not have to directly strike a diode to produce a signal in

that diode. The net effect is to increase the effective area or cross-section of each diode to several times its actual dimensions (which is 8.5×10^{-5} cm^2 for the Digicon diode). Both of these effects become less pronounced at higher proton energies as a consequence of the lower specific ionization produced in the bulk.

The shape of the differential pulse height spectra in Figures 6 and 7 substantiates these conclusions. Most of the counts appear to be associated with small charge values, presumably originating from particle tracks created exterior to and far from the diode boundaries. Since this region encompasses a greater area than that of the diode itself, the protons, which strike the array at random, have a greater probability of striking outside the diode, resulting in the observed distribution of counts. The largest charge values, occurring above the broad peak, presumably represent charge collected from particle tracks penetrating near the center of the diode, a relatively infrequent event. However, the factors contributing to the exact shape of the pulse height spectra are complex, and will be discussed in detail in "Analysis."

Coincidence Measurements

The close proximity of one diode to another, as well as the observation that the effective areas of adjacent diodes overlap, suggests that diffusing charge can leak to several diodes within a very short time interval, and thus create signals in adjacent diode pairs nearly coincidentally. This has indeed been observed in a 250-μ thick CCD array exposed to highly ionizing cosmic rays, whereby dozens of pixels were simultaneously activated (ref. 11). To study this effect, signal lines were connected from various combinations of diode pairs into a coincidence circuit with a one microsecond acceptance window. This unit produced one count for every current pulse which occurred in both diodes within one microsecond of each other. It was expected that the coincidence rate would decrease with increasing diode separation, as the diffusing charge would have to disperse over a larger area, resulting in less charge reaching both diodes.

The coincidence response of one diode with respect to another has been defined by dividing the total number of coincidence counts occurring between the two diodes during an arbitrary time interval by the average total number of counts obtained from both diodes during the same interval. Shown in Figure 8 is a plot of this fraction as a function of diode separation, for both proton energies used. Also shown are the results for 21.5 MeV and a 40 microsecond acceptance window. As expected, the coincidence response falls of with increasing didode separation; the largest values always occurring for adjacent diodes, although there is a measurable effect up to six diode spacings apart (for 21.5 MeV protons). Also indicated in Figure 8 is the strong energy dependence of the coincidence. This is due to the specific ionization loss of the proton being less at higher energies, thus producing less charge per unit length to be shared among the diodes. At energies below 21.5 MeV, larger coincidence fractions are to be expected.

Since the coincidence response for a given pair of diodes is presumably proportional to the extent to which each diode's effective sensitive area overlaps the other's, it should be possible to establish a dependence of this response on the geometrical arrangements of the diodes on the array. To experimentally verify this dependence we performed a two-parameter analysis using the IBM 360/44 data acquisition system available to users of the University of Maryland cyclotron. In this experiment, signals from a pair of diodes were each sent to separate analog-to-digital converters. If the conversion in one ADC occurred within 40 microseconds of that occurring in the other, both events were registered as a coincidence and sent to a dual parameter and display controller where the events were plotted and then stored on magnetic tape. A Z-intensified coutour display of several diode pairs is shown in Figure 9.

In each display, the amount of charge collected in one diode is plotted versus that collected in the other, and only those events which occurred in coincidence are plotted. The intensity of the data points is proportional to the number of counts each point represents. The figures suggest that adjacent diodes display somewhat different coincidence patterns than diodes separated by one diode. Based on our interpretation, the pattern observed in Figure 9 is not in any way fundamental, but depends on geometrical factors such as diode shape, relative spacing of each diode on the array, etc.

Consequently, a full discussion of the nature of the coincidence pattern must be postponed until "Analysis," when we use the diffusion model to discuss the results presented here.

DIFFUSION MODEL

Introduction

As described earlier, part of the kinetic energy associated with a penetrating charged particle is absorbed in the n-Si substrate of the diode array, creating hole-electron pairs. These ionization-generated charge pairs then diffuse away from their point of generation, some of which reach the depletion regions of the reverse-biased diodes. This chapter examines the physical theory behind the noise sensitivity of the diode array target as determined by hole diffusion and the discrete nature of the diode array.

Charge Creation

We consider protons entering the front surface of a silicon diode array at normal incidence. This surface is divided into two regions: exposed diodes and the $Si-SiO_2$ interface (see Figure 1). An energetic proton penetrating the face of the silicon wafer will generate in the substrate, through collective plasmon excitations and subsequent thermalization, electron-hole pairs at a rate of 1 e-h pair/3.62 eV of kinetic energy lost by the proton. Initially confined to the path of the proton, the charge pairs thermalize within a few picoseconds and spread to a radius of about 0.1 μ. The charges then immediately begin to diffuse in a direction opposite to the concentration gradient and disperse throughout the substrate of the wafer. For those which reach the edge of a diode depletion zone, the holes are swept into the depletion zone and the electrons are ohmically relaxed through the substrate contact. The fact of electron hole pairs that reach the $Si-SiO_2$ interface depends on the boundary conditions at this surface. Occasionally, a proton passes through both a diode's depletion region and the substrate beneath, where charge produced in both regions add quickly, producing a rather large current pulse. Protons penetrating the wafer outside the boundary of a diode enter only the substrate resulting in less charge reaching a diode. An exact solution of the diffusion equation, to be given shortly, shows the collection currents peak very rapidly after generation in the bulk and the collection process is complete within microseconds.

Other minor factors affecting the amount of charge collected include the electronic time constants of the input circuit to the diode, as well as dielectric relaxation effects in the equivalent circuit of the semiconductor substrate--depletion zone. We shall ignore these effects here for clarity of presentation, as they are significant only for large charge collection times.

Finally, mention should be made of a phenomenon discovered in the past year, known as "field-funneling." Recently, Hsieh et al., (ref. 26) presented definitive evidence that when an alpha-particle penetrates a p-n junction, the generated carriers drastically distort the junction field. After the alpha-particle penetration, the field, which was originally limited to the depletion region, extends far down into the bulk silicon along the length of the alpha-particle track and funnels a large number of carriers into the struck junction. After a few nanoseconds, the field recovers to its position in the normal depletion layer, and, if the track is long enough, a residue of carriers is left to be transported by diffusion. A first order analysis by Hu (ref. 27) shows the funneling depth is equal to 1 + μ_n/μ_p times the depletion region width for an n+/p junction (p-type substrates), where μ_n and μ_p are the drift mobilities for electrons and holes, respectively, in silicon. For n-type substrates, the ratio μ_n/μ_p becomes μ_p/μ_n. This result does not depend on charge density per cm along the track and should apply to proton tracks as well.

Boundary Value Problem

We begin by deriving an expression for the amount of charge reaching a diode from the substrate due to the passage of a charged particle. Making use of a Cartesian coordinate system, we approximate the silicon wafer by a homogeneous medium of infinite extent in x and y, and of finite thickness. In this and subsequent discussion, we shall assume this region to be of n-type conductivity. The front surface of the wafer, ($z = 0$), is partially implanted with diffused planar junctions, each of which is assumed to be a perfectly absorbing surface of zero thickness and finite area. (The details of the junction fabrication process do not concern us here). The remainder of the surface consists of the semiconductor-oxide interface boundary ($Si-SiO_2$), where we assume incomplete charge absorption takes place

due to the effect of fast surface states. Incomplete absorption also exists at the back surface of the wafer ($z = W$), although this boundary may be prepared under different conditions than the front surface.

As seen in Figure 10, the origin of a rectangular coordinate system is centered on the front surface of a typical diode with a rectangular cross-section of arbitrary dimensions. The $-z$ axis points into the silicon bulk. Passage of a ionizing particle, such as a proton, perpendicularly through the silicon wafer at $t = 0$ creates, nearly instantaneously, a line of charge parallel to the $-z$ axis. The density of charge generated along this track is generated non-uniform and will be formally represented by the function $\rho(z_o)$. The coordinates of the charged particle's point of entry is $(x_o, y_o, 0)$, that of any point along the trajectory is $(x_o, y_o, -z_o)$. We assume normal incidence for simplicity; experimentally this is easily realizable.

The volume density p_n of minority carriers (holes) in the quasi-neutral semiconductor medium under low injection conditions is governed by the time dependent diffusion equation given below (in Cartesian coordinates)

$$\frac{\partial p_n}{\partial t} + D_p\left(\frac{\partial^2 p_n}{\partial x^2} + \frac{\partial^2 p_n}{\partial y^2} + \frac{\partial^2 p_n}{\partial z^2}\right) + \frac{(p_n - p_{no})}{\tau_p} = \rho(z_o)\,\delta(t) \qquad (1)$$

where $\rho(z_o)$ is the source function, D_p the diffusion coefficient for holes in n-Si, and τ_p is the hole lifetime. This equation gives the minority carrier concentration at the location $r = (x, y, z)$ for a line of charge distributed along a track at $r' = (x_o, y_o)$ and created at $t = 0$.

In general, the solution to this equation must satisfy several boundary conditions at both the front and back surfaces of the wafer.

For the front surface:

$$J_z\Big|_{z=0} = -D_p \frac{\partial p_n}{\partial z}\Big|_{z=0} = v_o p_n \qquad \text{(at Si-O}_2\text{)} \qquad (2)$$

$$J_z\Big|_{z=0} = -D_p \frac{\partial p_n}{\partial z}\Big|_{z=0} = v_1 p_n \qquad \text{(at depletion layer)} \qquad (3)$$

For the back surfaces:

$$J_z\Big|_{z=W} = -D_p \frac{\partial p_n}{\partial z}\Big|_{z=W} = v_w p_n \qquad (4)$$

where v_n is the surface recombination velocity at the respective boundaries.

An analytical evaluation of the diffusion process in a mosaic target is quite involved. For a silicon wafer of finite thickness W, (1) becomes a boundary value problem with little chance of an exact solution. The reason for this is the need to specify three different homogeneous boundary conditions (of the third kind), one each for the diode depletion zone, the surface of the silicon wafer (z = 0) and its backside (z = W) (see Appendix 1). In fact, an exact solution would require detailed knowledge of the shape of the depletion regions and their geometrical arrangement on the array. Problems such as these with mixed boundary conditions (i.e., Dirchlet and Neumann boundary conditions specified on the same surface) are notoriously protracted but have been attempted by a few authors (refs. 28, 29, 30). As von Roos points out (refs. 28, 29), solutions are usually in the form of a series expansion of orthogonal functions appropriate to the coordinate system used, where the expansion coefficients are obtained by solving a set of dual inhomogeneous integral equations. To the author's knowledge, a solution to the particular problem posed here has not appeared in the diffusion theory literature.

Approximations

Mixed boundary values are necessary in theoretically evaluating experiments where surface effects predominate due to the close proximity of the charge source to the surface, such as the EBIC work described by Von Roos (ref. 28). However, simpler boundary conditions may not suffice even when the charge source lies deeper in the medium. For the case of long particle tracks penetrating deep into the silicon wafer, most of the charge is created away from the surface influences. However, it remains to be seen whether or not surface states continue to affect the amount of charge reaching the diode depletion zone. Nevertheless, there appear to be a

certain conditions under which it seems reasonable to relax boundary condition (2), and assume (3) applies over the entire surface. This approximation should adequately describe devices having a large fraction of their surface covered with diodes (such as CCD arrays). It should also hold for linear diode arrays and short particle tracks if the particle track is created well within the diode's boundary, away from the influence of surface effects at the silicon-oxide boundary. Also, as recombination velocities are usually quite high at depletion zones, ($>10^5$ m/s), due to the intense electric fields present at the junction, it is customary to let $V_1 \to \infty$, which is equivalent to demanding the charge density vanish at $z = 0$. Under these two approximations we are thus assuming the entire front surface to be a perfectly absorbing surface.

Solution

As shown in Appendix 1 for a medium unbounded in x and y, and infinite or semi-infinite in the z-coordinate, the Greens function solution to (1), under the approximations just covered, has the form

$$G_p = \frac{1}{4\pi D_p t} \exp\left(-\frac{r^2}{4D_p t} - \frac{t}{\tau_p}\right) \cdot \int_a^\infty \exp\left\{-n^2 D_p t\right\} K(n,z)\, K(n,z_o)\, dn \quad (5)$$

where $r^2 = (x - x_o)^2 + (y - y_o)^2$

and $a = 0 \qquad 0 < z < \infty \qquad$ (semi-infinite)

$a = -\infty \qquad -\infty < z < \infty \qquad$ (infinite)

and the $K(n,z)$ are eigenfunctions for the homogeneous problem corresponding to the boundary condition at $z = 0$.

For a medium of finite thickness the integral is replaced by a summation over eigenfunctions appropriate to the boundary conditions at $z = 0$ and $z = W$.

This solution was obtained by solving (1) using an impulse source function for a point along the track

$$G_s = g\,\delta(x-x_o)\,\delta(y-y_o)\,\delta(z-z_o)\,\delta(t) \qquad (6)$$

where g is the source strength at that point, and whose value we have chosen to be unity for the time being. Later we will integrate G_p over the charge density function $\rho(z_o)$ to obtain the final result.

By means of an example, the kernel $K(n,z)$ appropriate for an infinite medium, $K(n,z) = 1/\sqrt{2\pi}\,\exp(inz)$ when substituted in equation (5), gives

$$G_p = f(r,t) \int_{-\infty}^{\infty} \frac{1}{2\pi} \exp\left\{-n^2 D_p t - in(z-z_o)\right\} dn$$

resulting in the Greens function for an infinite medium

$$G_p = \frac{1}{(4\pi D_p t)^{3/2}} \exp\left(-\frac{r^2 + (z-z_o)}{4D_p t} - \frac{t}{\tau_p}\right) \qquad (7)$$

For a semi-infinite medium in which $V \to \infty$ at $z = 0$ the appropriate kernel is $K(n,z) = 2\pi\,\sin(nz)$, when substituted in equation (5) gives

$$G_p = \frac{1}{(4\pi D_p t)^{3/2}} \exp\left(-\frac{r^2}{4D_p t} - \frac{t}{\tau_p}\right)\left[\exp\left(-\frac{(z-z_o)^2}{4D_p t}\right) - \exp\left(-\frac{(z+z_o)^2}{4D_p t}\right)\right] \qquad (8)$$

The result, although obtained formally by integral transform techniques, is physically motivated by use of the method of images whereby the semi-infinite medium and a charge sink located at $+z_o$. Therefore, the charge density vanishes at $z = 0$, which is equivalent to demanding an infinite recombination velocity there.

Introducing a boundary at $z = W$ requires a different kernel to be substituted into equation (2). In this case, $K(n,z)$ is given by

$$K(n,z) = \left[2\,\frac{\beta_n^2 + (v_w/D_p)^2}{W\left(\beta_n^2 + (v_w/D_p)^2\right) + v_w/D_p}\right]^{1/2} \sin \beta_n z$$

for $v = \infty$ at $z = 0$. This results in the following expression

$$G_p = \frac{2}{4\pi D_p t} \exp\left(-\frac{r^2}{4D_p t} - \frac{t}{\tau_p}\right) \sum_{n=1}^{\infty} \exp\{-\beta_n^2 D_p t\}$$

$$\times \frac{\beta_n^2 + (v_w/D_p)^2}{W(\beta_n^2 + (v_w/D_p)^2) + v_w/D_p} \sin \beta_n z \sin \beta_n z_o$$

where β_n are the positive roots of $\beta * \cot(\beta W) + v_w/D_p = 0$.

For the limiting cases of $v_w \to 0$ and $v_w \to \infty$ at $z = W$ this Greens function reduces to

$$G_p = \frac{2}{4\pi D_p t} \exp\left(-\frac{r^2}{4D_p t} - \frac{t}{\tau_p}\right) \sum_{n=1}^{\infty} \exp\left(-\frac{(n - 1/2)^2 \pi^2 D_p t}{W^2}\right)$$

$$\times \sin\left(n - \frac{1}{2}\right)\frac{\pi}{W} z \sin\left(n - \frac{1}{2}\right)\frac{\pi}{W} z_o \qquad (10)$$

for $v_w = 0$ (perfect charge-reflecting back surface) with a similar expression for $v_w = \infty$ (perfect charge-absorbing back surface) with $\left(n - \frac{1}{2}\right)$ replaced by n.

The current density at a point $(x, y, 0)$ on the surface is given by

$$j(r, z_o, t) = - D_p \frac{\partial G_p}{\partial z}\bigg|_{z=0} \qquad (11)$$

Next, the current flowing into the entire diode from the point source at $(x_o, y_o, -z_o)$ is given by integrating equation (11) over x and y, where the integration limits corresponds to the physical dimensions of the diode.

$$i(r, z_o, t) = \int_{x_a}^{x_b} \int_{y_a}^{y_b} j(r, z_o, t)\, dy dx \qquad (12)$$

Upon integrating this expression over the tracklength L, we obtain the total current entering the diode resulting from charge diffusing away from the entire trajectory

$$I(r,t) = \int_o^L \rho(z_o)\, i(r,z_o,t)\, dz_o \tag{13}$$

where $\rho(z_o)$ is the generated electron-hole density per unit length.

Since $\rho(z_o)$ is usually non-uniform we may choose for the purposes of numerical computation to approximate the integral in equation (13) by a summation over thin segments or layers

$$I(r,t) = \sum_{n=1}^{N} \rho_n \int_{z_n}^{z_{n+1}} i(r,z_o,t)\, dz_o \tag{14}$$

where $z_1 = 0$, $z_n = L$ and N is the number of segments used to approximate $\rho(z_o)$. We assume ρ_n is uniform over each segment having thickness $s = z_{n+1} - z_n$. The average value of ρ_n is given by

$$\rho_n = e * (dE/dx)_n / w$$

where

e = electronic change
w = energy required to create 1 e-h pair
(dE/dx)n = stopping power for nth layer

Finally, the total charge Q_s collected by the diode from the substrate track is obtained by integrating over all time

$$Q_s = \int_o^\infty I(r,t)dt = D_p \sum_{n=1}^{\infty} \rho_n \int_o^t \int_{z_n}^{z_{n+1}} \int_{x_a}^{x_b} \int_{y_a}^{y_b} \left.\frac{\partial G_p}{\partial z}\right|_{z=0} dydxdz_o dt \tag{15a}$$

The integrations indicated in (15a) may be carried out analytically for both semi-infinite and finite solutions, with only the time integral requiring numerical integration. This results in the following expressions for Q_s

$$Q_s = \sum_{n=1}^{N} \rho_n W_n \tag{15b}$$

where

$$W_n = \frac{1}{\sqrt{16\pi}} \int_o^\infty f_\lambda(\text{erf}) \exp\left(-\frac{\lambda^2}{4L_d^2}\right) \left[\exp\left(-\frac{z_n^2}{\lambda^2}\right) - \exp\left(-\frac{z_{n+1}^2}{\lambda^2}\right)\right] d\lambda \tag{16}$$

for a semi-infinite medium, and

$$W_n = \frac{1}{2} \int_o^\infty \lambda f_\lambda \ (\text{erf}) \exp\left(-\frac{-\lambda^2}{4L_d^2}\right) \sum_{m=1}^{\infty} \exp\left(-\frac{\alpha_m^2\lambda^2}{4W^2}\right) \frac{\alpha_m^2 + b^2}{\alpha_m^2 + b^2 + b} \times \left(\cos\frac{\alpha_m z_n \pi}{W} - \cos\frac{\alpha_m z_{n+1}\pi}{W}\right) \tag{17}$$

for a wafer of thickness W having a finite recombination velocity v_w at $z = W$, and where

$$f_\lambda(\text{erf}) = \left[\text{erf}\left(\frac{x_b - x_o}{\lambda}\right) - \text{erf}\left(\frac{x_a - x_o}{\lambda}\right)\right]\left[\text{erf}\left(\frac{y_b - y_o}{\lambda}\right) - \text{erf}\left(\frac{y_a - y_o}{\lambda}\right)\right]$$

and where

$$\lambda^2 = 4D_p t, \quad \alpha_m = \beta_m W, \quad b = v_w W \quad \text{and} \quad L_d = D_p \tau_p$$

where α_m are the positive roots of $\alpha * \cot(\alpha) + b = 0$

Written this way, W_n represents an "effective track length" or the length of a track 'seen' by the diode with 100% efficiency, as opposed to the much smaller efficiency with which the actual track is seen, which we shall call the "charge collection efficiency" C_n, where $C_n = W_n (z_{n+1} - z_n)^{-1}$. We may write (15b) in terms of C_n as

$$Q_s = \sum_{n=1}^{N} q_n C_n \tag{18}$$

where q_n is the charge created along the segment of track having length $z_{n+1} - z_n$.

To equation (15) we must add Q_o, the charge collected from the depletion layer, the surface diffused layer, and the "funneling zone." Q_o may be written as

$$Q_o = \rho_o W_o$$

where

$$\rho_o = \text{charge density/unit length along } W_o$$

$$W_o = \left(1 + \frac{\mu_p}{\mu_n}\right) (2\varepsilon\rho\mu_n V_o)^{1/2} \tag{19}$$

and the physical parameters are defined in Table 1. Note $Q_o = 0$ if the proton enters the wafer at a point outside the perimeter of the diode.

Semi-Infinite vs. Finite Approximations

In the semi-infinite approximation, the total charge collected from the substrate depends only on the diffusion length L_d, plus geometrical

Table 1. Physical characteristics of digicon diode array.

SUBSTRATE	
Doping	n - type
Resistivity (ρ)	4.5 ohm-cm
Thickness (W)	400 μ
Dielectric constant (ε)	12-13
Hole Mobility (μ_p)	70 $cm^2/sec\text{-}v$
Electron mobility (μ_n)	1380 - 1400 $cm^2/sec\text{-}v$
Diffusion coefficient (D_p)	14.8 cm^2/sec
Bias voltage (V_o)	+5 V
DIODES	
Type	p+n diffused (0.7 μ) with Boron
Area	8.5×10^{-5} cm^2/diode
Pitch	50 μ
Width	40 μ
Length	250 μ
Depletion width	2.5 μ
Funneling depth	1 μ
No. diodes on array	512

factors involving diode dimensions and track length. The effect of the water back surface on the flow of the excess charge carriers is ignored. As a general rule, if the wafer thickness $W >> L_d$ this approximation is valid to a high degree. Another important geometrical ratio is that between diode size and W, which if small enough provides an independent criterion for ignoring the back surface. The importance of the magnitude of these geometrical factors cannot be overstated, for although the functional dependence on them appears complex, dimensionless ratios among them may be formed which shows more clearly the minimum number of variables upon which charge collection depends.

For a Digicon-type diode and substrate, both expressions equations (16) and (17) are plotted as a function of Ld and shown in Figure 11 for a charge track directly beneath the diode ($x_o = y_o = 0$). We have normalized the values plotted to the track length W, which has been set equal to 400 μ, corresponding to the physical situation in which the proton penetrates the wafer and thus track length and wafer thickness are the same. Notice we are assuming $\rho(z_o)$ is uniform along the entire track. As might be expected, increasing the diffusion length beyond the track length results in little additional charge collection, as evidenced by the leveling off of the curve around $L_d = 300\ \mu$. These curves are practically identical in both the semi-infinite and finite approximations, for both values of v_w, except for $L_d \to W$, where the curve for $v_w = \infty$ is slightly depressed.

Actually, only charge originating from that portion of the track nearest the back surface is affected by conditions there, as can be seen in Figure 12 where we show the collection efficiency from four 100 μ track segments plotted versus L_d for $v_w = 0$ and $v_w = \infty$. As the curves show, very little charge reaches the diode from the last 100 μ anyway, since the collection efficiencies barely exceeds 0.5%.

Although the amount of charge collected by the diode from a given particle track depends strongly on the diffusion length and the track depends strongly on the diffusion length and the track length, the maximum charge collectable from a track is ultimately determined by the diode area. This effect can be seen clearly in Figure 13 where the effective track length is plotted versus actual track length, for a number of values for L_d. Notice

that beyond a limit defined by the envelope of all the curves, additional increases in either L_d or W fail to further the amount of charge collected by the diode. In particular, the maximum theoretical charge collection efficiency from a 400 μ track is about 9%.

Summarizing, we find that unless L_d is of the same order as W, back-surface effects can be safely ignored and the much simpler semi-infinite approximation used in modeling charge diffusion from particle tracks. Second, if the wafer thickness is much greater than front surface diode dimensions, the semi-infinite model is valid irrespective of L_d, since the diode subtends vanishingly small solid angles from points far along the track. For the case of the Digicon diode/substrate, both considerations work to our advantages; consequently we shall employ the semi-infinite approximation in our modeling.

Diffusion Current Waveforms

Although we are primarily interested in the total charge collected at the diode, it is of some interest to examine the diffusion current waveforms in order to explore the physical soundness of the results of our derivation. We confine our attention to the Digicon type diode-substrate whose relevant physical parameters are summarized in Table 1. The general shape of the diffusion current versus time waveforms is illustrated in Figures 14, 15, 16 for a track created by a proton entering the wafer at $y_o = 0$, $x_o = 0$, 50 and 100 μ, respectively (using the same coordinate system defined at the beginning of the chapter and in Figure 10). These curves are plotted using equation (13) and the semi-infinite Greens function with a track length W of 400 μ, as before. We do not show drift currents due to charge collection in the depletion layer or the funneling zone, as these occur on subnanosecond time scales. Evident is the strong dependence of the shape and magnitude of the current pulse on the distance from the proton's entry point to the center of the diode. In addition to the expected decrease in current with increasing distance of entry, both a peak shift and width increase is apparent. The time delay arises naturally as a result of the longer distances over which charge must diffuse to reach the diode. This also produces in a smearing out of the arrival times of each charge carrier, due to the random nature of the diffusion process, resulting in larger peak widths.

Decreasing the diffusion length L_d also has a pronounced effect on both the shape and magnitude of the current, as indicated in the series of figures beginning with Figure 17. Since L_d controls the depth to which the diode "sees" into the silicon bulk, it is to be expected that smaller values of L_d will lead to a reduction in the magnitude of the current, as well as the time spread of the current pulse. This latter effect follows from the smaller time differential for charge arriving at the diode from the beginning and end of the track, resulting from a decrease in the effective length of the track, (see Figure 13).

Since the magnitude of each current pulse is extremely small, (no more than 100 pA at the peak for a 20 MeV proton), and lasts for less than a microsecond, it is unlikely that diffusion current waveforms due to particle tracks can be measured with much precision at present. Fortunately, much of the relevant information can be derived from the integrated charge. Experiments obtaining this information were described and, in the next section, those results are interpreted in light of the model presented here.

ANALYSIS

Introduction

Our primary task in this chapter is to account for the experimental frequency distribution of noise charge observed during irradiation of the Digicon diode array with 21.5 and 75.4 MeV protons, and presented in "Experimental Work." These pulse-height spectra of collected charge represent the accumulation of tens of thousands of separate events each consisting of a proton entering the wafer at some random point (x_o, y_o) and generating charge along a straight line path. The electron-hole pairs subsequently spread in all directions, inducing a transient diffusion current in a p-n junction diode at the surface of the wafer. Thus, all pulse-height spectra simulation algorithms in this area are faced with two fundamental physics problems: charge creation and charge transport.

Once charge is created at a point in the wafer, the subsequent transport and collection of that charge at a diode is a rather complex diffusion theory boundary value problem but one which can be solved under the simplifying approximations outlined in "Diffusion Model." However, it is well known that the ionization losses of fast charged particles fluctuate, even if the particles are monoenergetic, due to the statistical nature of the energy-loss process. Thus, the number of charge carriers created in the silicon by each proton is not constant, but characterized by a probability function we shall refer to as the energy-loss straggling distribution. This means the magnitude of charge collected by a diode from each event is determined not only by diffusion, but also by statistical considerations involving the ionization process itself.

To clarify this point, consider the magnitude of the charge Q at the endpoint of the integral pulse height spectra in "Experimental Work." This point, Q_{max}, represents the largest amount of charge collected by the diode for that particular energy. For the 21.5 MeV data shown in Figure 6, Q_{max} is around 11.2 fC, which is equalivent to about 70,000 charge carriers collected. At 75.4 MeV this point occurs at around 5.4 fC. From symmetry considerations, these events should be due to protons penetrating near the center of the diode's collecting area, where the largest solid angle is

available to the ionization track. Diffusion theory, however, predicts a maximum collectable charge Q of only about 7.1 fC from a 21.5 MeV proton track, (assuming a uniform $\rho(z_o)$ and no statistical fluctuations from track to track). Furthermore, as will be illustrated shortly, calculated pulse height distributions using this assumption result in spectra which poorly approximate most of the upper half of the experimental distribution. Clearly a more rigorous approach is needed. The next section outlines these ideas in more detail.

Diffusion-Predicted Pulse-Height Spectra

Before we introduce energy loss fluctuations, let us examine the degree to which diffusion theory alone accounts for the experimental results. To do this we must provide some familiarity with the simulation techniques used in this work and the assumptions behind them. To simplify matters, we begin by plotting as a function of x_o and y_o the two dimensional charge collection efficiency matrix C_w defined in expression (18), for a uniform track of length W = 400 u. This is shown in a three-dimensional representation in Figure 20 for a Digicon type diode/substrate, and L_d = 90 μ. As expected, the largest values corresponds to tracks located beneath the center of the diode, falling off most nearly exponentially with increasing distance from the diode boundaries. (The peaked structure in Figure 20 has no special significance and is due to the particular shape of the collection area of the Digicon diode). When each value in this matrix is multiplied by the total charge generated in the silicon by a proton (not including the depletion zone), Figure 20 represents the amount of charge collected by the diode from the substrate, plotted as a function of the proton's entry point. A computer program can then be used to sort these values into a frequency distribution which represents a rather crude approximation to the experimental distribution of collected charge.

This calculation was carried out and is shown plotted in Figure 21 in integral form alongside the experimental result for 21.5 MeV protons, while Figure 22 shows the 75.4 MeV result. In both figures curve (a) corresponds to W_o = 0 (no depletion layer), while (b) corresponds to W_o = 3.5 μ (given by expression (19) in "Diffusion Model"). In both cases the lack of a statistical treatment results in a gross understimation of the maximum

charge collected, and fails to account for the overall shape of the distribution for large values of charge. Fairly good agreement is seen in ther lower half of the spectrum, at both energies, which is also that portion of the spectrum whose shape is independent of W_o. This suggests diffusion theory alone suffices in accounting for charge collection from distance particle tracks, or at least tracks not directly underneath the diode collection area.

Energy Loss Fluctuations

A better approximation can be constructed by allowing for fluctuations in the amount of ionization produced in the silicon from event to event (track to track). In the previous treatment we simply multiplied each value in the collection efficiency matrix by the mean energy loss, $\bar{\Delta}$, given by the familiar expression due to Bethe [see for example, Rossi, (ref. 44)]

$$\Delta = 0.30058 \frac{mc^2}{\beta^2} \frac{Z}{A} s \left[\log\left(\frac{2mc^2\beta^2\varepsilon_{max}}{I^2(1-\beta^2)} \right) - 2\beta^2 - 2\frac{C}{Z} - \delta \right], \qquad (20)$$

where Z, A, and I are, respectively, the atomic number, atomic weight, and mean excitation energy of the medium, $2\frac{C}{Z}$ is the shell correction, and δ is the density effect correction.

where

$$\varepsilon_{max} = \frac{2mc^2\beta^2}{1-\beta^2} \left[1 + \frac{2m}{M} \frac{1}{1-\beta^2} + \left(\frac{m}{M}\right)^2 \right]^{-1}$$

on mass where mc^2 is the electron rest energy and βc the velocity of the particle. For small β, ε_{max} is also very small. Because of the small value of m/M for protons or mesons, the factor in square brackets is practically unity, except when $\beta \to 1$. For $\beta \to 1$, $\varepsilon_{max} \to \frac{mc^2\beta^2}{1-\beta^2}$, which means that almost the entire energy of the particle can then be transferred in a single collision. (We have neglected the shell correction and density effect correction in (20) as they are insignificant for our range of β).

Now the energy lost by a charged particle in a thin absorber is subject to fluctuations as previously mentioned. Landau (ref. 31) derived a transport equation for the straggling function for the energy losses Δ small compared to the initial energy of the incident particle:

$$\frac{\partial f(\Delta,s)}{\partial s} = \int_0^b w(\varepsilon)\, f(\Delta - \varepsilon, s)\, d\varepsilon - f(\Delta,s) \int_0^{\varepsilon_{max}} w(\varepsilon)\, d\varepsilon \qquad (21)$$

($b = \Delta$ for $\Delta < \varepsilon_{max}$; $b = \varepsilon_{max}$ for $\Delta > \varepsilon_{max}$).

where $f(\Delta,s)d\Delta$ denotes the probability that a proton in penetrating a distance s in the target, will experience an energy loss between Δ and $\Delta + d\Delta$ as a result of collisions with atomic electrons; and $w(\varepsilon)d\varepsilon$ is the differential collision cross-section for single collisions with an energy loss ε.

Thus, the mean energy loss $\bar{\Delta}$ is given by

$$\bar{\Delta} = \int_0^\infty f(\Delta,s)\Delta\, d\Delta$$

A rigorous solution to equation (21) has been given by Vavilov (ref. 32), who showed that the shape of $f(\Delta,s)$ was characterized by the ratio of Δ to ε_{max}. This we denote by κ, where

$$\kappa = 0.30058 \frac{mc^2}{\beta^2} \frac{Z}{A} s/\varepsilon_{max} = \frac{\xi}{\varepsilon_{max}} . \qquad (22)$$

If each of the energy-transfer to electrons is small compared to Δ, which is the case if $\kappa >> 1$, $f(\Delta,s)$ is approximately Gaussian, given by

$$f(\Delta,s) \sim \frac{1}{\xi \frac{2\pi}{\kappa} (1 - \beta^2/2)} \exp\left\{-(\Delta - \bar{\Delta})^2\, \kappa/2\xi^2\, (1 - \beta^2/2)\right\} \qquad (23)$$

(see also Jackson (ref. 33)).

If the total number of atomic collisions is small, which occurs for both thin absorbers or fast particles, (i.e., $\kappa << 1$), then individual

collisions can make significant contributions to Δ, and the distribution is asymmetric, with a tail corresponding to large values of Δ. This is the so-called Landau distribution, given by

$$\lim_{\kappa \to 0} f(\Delta, s) = \frac{1}{\pi\xi} \int_0^\infty e^{-\frac{\pi x}{2}} \cos\left[x(\log x + \lambda)\right] dx. \qquad (24)$$

where

$$\lambda = \lambda_v/\kappa - \log \kappa = \frac{\Delta - \overline{\Delta}}{\xi} - 1 - \beta^2 + \gamma - \log \kappa,$$

$\gamma = 0.577216 \ldots$ (Euler's constant). The shape of the Landau distribution is indicated in Figure 23.

For intermediate values of κ, the rather complex but exact solution due to Vavilov applies, and is given in Appendix 2. Both the Landau and Gaussian distributions are limiting cases of the exact Vavilov solution. For the Digicon diode/substrate all of these types of fluctuations contribute to the overall shape of the pulse-height spectra in Figures 6 and 7. In addition, at the lower proton energy (21.5 MeV), this shape function is dominated by fluctuations in the 3.5 μ depletion layer/funneling zone, where $\kappa \lll 1$ and the above theoretical treatments are not valid.

Computer Program PULHGT

To correctly simulate the observed pulse height distributions, the above considerations force us to treat each incoming proton as a separate event. A computer program called PULHGT was developed in order to accomplish this task. PULHGT performs the calculations indicated in (18), and using Monte Carlo techniques to determine x_o, y_o, and q_n, calculates pulse height distribution of charge which is collected as the result of N protons striking the diode array at random. This is accomplished by first calculating the three-dimensional charge collection efficiency matrix $C_n(x_o, y_o, z_n)$ for a large number of points representing the volume in the

substrate to which the diode is sensitive. This matrix is stored in PULHGT and during the simulation each point in this matrix corresponding to a particle track at x_o, y_o is multiplied by the charge created along each segment of the track having length $z_{n+1} - z_n$. The number of charge carriers created by each proton in either the depletion zone or along a segment is determined by computing the energy loss straggling function $f(\Delta,s)$ appropriate for the region through which the proton is passing, and using a random number generated on an interval from 0 to 1 to select values from the normalized integral of $f(\Delta,s)$. In this way, q_n is calculated independently for each segment z_n in expression (18) as well as for the depletion layer W_o, and the process is literated for as many times as is necessary to build up to the equivalent statistical accuracy of the experimental distribution.

In some situations it is convenient to allow the ionization to vary from event to event, but to retain the assumption that the ionization density remains constant over the track length. In this case our simulation is essentially two-dimensional, as we are calculating for each point x_o, y_o an average charge collection efficiency for the entire 400 μ track, and multiplying this value by the charge produced along the track. (This was the procedure used in the diffusion-only simulations previously, where we neglected energy-loss fluctuations completely).

This latter procedure was followed in building up the theoretical pulse height distributions shown in Figure 24. The Vavilov parameter for a 400 μ track is large enough (>1) to assume a Gaussian distribution of energy losses in the substrate. For the 3.5 μ depletion layer/funneling zone, κ = 0.0297, meaning we should use the Landau distribution to determine energy loss in this region. The program PULHGT computed the energy of the 40 MeV protons after passing through the 10 mil tantalum beam port and the 3 mm MgF_2 window also using a Gaussian distribution of energy losses. Two random numbers were used to determine x_o and y_o for each proton.

We show the corresponding predicted and observed integral/differential distributions at 21.5 MeV in Figure 24. A trial-and-error procedure was used to determine the value of L_d needed to produce the best fit. This turned out to be L_d = 90 μ. We have normalized the theoretical integral

distribution to the experimental distribution at a point around 3.5 fC, as this seems to produce the best overall fit. From Figure 24 we see that agreement between theory and experiment is fair except for the very low (<1.4 fC) charge events, in which case the simulation underestimates the amount of charge collected. Notice also that most of the large charge events (>6 fC) appear to be due to energy-loss fluctuations in the depletion layer.

When a similar simulation is performed for 75.4 MeV protons, the agreement between the integral distributions is excellent until around 1.2 fC, where the two curves dramatically part company (see Figure 25). Unlike the previous result at 21.5 MeV, here the fit is poor for both $W_o = 0$ and $W_o = 3.5\,\mu$. Evidently, energy loss fluctuations in the depletion layer do not fully account for large Q events at this higher energy.

Three-Dimensional Simulations

Explaining the discrepancy in the 75.4 MeV integral spectra at large charge values requires rejecting the assumption of a uniform $\rho(z_o)$. Initially we assumed a uniform density of electron hole pairs along the particle track to simplify the derivations and expedite the calculations, as full three-dimensional simulations require substantial computing time. The reason this assumption must be rejected lies in realizing that the diode "sees" different segments of nearby particle tracks with different degrees of efficiency, determined mainly by two factors: the geometrical solid angle subtended by the diode at a point on the track segment, and of course the diffusion length. (By 'nearby' tracks we mean those occurring directly beneath the diode collecting area.) Thus, the diode is somewhat sensitive to large fluctuations in the charge density along these tracks, and this in turn affects the number of large charge events seen. Of course, these fluctuations are more severe at higher proton energies, since the number of collisions per unit length is smaller. We show the dependency of C_n on z_o for a track centered at $x_o = y_o = 0$ in Figure 26.

Charge collection from distant tracks is less influenced by variations in $\rho(z_o)$. Indicated in Figure 27 is $C_n(z_o)$ for a track entering at $x_o = 100\,\mu$, $y = 0$. Peak sensitivity occurs around $z_o = 50\,\mu$, dropping

rather sharply on both sides. Only the portion of the track centered on the peak is seen by the diode, compared to the larger fraction seen for nearby tracks. This analysis suggests why diffusion theory alone suffices in determining the experimental charge distributions for low to medium Q (due to distance tracks), but fails in the high Q part of spectrum (due to nearby tracks).

To simulate the 75.4 MeV data we chose to divide the track into 10 segments each having a length of 20 μ for a total track length of 200 μ. (Although the actual track length is 400 μ, we have shown that for $L_d <$ 150 μ, very little charge is calculated to reach the diode from points along the track beyond 200 μ). This choice was a reasonable compromise between a desire to adequately sample the varying collection efficiency along the track, and budget the expensive computing time. The theoretical spectrum obtained for 75.4 MeV protons is presented in Figure 28. Although a slight deviation remains for very small Q, the overall agreement between theory and experiment is much improved.

At 21.5 MeV the fit is not as precise (Figure 29). There occurs a discrepancy for very small Q which we have attributed to surface effects not adequately modeled here. The rest of the calculated spectrum follows its experimental counterpart about as well using the three-dimensional treatment as it did with the two-dimensional approximation. This further indicates the insensitivity at low proton energies to fluctuations along the substrate track, in striking contrast to the 75.4 MeV result, in which substrate fluctuations dominate the spectrum.

Low Q: Surface Effects

A possible reason for the improved fit at 75.4 MeV for events occurring below 1.4 fC may be seen by considering where the protons which cause these events enter the diode array. Using the program PULHGT we plotted the values of x_o and y_o responsible for causing counts within a 'window' of charge values occurring in the pulse height spectrum, whose width and possible could be varied at will. Such a plot is shown superimposed on the diode array pattern in Figures 30 and 31 for 21.5 and 75.4 MeV protons, respectively. These plots show where protons had to enter the wafer in order to result in charge between 0.5 and 1.4 fC being collected by the center diode.

At 21.5 MeV most of the events originate in particle tracks created well outside (>100 μ) the boundary of the center or 'reference' diode. This is a region in which much of the charge must diffuse under the Si/SiO_2 interface portion of the diode array pattern in order to reach the diode. Much of this charge will reach the surface before getting to the diode depletion zone, and according to the boundary condition $v_o = \infty$, be completely absorbed there. If this boundary condition is not valid then some charge would be 'reflected' at this interface and reach the diode. This would probably result in more counts being observed at low charge values, but we do not attempt the calculation here. (This was partly our reason for not normalizing the theoretical spectrum to the experimental one at the noise threshold at 0.5 fC).

However, we remarked in "Experimental Work" that if protons enter the array within the 'protective' region near the diode elements, where surface effects should be minimal in determining the amount of charge reaching each diode, then our assumption of a completely absorbing surface at $z = 0$ may be a valid approximation. This is borne out in Figure 31, since most of the protons at 75.4 MeV causing counts in the above region of interest apparently enter the array close to the center diode's boundaries.

High Q: Incorrect Distribution Function?

Returning to the problem of large charge values in the spectrum, we have found for charge values above 3.2 fC (at 21.5 MeV) that aside from being confined to the interior of the diode, there is little correlation between the location of the "charge window" and x_o, y_o. Actually, the region near the endpoint of the spectrum represents relatively infrequent events when large energy transfers occurred in the depletion zone and substrate. This effectively increases the charge collection efficiency beyond that predicted by expression (16), explaining the discrepancy described at the beginning of the chapter.

Unfortunately, theoretical treatments of energy loss in extremely thin absorbers, such as the depletion layer, are not yet consistent with experimental results. Vavilov/Landau theory does not include the effect of

resonant collisions with distant atomic electrons, which can significantly alter the shape of $f(\Delta,s)$ in these regions (ref. 42). Our use of the Landau distribution in this region is therefore probably incorrect, and may explain the poorer fit seen for large Q at 21.5 MeV. Corrections to the Vavilov theory, most notable that given by Blunck and Leisegang (ref. 34), have been shown not to agree with experiment (ref. 38), although recent efforts appear to be more successful (ref. 39). Vavilov's theory works very well in the range of κ used at 75.4 MeV to model the substrate $\rho(z_o)$ (ref. 40, 41). We assume this is responsible for the excellent fit seen there.

Analysis of Coincidence Results

An important aspect of charge diffusion from particle tracks created in multi-diode thin silicon chips is the near simultaneous triggering of several diodes from a single proton event. Every diode in the vicinity of a proton track sees the track with differing degrees of effectiveness, and at slightly different moments in time, depending on the solid angles and diffusion time constants of the situation. This effect, besides providing an opportunity for further testing the validiaty of various physical models, can have many practical consequences with respect to the use of thse devices as paraticle detectors. Some proton-induced noise-rejection schemes to be employed when the Space Telescope Digicon diode array is flown in orbit depend on various anti-coincidence decisions whose effectiveness is determined by the magnitude of the coincidence effect.

We have not been as successful in modeling the coincidence and effective area results indicated in "Experimental Work," as these phenomena depend rather strongly on the number of low Q events collected, which our model underestimates at low proton energies. We do see qualitative agreement, however, indicating the physical principles involved are probably sound. In the limit of infinite front surface charge absorption, we predict crosstalk and enhanced collection is reduced by 50% over the absorbed amount. Our results suggest, at least, that these effects may be controlled by altering the surface preparation of the wafer during manufacture.

Summary and Conclusions

The combined problem of generation/transport of ionizing-radiation created charge carriers in a silicon microelectronic device has been treated here for the first time. Given the extreme complexity of this process, conventional wisdom would dictate that a useful simulation procedure is practically impossible by any except Monte Carlo methods. Indeed, Monte Carlo techniques have proven successful in modeling energy loss distribution (ref. 35) as well as charge transport simulations in integrated circuits (refs. 13, 14). However, a full scale Monte Carlo simulation of the combined generation/transport problem would probably tax the limits of most computer installations. From this viewpoint, it is encouraging that the predominately analytical approach pursued in this paper, with the unavoidable simplifying assumptions, has met with reasonable success.

Furthermore, we have clearly delineated the areas in which the model fails to work, by establishing a connection between those areas and the assumptions which underly them. This is most important if Monte Carlo modeling is attempted in future work, as this approach requires a clear understanding of the physical processes occurring in the system, and their relative importance. Two important problem areas brought out in this work are surface effects and energy loss in thin depletion layers, the latter being of critical importance in simulating proton-induced charge noise in digital circuits having very low Q_{crit}.

Finally, we believe the interaction of protons with these devices presents a challenge to both the experimentalist and the theoretician by providing a simple tool with which to study charge creation and transport in a semi-classical environment. Future devices with their even greater levels of integration will surely require quantum mechanical modeling, and the considerations raised here will continue to be relevant, if not dominating.

APPENDIX I

GREEN FUNCTION SOLUTION TO DIFFUSION EQUATION

In the absence of electric fields, the continuity and current density equations for holes in n-type silicon are:

$$\frac{\partial p_n}{\partial t} = S_p - U_p - \nabla \cdot \vec{J}_p \qquad (I.1)$$

and

$$|J_p| = -D_p \nabla \cdot p_n \qquad (I.2)$$

where p_n = number density of holes in holes/cm**3
S_p = hole generation rate
U_p = hole recombination rate
J_p = hole current density
D_p = hole diffusion constant

Under low injection conditions (i.e., where the injected carrier density is much less than the equilibrium majority carrier density), U_p can be approximated by $(p_n - p_{no})/\tau_p$, where p_{no} is the thermal equilibrium minority carrier density and τ_p the hole lifetime.

For the three-dimensional case under low injection conditions, equations (I.1) and (I.2) combine and reduce to

$$\frac{\partial p_n}{\partial t} = D_p \nabla^2 p_n - \frac{(p_n - p_{no})}{\tau_p} + S_p \qquad (I.3)$$

For an instantaneous line source of charge created at t = 0, we have $S_p = \rho(z_o)\delta(t)$, where $\rho(z_o)$ is the generated charge per unit length.

For $t > 0$ (I.3) is homogeneous and we may substitute $p = (p - p_{no}) \exp(t/\tau_p)$ leaving, in Cartesian coordinates

$$-D_p\left(\frac{\partial^2 p}{\partial x^2} + \frac{\partial^2 p}{\partial y^2} + \frac{\partial^2 p}{\partial z^2}\right) + \frac{\partial p}{\partial t} = \rho(z_o)\,\delta(t) \qquad \text{(I.4a)}$$

The Green function $G(x,x')$ appropriate to (I.4a) satisfies the in homogeneous equation

$$-D_p\left(\frac{\partial^2 G}{\partial x^2} + \frac{\partial^2 G}{\partial y^2} + \frac{\partial^2 G}{\partial z^2}\right) + \frac{\partial G}{\partial t} = \delta(x-x_o)\,\delta(y-y_o)\,\delta(z-z_o)\,\delta(t) \qquad \text{(I.4b)}$$

Equations (I.4) are familiar from the theory of heat conduction. Ozisik (ref. 43) has developed Green function solutions to equation (I.4) under a number of different boundary conditions, using Fourier integral transform techniques. We may define the Fourier transforms needed to solve equation (I.4) as follows. For a medium infinite in x and y and infinite, semi-infinite or finite in z, the transform is defined as

$$\bar{p}(\beta,\nu,\eta,t) = \int_{-\infty}^{\infty}\int_{-\infty}^{\infty}\int_{-\infty}^{\infty} e^{i(\beta x + \nu y)}\, K(\eta,z)\, p(x,y,z,t)\, dxdydz \qquad \text{(I.5)}$$

along with the inverse transform for a semi-infinite or infinite medium

$$p(x,y,z,t) = \int_{-\infty}^{\infty}\int_{-\infty}^{\infty}\int_{-\alpha}^{\infty} e^{-i(\beta x + \nu y)}\, K(\eta,z)\, \bar{p}(\beta,\nu,\eta,t)\, d\beta d\nu d\eta \qquad \text{(I.6a)}$$

where $\alpha = \begin{cases} 0 & \text{semi-infinite} \quad 0 \le z \le \infty \\ -\infty & \text{infinite} \quad -\infty \le z \le \infty \end{cases}$

and for a finite medium $0 < z < W$

$$p(x,y,z,t) = \int_{-\infty}^{\infty}\int_{-\infty}^{\infty}\sum_{M=1}^{\infty} \frac{e^{-i(\beta x + \nu y)}}{(2\pi)^2}\, K(\eta_m,z)\, p(\beta,\nu,\eta_m,t)\, d\beta d\nu \qquad \text{(I.6b)}$$

The function $K(\eta_m,z)$ is called the transform kernel and the η_m's are the eigenvalues. The type of kernels and the equations for the eigen-

values depend on the combinations of boundary conditions at $z = 0$ and $z = W$, and are tabulated on page 50-52 and 481-483 in Ozisik.

Solution

We first remove the time dependence in (I.4b) by applying the Laplace transform to both sides of the equation, giving

$$-D_p \frac{\partial^2 \overline{G}}{\partial x^2} + \frac{\partial^2 \overline{G}}{\partial y^2} + \frac{\partial^2 \overline{G}}{\partial z^2} - s\,\overline{G} = \delta(x-x_o)\,\delta(y-y_o)\,\delta(z-z_o) \qquad (I.7)$$

where

$$\overline{G} = L[G] \quad \text{and} \quad L[\delta(t)] = 1$$

Applying the transform defined in equation (I.5) to both sides of equation (I.7) we get

$$-D_p\,(\beta^2 + \nu^2 + \eta^2)\,\bar{\bar{G}} - s\,\bar{\bar{G}} = e^{i(\beta x_o + \nu y_o)}\,K(\eta, z_o)$$

a simple algebraic equation whose solution is

$$\bar{\bar{G}} = \frac{-e^{i(\beta x_o + \nu y_o)}\,K(\eta, z_o)}{D_p(\beta^2 + \nu^2 + \eta^2) + s} \qquad (I.8)$$

Applying the inverse Laplace transform to equation (I.8) yields

$$\bar{\bar{G}} = e^{i(\beta x_o + \nu y_o)}\; e^{D_p(\beta^2 + \nu^2 + \eta^2)t}\,K(\eta, z_o) \qquad (I.9)$$

since

$$L^{-1}\,\frac{k}{s + a} = e^{-at}$$

Finally, applying the remaining inverse transform (I.6a) to (I.9) and using the integral formula

$$\frac{1}{2\pi}\int_{-\infty}^{\infty} e^{-\alpha\beta^2 t - i\beta(x-x')}\, d\beta = \frac{1}{(4\pi\alpha t)^{1/2}}\, e^{-\frac{(x-x')^2}{4\alpha t}}$$

we obtain for a semi-infinite medium

$$G = \frac{1}{4\pi D_p t}\exp - \frac{(x-x_o)^2 + (y-y_o)^2}{4D_p t}\int_o^{\infty} e^{-D_p\eta^2 t}\, K(\eta,z)\, K(\eta,z_o)d\eta \quad (I.10)$$

and $G_p = G\exp(-t/\tau_p)$.

APPENDIX II

VAVILOV SOLUTION TO LANDAU TRANSPORT EQUATION

Details on Vavilov's treatment of energy loss fluctuations can be found in the literature (ref. 32). His solution to the transport equation is as follows:

$$f(\Delta,s)\, d\Delta = \frac{1}{\xi}\, \phi_v(\lambda_v,\kappa,\beta^2)d\lambda_v,$$

$$\phi_v(\lambda_v,\kappa,\beta^2) = \frac{\kappa}{\pi}\, e^{\kappa(1 + \beta^2\gamma)} \int_0^\infty e^{\kappa f_1} \cos(y\lambda_v + \kappa f_2)dy$$

$$\lambda_v = \frac{\Delta - \overline{\Delta}}{\epsilon_{max}} - \kappa(1 + \beta^2 - \gamma)$$

$$\gamma = 0.577216 \text{ --- (Euler's constant)}$$

$$f_1(y) = \beta^2[\log y + Ci(y)] - \cos y - y\, Si(y)$$

$$f_2(y) = y[\log y + Ci(y)] - \cos y - y\, Si(y)$$

$$Si(y) = \int_0^y \frac{\sin u}{u}\, du \text{ (sine integral)}$$

$$Ci(y) = \int_{-\infty}^y \frac{\cos u}{u}\, du \text{ (cosine integral).}$$

Tabulations of the Vavilov distribution have been performed by Seltzer and Berger (ref. 36) for protons and mesons, and the computer code used in their numerical integration was graciously supplied to us by Steve Seltzer. Modifications of this code were necessary in order to calculate the integral of $f(\Delta,s)$, which is performed in the program VAVINT. The original code may be found in NBS Report 9498 (ref. 37).

APPENDIX III

COMPUTER PROGRAMS

These are the FORTRAN codes used in the simulations presented in this paper. DIODE generates the charge collection efficiency matrix $C_n(x_o, y_o, Z_n)$ given the circuit geometry and substrate diffusion length. The integration indicated in (16) uses IMSL routine DCADRE, which performs numerical integration of a function using cautious adaptive Romberg extrapolation. The integrand in (16) is contained in the function routine XYZTL. The C_n matrix is written onto a disk file for use by the simulation routine PULHGT.

Simulations are carried out by transporting a proton through the wafer, layer by layer, and computing the charge generated in each layer. Charge reaching the diode is determined by multiplying this dE/dx vector by the charge collection matrix C_n as in (18). Proton entry point (x_o, y_o) is generated using random numbers, and the energy loss in each layer is determined by sampling the appropriate probability density function $f(\Delta,s)$. The latter is accomplished in the following way. First the density function is converted into a integral distribution function $P(\Delta,s)$ given by

$$P(\Delta,s) = 1 - \int_{-\infty}^{\Delta} f(\Delta',s)d\Delta \qquad \text{(III.1)}$$

If $f(\Delta,s)$ was properly normalized, $P(\Delta,s)$ will be uniformly distributed on the interval (0, 1), and be a proper distribution from which to sample $f(\Delta,s)$. Actually, this can be accomplished analytically only if (III.1) can be solved for Δ in terms of $P(\Delta,s)$. Since this is generally not possible, numerous interpolation schemes are employed to sample from tabulated values of $P(\Delta,s)$. These values are generated in program VAV, where both $f(\Delta,s)$ and $P(\Delta,s)$ are calculated for either Vavilov or Blunck-Leisegang theories.

The actual simulations are carried out in PULGHT, which contains sufficient documentation for understanding. These programs were written on a

DEC-10 using version 5 of FORTRAN 10, and version 8 of the International Mathematical Subroutine Library (IMSL). The graphics program PLTGEN was written from PLOT-10/ADVANCED GRAPHING II, Release 1.2, and from the LEVEL 1 version of the 4010A01 PLOT 10 TERMINAL CONTROL SYSTEM, Release 3.3, available from TEKTRONIX.

The interpolation subroutine INTERP was taken from Bevington (ref. 45).

```
C       PROGRAM DIODE
C
C       CALLING PROGRAM TO CREATE CHARGE COLLECTION EFFICIENCY
C       MATRIX, Cn(X0,Y0,Zn), USED IN PULSE-HEIGHT SIMULATIONS
C
        DIMENSION XYTOT(35,121,10),DIODE(3,4)
        COMMON /PARAM/X0,Y0,DL,THICK,A,B,BETA
        COMMON /LIMITS/XMIN,XMAX,YMIN,YMAX
        EXTERNAL XYZTL
        DOUBLE PRECISION FNAME
C
C       DIGICON DIODE DIMENSIONS (MICRONS)
C
        DATA ((DIODE(I,J),I=1,3),J=1,4)/-20,-20,-6.858,20,20,
     16.868,-75,125,75,75,175,125/
        CALL UERSET(0,LEVOLD)              ! SUPRESS IMSL ERROR PRINTOUT
        TYPE 100
100     FORMAT(1X/1X'ENTER DIFFUSION LENGTH, X INC, Y INC:'$)
        ACCEPT *, DL, IC, ID
        CALL CNFIG(XYTOT,DIODE,IC,ID,STEP)
        TYPE 300
300     FORMAT(1X/1X'ENTER OUTPUT FILE NAME:'$)
        ACCEPT 20, FNAME
20      FORMAT(A6)
        OPEN(UNIT=21,FILE=FNAME)
        WRITE(21,*) STEP
        WRITE(21,200)(((XYTOT(I,J,N),I=1,35),J=1,121),N=1,10)
200     FORMAT(35E10.4)
        CLOSE(UNIT=21,FILE=FNAME)
        CALL EXIT
        END
```

```
C
C       CREATES CHARGE COLLECTION EFFICIENCY MATRIX Cn(Xo,Yo,Zn)
C
        SUBROUTINE CNFIG1(XYTOT,DIODE,IC,ID,STEP)
        DIMENSION DIODE(3,4)
        DIMENSION XYTOT(35,121,10)
        COMMON /PARAM/X0,Y0,DL,THICK,A,B,BETA
        COMMON /LIMITS/XMIN,XMAX,YMIN,YMAX
        EXTERNAL XYZTL
        PI=3.141592654; AA=0.;U=40.
        CON=1./SQRT(16*PI)          ! SEMI-INFINITE NORMALIZATION
        A=0.;B=20.
        THICK=B-A                   ! SEGMENT THICKNESS
        X0=0.0;Y0=-12.
        STEP=3.                     ! RESOLUTION (MICRONS)
        DO 1 J=1,121,ID             ! INCREMENT Y0
        DO 2 I=1,35,IC              ! INCREMENT X0
        DO 3 N=1,10                 ! INCREMENT ZC
        DO 4 M=1,3                  ! DIGICON DIODE HAS THREE PARTS
        XMIN=DIODE(M,1)
        XMAX=DIODE(M,2)
        YMIN=DIODE(M,3)
        YMAX=DIODE(M,4)
C
C       NUMERICAL INTEGRATION OVER TIME FROM AA -> U USING DCADRE,
        IMSL ROMBERG INTEGRATION ROUTINE
C
        XYTOT(I,J,N)=XYTOT(I,J,N) + DCADRE(XYZTL,AA,U,1.0E-3,0.,E,NN)
4       CONTINUE
        A=A + THICK;B=B + THICK
        XYTOT(I,J,N)=XYTOT(I,J,N)*CON/THICK
3       CONTINUE
        A=0.0;B=THICK
        X0=X0+STEP*IC
2       CONTINUE
        X0=0.0
        Y0=Y0+STEP*ID
1       CONTINUE
        RETURN
        END
```

```
C
      FUNCTION XYZTL(P)
C
C     SEMI-INFINITE CHARGE COLLECTION EFFICIENCY
C     INTEGRAND FOR NUMERICAL INTEGRATION OVER TIME
C     ERF(X) IS AN IMSL CALLABLE FUNCTION
C
      COMMON /PARAM/X0,Y0,DL,THICK,A,B,BETA
      COMMON /LIMITS/XMIN,XMAX,YMIN,YMAX
      ARG1=(XMAX-X0)/R
      ARG2=(XMIN-X0)/R
      ARG3=(YMAX-Y0)/R
      ARG4=(YMIN-Y0)/R
      ERF1=ERF(ARG1)
      ERF2=ERF(ARG2)
      ERF3=ERF(ARG3)
      ERF4=ERF(ARG4)
      X=ERF1-ERF2
      Y=ERF3-ERF4
      Z=EXP(-(A/R)**2) - EXP(-(B/R)**2)
      T=EXP(-(R/(2*DL))**2)
      XYZTL=X*Y*Z*T
      RETURN
      END
```

```
C
C       PROGRAM PULHGT
C
C       PERFORMS SIMULATIONS OF PULSE-HEIGHT DATA
C
        DIMENSION CN(35,121,10),C(6),COUNT(1500)
        DIMENSION X(1500),DUAL(1,5,5)
        DIMENSION C40(4),C240(4),C85(4),XC(4),XTC(6),CT40(6)
        DIMENSION XC1(2),C840(2)
        DIMENSION XLABL1(59),XLABL2(59),XLAB 3(59),YLABL1(59)
        DIMENSION YLABL2(59)
        COMMON/THIN/GP03(70),GP0325(70),GP035(70)
        COMMON/THICK/GP17(40),GP19(40),GP21(40),GP23(40),GP25(40)
        COMMON/SIMPLE/GTHIN(100),GTHICK(100),NUM1,NUM2
        COMMON/YVALUE/YL1(100),YL2(100)
        COMMON /THINGS/ENRG,DSEED,KMAX,NHOL,LLDA,LLDB,NRSUM1,NSUM
     1,XA,YA,T1,T2,LA,LB,NID,LLD1,LLD2,LLD3,LLD4,T,NSUM3,NWD,STEP
     2,NWD1,NWD2,NSTAT
        COMMON /PLOT/NPTS,XMIN,XMAX,YMIN,YMAX,X1,X2,X3,X4,NP,NG,LT,
     1ISTP,ISYM,ITX,ITY,IG
        DOUBLE PRECISION FINAME,DSEED
        REAL NCPTS
C
C       COINCIDENCE DATA FROM DIGICON TEST RUN
C
        DATA C40/0.28,0.23,0.13,0.03/
        DATA C240/0.73,0.61,0.34,0.22/
        DATA C85/0.20,0.077,-1.,.014/
        DATA C840/0.36,0.29/
        DATA XC1/1.,2./
        DATA XC/1.,2.,3.,6./
        DATA XTC/1.,2.,3.,4.,5.,6./
C
C       LABELS FOR TEKTRONIX PLOTTING
C
        DATA XLABL1/'N','u','m','b','e','r',' ','o','f',' ','C','h',
     a'a','r','g','e',' ','C','a','r','r','i','e','r','s',' ','(','h',
     b'o','l',
     i'e','s',')',' ','C','o','l','l','e','c','t','e','d',16*' '/
        DATA YLABL1/'C','o','u','n','t','s',53*' '/
        DATA XLABL2/'C','h','a','r','g','e',' ','C','o','l','l',
     1'e','c','t','e','d',43*' '/
        DATA XLABL3/'D','i','o','d','e',' ','N','u','m','b','e',
     1'r',47*' '/
        DATA YLABL2/'C','o','i','n','c','i','d','e','n','c','e',
     1' ','F','r','a','c','t','i','o','n',39*' '/
C
C       READ IN VAVILOV INTEGRAL PROBABILITY DISTRIBUTIONS
C
        CALL READIN
        WRITE(5,*) (YL1(I),GTHIN(I),I=1,NUM1)
        TYPE  40
        ACCEPT 41,FINAME
        OPEN(UNIT=23,FILE=FINAME)
C
C       READ IN CHARGE  COLLECTION EFFICIENCY MATRIX  Cn
C
        READ (23,*) STEP
        READ (23,100,END=70) (((CN(I,J,K),I=1,35),J=1,121),K=1,10)
70      CLOSE(UNIT=23,FILE=FINAME)
```

```
 100     FORMAT (35E10.4)
  40     FORMAT(' INPUT FILE NAME? ')
  41     FORMAT(A10)
         LAYER=K-1
         TYPE 97
97       FORMAT(1X/1X'ENTER SPECTRUM RESOLUTION (E-H PAIRS):'$)
         ACCEPT *, NHOL
71       TYPE 501
501      FORMAT(1X/1X'ENTER PROTON ENERGY < WINDOW (MEV): '$)
         ACCEPT *, ENERGY
         TYPE 93
93       FORMAT(1X/1X'REJECT PROTONS NOT ENTERING AREA DEFINED
     1 BY -X,X,-Y,Y:'$)
         ACCEPT *, XAMIN,XAMAX,YAMIN,YAMAX
         TYPE 43
43       FORMAT(1X/1X'FOR PRIMARY SPECTRUM ENTER LLD,ULD:'$)
C
C        LLD: LOWER LEVEL DISCRIMINATOR, ULD: UPPER LEVEL DISCRIM.
C
         ACCEPT *, LLDA,LLDB
         TYPE 44
44       FORMAT(1X/1X'FOR PROTON ENTRY POINT MAP ENTER LLD,ULD:'$)
         ACCEPT *, LLD1,LLD2
         TYPE 46
46       FORMAT(1X/1X'FOR COINCIDENCE DETECTION ENTER DIODE NO.
     1,LLD,ULD:'$)
         ACCEPT *, NWD,NWD1,NWD2
         TYPE 92
92       FORMAT(1X/1X'STOP SIMULATION WHEN TOTAL COUNTS
     1 BETWEEN X1 AND X2  EXCEED Y:'$)
         ACCEPT *, LLD3,LLD4,NIT
         TYPE 69, LAYER
69       FORMAT(1X/1X'ENTER THICKNESS OF DEPLETION LAYER AND EACH OF
     1 'I2' LAYERS:'$)
         ACCEPT *, T1,T2
         TYPE 89
89       FORMAT(1X/1X'ENTER WHICH LAYER AND HOW MANY DIODES:'$)
         ACCEPT *, LB,NID
         LA=LB
         IF(LB.EQ.0) LA=1
         IF(LB.EQ.6) LB=LAYER
         TYPE 888
888      FORMAT(1X/1X' NAME FOR PROTON ENTRY MAP FILE:'$)
         ACCEPT 41, FINAME
         OPEN(UNIT=21,FILE=FINAME)
         WRITE(21,*) LLD1,LLD2,NIT
         TYPE 910
910      FORMAT(1X/1X'STRAGGLING ?:'$)
         ACCEPT *, NSTAT
         TYPE 887
887      FORMAT(1X/1X'TYPE 1 FOR DEBUG')
         ACCEPT *, T
C
C        INITIALIZE  PARAMETERS FOR WINDOW MATERIAL AND
C        DETERMINE ENERGY LOSS OF PROTON PASSING THROUGH DIGICON WINDOW
C
         ZA=.454;ZI=.09088;DENSE=2.601    ! LITHIUM FLOURIDE
         BETA=BTA(ENERGY)
         CALL IONIZ(BETA,3000.,ZA,ZI,DENSE,EWO,DWO,EMAX,DUM,DUM)
C
```

```
C       ZERO ACCUMULATOR ARRAYS
C
        DO 1 K=1,1500
        COUNT(K)=0
 1      CONTINUE
        DO 2 K=1,5
        DO 2 J=1,5
2       DUAL(1,K,J)=0.0
        DO 3 J=1,6
3       C(J)=0.0
C
C       BEGIN PROTON IRRADIATION SIMULATION
C
        DSEED=121212.D0                 ! ASSIGN SEED TO GGUBFS(DSEED)
        AMINX=XAMIN - XAMAX
        AMINY=YAMIN - YAMAX
        DO 33 NPROT=1,10000000          ! ITERATION LOOP
        XA=GGUBFS(DSEED)*AMINX + XAMAX  ! GENERATE RANDOM X
        YA=GGUBFS(DSEED)*AMINY + YAMAX  ! GENERATE RANDOM Y
C
C       DETERMINE ENERGY OF PROTON AFTER WINDOW BUT BEFORE DIODE ARRAY
C
        DELW=GAUSS(EW0,D*0,DSEED)
        ENRG=ENERGY-(DELW/1000.)! ENERGY AFTER WINDOW
C
C       INCREMENT PULSE HEIGHT SPECTRUM
C
        CALL PULHGT(XY,C,COUNT,DUAL)
        IF(NSUM3.EQ.NIT) GO TO 659      ! JUMP OUT OF ITERATION
33      CONTINUE
659     CLOSE(UNIT=21,FILE=FINAME)

C
C       SUMMARIZE PARAMETERS AND RESULTS
C
        A3=ENERGY-(EW0/1000)
        Z=14;A=28.085;ZA=Z/A;ZI=.170;DENSE=2.328        ! SILICON
        BETA=BTA(A3)
        CALL LANDAU(BETA,T1,ZA,ZI,DENSE,DE1,E1,DLAM,V,V,V)
        CALL LANDAU(BETA,T2,ZA,ZI,DENSE,DE2,E2,DLAM,V,V,V)
        WTHK=3.0;DWT=T1;BT=T2
        A1=ENERGY;A2=WTHK;A4=DW0/1000;A5=DWT;A6=E1
        A7=E1*1000/3.62;A8=DE1;A9=DE1*1000/3.62;A10=BT
        A11=E2;A12=E2*1000/3.62;A13=DE2;A14=DE2*1000/3.6
        A15=4.72E2*NPROT;A16=FLOAT(NSUM)/FLOAT(NRSUM1)
C
C       DEFINE OUTPUT ABOVE...TYPE OUT BELOW
C
        TYPE 999,A1,A2,A3,A4,A5,A6,A7,A8,A9,A10,A11,A12,A13,A14,A15,A16
999     FORMAT(1X/1X'INCIDENT PROTON ENERGY: 'F4.1' MEV'
     1/1X'AFTER 'F2' MM WINDOW: 'F5.1' MEV +/- 'F6.4' MEV'/
     2' AVERAGE ENERGY LOSS 'F1X/1X'IN 'F5.1' MICRON DEPLETION WIDTH: '
     3F6.2' KEV  'F5' E-H PAIRS'1X/30X'+/- 'F7.3' KEV  'F5'E-H PAIRS'1X
     4/' IN 'F5.1' MICRON BULK:'F7.2' KEV  'F7' E-H PAIRS'1X/17X'+/-
     5 'F7.3' KEV  'F6' E-H PAIRS'
     6/' TOTAL DOSE: 'E' P+/CM**2'1X/1X
     7'EFFECTIVE AREA/DIODE AREA: 'F5.2)
        TYPE 883, LLDA,NSUM,LLD3,NSUM3,NRSUM1,NPROT
883     FORMAT(1X/1X'TOTAL COUNTS ABOVE 'I5' WERE ' I7,1X/
     11X,'TOTAL COUNTS ABOVE 'I5' WERE 'I7,1X/1X,
```

```
     2"TOTAL PROTONS TO HIT DICDE WERE "I5,1X/1X
     3"NUMBER OF ITERATIONS WAS "I6)
        TYPE 884,XAMIN,XAMAX,YAMIN,YAMAX,NUMWIN
884     FORMAT(1X/1X"NUMBER OF PROTONS TO HIT WINDOW DEFINED BY "
     14F5" WAS "I6)
C
C       PLOT PULSE HEIGHT DISTRIBUTIONS BELOW
C
        X1=1.;X2=1.;X3=7.75;X4=5.75;NG="YES";NP="YES"
        LT=-4;ISTP=1
        ISYM=0;ITX=1;ITY=2;IG=2;NPTS=KMAX-1
        TYPE 10010
10010   FORMAT(1X/1X"GRAPH PULSE HEIGHT DISTRIBUTION ? 1=YES")
        ACCEPT *, GRAF
        IF(GRAF.EQ.0) GO TO 10011
        DO 8 I=1,KMAX
8      X(I)=FLOAT(NHOL*(I-1))
45      TYPE 50
50      FORMAT(1X/1X"ENTER XMIN,XMAX,YMIN,YMAX")
        ACCEPT *, XMIN,XMAX,YMIN,YMAX
        CALL PLTGEN(X,COUNT)
        CALL LABL(1.9,0.25,"H",XLABL1,0.,1.5,1.5,10,0)
        CALL LABL(0.2,3.,"V",YLABL1,0.,1.5,1.5,10,0)
        CALL TINPUT(JK)
        CALL ERASE
        TYPE 121
121      FORMAT(1X/1X"GRAPH AGAIN? 1=YES")
        ACCEPT *, GRAG
        IF(GRAG.EQ.1) GO TO 45
        IF(FLAG.EQ.1) GO TO 10011
C
C       OUTPUT PULSE HEIGHT SPECTRUM TO DSK FILE
C
        TYPE  40
        ACCEPT 41, FINAME
        OPEN(UNIT=21,FILE=FINAME)
        WRITE(21,*) (X(K),COUNT(K),K=1,NPTS)
        CLOSE(UNIT=21,FILE=FINAME)
C
C       PLOT INTEGRAL OF SPECTRUM
C
        TYPE 1122
1122    FORMAT(1X/1X"PLOT INTEGRAL OF SPECTRUM--TYPE 1:"$)
        ACCEPT *, INT
        IF(INT.NE.1) GO TO 10011
        FLAG=1;SUMM=0.0
        DO 1124 I=NPTS,1,-1
        SUMM=SUMM + COUNT(I)
        COUNT(I)=SUMM
1124    CONTINUE
        GO TO 45
C
C       PLOT DUAL PARAMETER; X VRS. Y VRS. COINCIDENCE INTENSITY
C
10011   TYPE 51
51      FORMAT(1X/1X" WISH TO PLOT DUAL PARAMETER?")
        ACCEPT *, GRAG
        IF(GRAG.EQ.0) GO TO 56
        ITY=1;X3=6.;X4=6.
913     TYPE 52
```

```
      ACCEPT *, NDIODE
      TYPE 50
      ACCEPT *, XMIN,XMAX,YMIN,YMAX
      DO 10 I=1,5
      COUNT(1)=(I-1)*1000
      DO 10 J=1,5
      M=0
      IF(DUAL(NDIODE,I,J).GT.1) M=ALOG10(DUAL(NDIODE,I,J)) + 0.5
      X(1)=(J-1)*1000
      ISYM=M;NPTS=1
      CALL PLTGEN(X,COUNT)
      NP="NO";NG="NO"
10    CONTINUE
      CALL LABL(2.6,0.25,"H",XLABL2,0.,1.5,1.5,10,0)
      CALL LABL(0.25,2.6,"V",XLABL2,0.,1.5,1.5,10,0)
      CALL TINPUT(KJ)
      CALL ERASE
      NP="YES";NG="YES"
      TYPE 121
      ACCEPT *, GRAG
      IF(GRAG.EQ.1) GO TO 913
C
C     PLOT COINCIDENCE INTENSITY VRS. X
C
56    DO 57 J=1,1000
      COUNT(J)=0.0
57    CONTINUE
      DO 58 J=1,5
      X(J)=(J-1)*1000
58    CONTINUE
      TYPE 52
52    FORMAT(1X/1X"CHOOSE DIODE 1 OR DIODE 2 :"$)
      ACCEPT *, NDIODE
      IF(NDIODE.EQ.0) GO TO 11111
      TYPE 53
53    FORMAT(1X/1X"CHOOSE CHANNEL NO. TO PLOT:"$)
      ACCEPT *, NCHAN
      TYPE 54
54    FORMAT(1X/1X"ENTER 1 TO NORMALIZE:"$)
      ACCEPT *, NNORM
      DO 55 I=1,5
      COUNT(I)=DUAL(NDIODE,NCHAN,I)
      IF(NNORM.EQ.1) COUNT(I)=DUAL(NDIODE,NCHAN,I)/COUNT(1)
55    CONTINUE
      NPTS=5;NP="YES";NG="YES";LT=0;ISTP=1;ISYM=0
      TYPE 50
      ACCEPT *, XMIN,XMAX,YMIN,YMAX
      X3=7.75;X4=5.75
      TYPE 59
59    FORMAT(1X/1X"LIN Y (1) OR LOG Y (2) ?:"$)
      ACCEPT *, ITY
      CALL PLTGEN(X,COUNT)
      CALL LABL(3.4,0.25,"H",XLABL2,0.,1.5,1.5,10,0)
      CALL LABL(0.25,3.,"V",YLABL1,0.,1.5,1.5,10,0)
      CALL TINPUT(M)
      CALL ERASE
      GO TO 56
C
C     PLOT COINCIDENCE FRACTIONS VERSUS DIODE POSITION
C
```

```
11111   LT=-4;ITY=1;X3=7.75;X4=5.75
        DO 151 II=1,NID-1
        C(II)=C(II)/NSUM
151     CONTINUE
        XMIN=1;XMAX=6;YMIN=0;YMAX=1.
2323    NPTS=4;ISYM=1;ISTP=1;NP="YES";NG="YES";
        TYPE 10101
10101   FORMAT(1X/1X"LIN Y (1) OR LOG Y (2):"$)
        ACCEPT *, ITY
        IF(ITY.EQ.2) YMIN=.01
        CALL PLTGEN(XC,C40)
        NG="NO";NP="NO";ISYM=2
        CALL PLTGEN(XC,C240);ISYM=3
        CALL PLTGEN(XC,C85);ISYM=4;NPTS=NID-1
        CALL PLTGEN(XTC,C);ISYM=5;NPTS=2
        CALL PLTGEN(XC1,C840)
        CALL LABL(3.6,0.25,"H",XLABL3,0.,1.5,1.5,10,0)
        CALL LABL(0.25,2.3,"V",YLABL2,0.,1.5,1.5,10,0)
        CALL TINPUT(JJ)
        CALL ERASE
        NP="YES";NG="YES"
        TYPE 121
        ACCEPT *, GRAG
        IF(GRAG.EQ.1) GO TO 2323
        CALL EXIT
        END
C
C
C
C
C
        SUBROUTINE PULHGT(XY,C,COUNT,DUAL)
C
C       THIS SUBROUTINE INCREMENTS THE PULSE-HEIGHT SPECTRUM AND
C       PERFORMS COINCIDENCE DATA SIMULATIONS
C
        DIMENSION CN(35,121,10),COUNT(1),C(1)
        DIMENSION DUAL(1,5,5),DEDX(10)
        COMMON /THINGS/ENRG,DSEED,KMAX,NHOL,LLDA,LLDB,NRSUM1,NSUM
     1,XA,YA,T1,T2,LA,LB,NID,LLD1,LLD2,LLD3,LLD4,T,NSUM3,NWD,STEP
     2,NWD1,NWD2,NSTAT
        DOUBLE PRECISION DSEED
C
C       FIND CHARGE DEPOSITED AT XA, YA , Z
C
        CALL CHARGE(DEPLT,DEDX,NSAV)
C
C       COMPUTE COINCIDENCE AND DUAL PARAMETER DATA
C
        NX=0
        DO 299 K=1,NID
        DEPLET=0.0;SUM=0.0
        XANX=XA - NX
        YANX=-YA
        IF((NX/50)/2*2.EQ.NX/50) YANX=YA
        NX=NX + 50
        II=INT(ABS(XANX/STEP) + 1.5)
        JJ=INT(YANX/STEP + 51.5)
        IF(II.GT.35.OR.JJ.GT.121.OR.JJ.LT.1) GO TO 299
        IF(K.EQ.NSAV) DEPLET=DEPLT
```

```
C
C       DETERMINE CONTRIBUTION OF CHARGE FROM EACH LAYER
C
        DO 23 LL=LA,LB
        SUM=SUM + DEDX(LL)*CN(II,JJ,LL)
23      CONTINUE
C
C       ADD DEPLETION ZONE CONTRIBUTION
C
        TEST=SUM + DEPLET
        IF(K.EQ.1) REF=TEST      ! SAVE VALUE OF DIODE 1
        IF(K.EQ.NWD) REF1=TEST   ! SAVE VALUE OF DIODE NWD
        IF(K.EQ.1) GO TO 299
C
C       INCREMENT COINCIDENCE AND DUAL PARAMETER COUNTERS
C
        IF(REF.GE.LLDA.AND.TEST.GE.LLDA) C(K-1)=C(K-1) + 1
        GO TO 299
        ID=REF/1000. + 1.5;JD=TEST/1000. + 1.5
        IF(ID.GE.5) ID=5
        IF(JD.GE.5) JD=5
        IF(K.EQ.2) DUAL(K-1,ID,JD)=DUAL(K-1,ID,JD) + 1.
299     CONTINUE
C
C       REJECT IF NWD COUNTS OUTSIDE THIS WINDOW
C
        IF(REF1.LT.NWD1.OR.REF1.GT.NWD2) RETURN
C
C       WRITE INFORMATION TO DISK FILE
C
        IF(REF.GE.LLD1.AND.REF.LE.LLD2) WRITE(21,*) REF,
     1XA,YA,DEPLET,DEDX(LA)
C
C       ACCUMULATE PULSE HEIGHT DISTRIBUTION
C
        IF(REF.GE.LLDA.AND.REF.LE.LLDB) NSUM=NSUM + 1
        IF(REF.GE.LLD3.AND.REF.LE.LLD4) NSUM3=NSUM3 + 1
        K=REF/NHOL + 1.5
        IF (K-KMAX) 4,4,2
 2      IF(K-1500)15,3,3
 15     KMAX=K
        GO TO 4
 3      K=1500
        KMAX=K
 4      COUNT(K)=COUNT(K) + 1
        RETURN
        END
C
C
C
        FUNCTION INSIDE(X,Y)
C
C       THIS FUNCTION DEPENDS ON SHAPE OF DIODE COLLECTION AREA
C       HERE WE ARE USING UDT/ELECTRON VISION DIGICON DIODE MASK
C
        INSIDE=0
        XAB=ABS(X);YAB=ABS(Y)
C
C       AM I INSIDE DICDE BOUNDARIES ?
C
```

```
      IF(XAB.LE.22.5.AND.YAB.LE.77.5) INSIDE=1
      IF(XAB.LE.9.35.AND.Y.GE.77.5.AND.Y.LE.122.5) INSIDE=1
      IF(XAB.LE.22.5.AND.Y.GE.122.5.AND.Y.LE.177.5) INSIDE=1
      RETURN
      END
C
CC
C
      SUBROUTINE CHARGE(DEPLT,DEDX,NSAV)
C
C     THIS SUBROUTINE DETERMINES Pn(Zn)--CHARGE DENSITY/SEGMENT
C
      DIMENSION DEDX(1)
      COMMON/THIN/GP03(70),GP0325(70),GP035(70)
      COMMON/THICK/GP17(40),GP19(40),GP21(40),GP23(40),GP25(40)
      COMMON/SIMPLE/GTHIN(100),GTHICK(100),NUM1,NUM2
      COMMON/YVALUE/YL1(100),YL2(100)
      COMMON /THINGS/ENRG,DSEED,KMAX,NHOL,LLDA,LLDB,NRSUM1,NSUM
     1,XA,YA,T1,T2,LA,LB,NID,LLD1,LLD2,LLD3,LLD4,T,NSUM3,NWD,STEP
     2,NWD1,NWD2,NSTAT
      DOUBLE PRECISION DSEED
C
CC    INITIALIZE VARIABLES
C
      NTERMS=2;NPTS=70;NSAV=0
C
CC    INITIALIZE  PARAMETERS FOR ABSORBING MEDIUM
C
      Z=14;A=28.085;ZA=Z/A;ZI=.170;DENSE=2.328          ! SILICON
C
CC    DID PROTON PASS THROUGH A DIODE?
C
      NX=0
      DO 5 K=1,NID
      XANX=XA - NX
      YANX=-YA
      IF((NX/50)/2*2.EQ.NX/50) YANX=YA
      NX=NX + 50
      I=INT(ABS(XANX/STEP) + 1.5)
      J=INT(YANX/STEP + 51.5)
      IF(I.GT.35.OR.J.GT.121.OR.J.LT.1) GO TO 5
      FLAG=INSIDE(XANX,YANX)
      IF(FLAG.EQ.1) GO TO 7
5     CONTINUE
CC
CC    IF NOT GO ON TO COMPUTE ENERGY LOSS IN BULK
C
      GO TO 337
C
CC    IF SO REMEMBER WHICH DIODE PROTON HIT
C
7     NSAV=K
      IF(K.EQ.1) NRSUM1=NRSUM1 + 1
C
CC    IF SO COMPUTE ENERGY LOSS IN DEPLETION ZONE
C
      IF(T1.EQ.0) GO TO 337
      NPTS=NUM1
      BETA=BTA(ENRG)
      CALL IONIZ(BETA,T1,ZA,ZI,DENSE,E,DE,K,G,DUM)
```

```
      IF(NSTAT.EQ.0) GO TO 335
      U1=GGUBFS(DSEED)
      CALL INTERP(GTHIN,YL1,NPTS,NTERMS,U1,THIN)
      FAC1=G*W
      FAC2=1 + BETA**2 - 0.577216 + ALOG(G)
      E=E + FAC1*(THIN + FAC2)
335   DEPLT=E*1000./3.62
      ENRG=ENRG - E/1000.
C
C     DETERMINE ENERGY LOSS IN EACH LAYER OF BULK
C
337   NPTS=NUM2
      DO 10 K=1,LB
      BETA=BTA(ENRG)
      CALL IONIZ(BETA,T2,ZA,ZI,DENSE,E,DE,W,G,DUM)
      IF(NSTAT.EQ.0) GO TO 338
      IF(G.GE.1) E=GAUSS(E,DE,DSEED)
      IF(G.GE.1) GO TO 338
      U1=GGUBFS(DSEED)
      CALL INTERP(GTHICK,YL2,NPTS,NTERMS,U1,THIN)
      FAC1=G*W
      FAC2=1 + BETA**2 - 0.577216 + ALOG(G)
      E=E + FAC1*(THIN + FAC2)
338   DEDX(K)=E*1000./3.62
      KT2=K*T2
      ENRG=ENRG - E/1000.
      IF(T.EQ.1) TYPE *, ENRG,XA,YA,KT2,DEPLT,DEDX(K),THIN,G
10    CONTINUE
      RETURN
      END
C
C
C
      FUNCTION GAUSS(E,DE,DSEED)
C
C     OUTPUT IS NORMALLY DISTRIBUTED AROUND E WITH SIGMA=DE
C
      DOUBLE PRECISION DSEED
      RAN1=GGUBFS(DSEED)
      RAN2=GGUBFS(DSEED)
      GAUSS=(SQRT(-2*ALOG(RAN1))*COS(2*3.14159*RAN2)*DE)+E
      RETURN
      END
```

```
C
      SUBROUTINE READN2
C
C     PROGRAM PULHGT USES THIS SUBROUTINE TO READ IN INTEGRAL
C     INTEGRAL ENERGY LOSS DISTRIBUTION FUNCTIONS FOR THE
C     DEPLETION LAYER, DEFINED IN GTHIN, AND EACH SEGMENT
C     OF THE SUBSTRATE TRACK, DEFINED IN GTHICK.  THESE FILES
C     ARE CREATED IN VAV.
C
      COMMON/SIMPLE/GTHIN(100),GTHICK(100),NUM1,NUM2
      COMMON/YVALUE/YL1(100),YL2(100)
      TYPE 10
10    FORMAT(1X/1X'SUBROUTINE READN2')
      OPEN(UNIT=21,FILE='GTHIN.DAT')
      READ(21,*) NUM1
      READ(21,*) (YL1(I),GTHIN(I),DUM,I=NUM1,1,-1)
      CLOSE(UNIT=21)
      TYPE 20 , NUM1
20    FORMAT(1X/1X'GTHIN READ IN ... NPTS = 'I3)
      OPEN(UNIT=21,FILE='GTHICK.DAT')
      READ(21,*) NUM2
      READ(21,*) (YL2(I),GTHICK(I),DUM,I=NUM2,1,-1)
      CLOSE(UNIT=21)
      TYPE 30, NUM2
30    FORMAT(1X/1X'GTHICK READ IN ... NPTS = 'I3)
      RETURN
      END
```

```
      SUBROUTINE IONIZ(BETA,THICK,ZA,ZI,DEN,DELBAR,SIG,EMAX,G,BL)
C
C     SUBROUTINE IONIZ
C
C     PURPOSE
C        CALCULATE IONIZATION LOSS FOR PROTONS USING BETHE-BLOCH
C        FORMULA WITHOUT DENSITY EFFECT OR SHELL CORRECTION
C
C     DESCRIPTION OF PARAMETERS
C       BETA           - VELOCITY OF PROTON/SPEED OF LIGHT
C       THICK          - THICKNESS IN MICRONS OF ABSORBER
C       ZA             - ATOMIC NUMBER/ATOMIC MASS OF ABSORBER
C       ZI             - MEAN IONIZATION POTENTIAL
C       DEN            - DENSITY OF ABSORBER
C       DELBAR         - MEAN ENERGY LOSS (DE/DX) KEV/MICRON
C       SIG            - STANDARD DEVIATION OF MEAN ENERGY LOSS
C       EMAX           - MAXIMUM ENERGY TRANSFER TO ELECTRON IN
C                        SINGLE COLLISION
C       G              - KAPPA FACTOR OF VAVILOV AND LANDAU
C       BL             - BLUNCK-LEISEGANG FACTOR
C
      ERM=511
      THK=1.0E-4*THICK*DEN
      BETA2=BETA**2
      EMAX=2*ERM*BETA2/(1-BETA2)
      G=0.30058*ERM*ZA*THK/(BETA2*EMAX)
      FAC=G*EMAX
      ARG=(EMAX/ZI)**2
      DELBAR=FAC*(ALOG(ARG) - 2*BETA2)
      SIG=EMAX*SQRT(G*(1 - BETA2/2.))
      BL=DELBAR*0.6748/FAC**2          ! SILICON
      RETURN
      END
```

```
      FUNCTION BTA(ENERGY)
C
C     INPUT IS KINETIC ENERGY OF PROTON
C     OUTPUT IS BETA=V/C
C
      PRM=938.213
      ROOT=(PRM/(PRM + ENERGY))**2
      BTA=SQRT(1-ROOT)
      RETURN
      END
```

```
C
C       PROGRAM VAV.FOR
C
C       GENERATES DIFFERENTIAL AND INTEGRAL ENERGY LOSS DISTRIBUTIONS
C       FOR BOTH VAVILOV AND BLUNCK-LEISEGANG THEORIES.  PLOTS ON
C       TEKTRONIX AND WRITES DISK FILE FOR USE IN PROGRAM PULHGT
C
        DIMENSION X(100),XV(100),XKEV(100),Y(100),YSUM(100)
        DIMENSION YB(100),YBSUM(100)
        DIMENSION LAB1(59),LAB2(59),LAB3(59),LAB4(6),LAB5(8)
        DIMENSION LAB0(59),LAB6(5)
        COMMON/STUFF/NCOMP,COMP,DY,NMAX,MAXB,MAXT,MAXY
        COMMON/RETKAP/BSQ,D,PV,PMIN
        COMMON/PLOT/N,XMN,XMX,YMN,YMX,X1,X2,X3,X4,NP,NG,
     1LT,ISTP,ISYM,ITX,ITY,IG
        DOUBLE PRECISION FINAME
C
C       PLOTTING LABELS
C
        DATA LAB0/'P','r','o','b','a','b','i','l','i','t','y',
     148*' '/
        DATA LAB3/'E','n','e','r','g','y',' ','L','o','s','s',
     1' ','(','k','e','v',')',42*' '/
        DATA LAB1/'L','a','m','b','d','a',' ','(','L','a','n','d',
     1'a','u',')',44*' '/
        DATA LAB2/'L','a','m','b','d','a',' ','(','V','a','v','i',
     1'l','o','v',')',43*' '/
        DATA LAB4/'K','a','p','p','a','='/
        DATA LAB5/'B','e','t','a','*','*','2','='/
        DATA LAB6/'B','*','*','2','='/
C
C       INITIALIZE PLOTTING PARAMETERS
C
        X1=1.;X2=1.;X3=7.75;X4=5.75;NP='YES';NG='YES';LT=0;ISTP=1;
     1ISYM=0;IG=2.;ITX=1;ITY=1
C
C       INITIALIZE PARAMENTERS FOR 3-POINT SIMPSON RULE INTEGRALS
C
        NCOMP=10
        COMP=1.00E-05
        NMAX=1001
        MAXY=0
        MAXB=0
C
C       PROVIDE INPUT OPTION
C
        TYPE 5
5       FORMAT(1X/1X'INPUT OPTION: ENERGY-THICKNESS (1) OR KAPPA-
     1BETA**2 (2):'$)
        ACCEPT *, OPTION
        IF(OPTION.EQ.1) GO TO 15
C
C       INPUT KAPPA AND BETA**2
C
        TYPE 25
25      FORMAT(1X/1X'ENTER KAPPA AND BETA**2:'$)
        ACCEPT *, D, BSQ
        GO TO 30
C
C       INPUT PROTON ENERGY AND SILICON WAFER THICKNESS
```

```
C
15      TYPE 10
10      FORMAT(1X/1X'ENTER PROTON KINETIC ENERGY (MEV):'$)
        ACCEPT *, ENERGY
        TYPE 20
20      FORMAT(1X/1X'ENTER SILICON THICKNESS (MICRONS):'$)
        ACCEPT *, THICK
C
C       DEFINE SOME MORE VARIABLES NEEDED IN INTEGRATION
C
        Z=14;A=28.085;ZA=Z/A;DENSE=2.328;ZI=.170          ! SILICON
        BETA=BTA(ENERGY)
        CALL IONIZ(BETA,THICK,ZA,ZI,DENSE,DELBAR,DUM,W,D,BL)
        BSQ=BETA**2
30      ERM=511
        W=2*ERM*BSQ/(1-BSQ)
        FAC1=D*W
        FAC2=1+BSQ-0.577216+ALOG(D)
        DY=0.02/D
        SUM=0.0
C
C       ESTABLISH LIMITS OF COMPUTATION
C
        TYPE 150
150     FORMAT(1X/1X'ENTER PMIN,PMAX:'$)
        ACCEPT *, PMIN,PMAX
        N=2*(PMAX - PMIN) + 1
C
C       WHAT TO COMPUTE
C
        TYPE 35
35      FORMAT(1X/1X'COMPUTE DIFF(1),INT(2) OR BOTH(3) ?:'$)
        ACCEPT *, LP
C
C       ACCUMULATE POINTS FOR GRAPH
C
        IF(LP.EQ.2) GO TO 105
C
C       DIFFERENTIAL SPECTRUM
C
        DO 100 I=1,N
        P=PMIN + (I-1)*0.5
        Y(I)=VAVDIF(P)
        YB(I)=BLDIF(P,BL)
        X(I)=P
        XV(I)=PV
        XKEV(I)=DELBAR + FAC1*(P+FAC2)
100     CONTINUE
        IF(LP.EQ.1) GO TO 250
C
C       INTEGRAL SPECTRUM
C
105     MAXY=0
        MAXB=0
        MAXT=0
        DO 110 I=1,N
        P=PMIN + (I-1)*0.5
        YSUM(I)=1. - VAVINT(P)
        YBSUM(I)=1. - BLINT(PMIN,P,BL)
        X(I)=P
```

```
      XV(I)=PV
      XKEV(I)=DELBAR + FAC1*(P+FAC2)
110   CONTINUE
250   TYPE 300
300   FORMAT(1X/1X"X VALUES: LANDAU (1), VAVILOV(2) OR KEV(3):"$)
      ACCEPT *, NVAL
      TYPE 350
350   FORMAT(1X/1X"ENTER XMIN,XMAX,YMIN,YMAX")
      ACCEPT *, XMN,XMX,YMN,YMX
      IF(NVAL.EQ.1) CALL PLTGEN(X,Y)
      NP="NO";NG="NO"
      IF(LP.EQ.2.OR.LP.EQ.3.AND.NVAL.EQ.1) CALL PLTGEN(X,YSUM)
C     IF(NVAL.EQ.1) CALL PLTGEN(X,YB)
      IF(LP.EQ.2.OR.LP.EQ.3.AND.NVAL.EQ.1) CALL PLTGEN(X,YBSUM)
      IF(NVAL.EQ.1) CALL LABL(3.,0.25,"H",LAB1,0.,1.5,1.5,10,0)
      NP="YES";NG="YES"
      IF(NVAL.EQ.2) CALL PLTGEN(XV,Y)
      NP="NO";NG="NO"
      IF(LP.EQ.2.OR.LP.EQ.3.AND.NVAL.EQ.2) CALL PLTGEN(XV,YSUM)
      IF(NVAL.EQ.2) CALL PLTGEN(XV,YB)
      IF(NVAL.EQ.2) CALL LABL(3.,0.25,"H",LAB2,0.,1.5,1.5,10,0)
      NP="YES";NG="YES"
      IF(NVAL.EQ.3) CALL PLTGEN(XKEV,Y)
      NP="NO";NG="NO"
      IF(LP.EQ.2.OR.LP.EQ.3.AND.NVAL.EQ.3) CALL PLTGEN(XKEV,YSUM)
      IF(NVAL.EQ.3) CALL PLTGEN(XKEV,YB)
      IF(LP.EQ.2.OR.LP.EQ.3.AND.NVAL.EQ.3) CALL PLTGEN(XKEV,YBSUM)
      IF(NVAL.EQ.3) CALL LABL(3.,0.25,"H",LAB3,0.,1.5,1.5,10,0)
      CALL LABL(0.25,2.75,"V",LAB0,0.,1.5,1.5,10,0)
      CALL LABL(1.,5.8,"H",LAB4,0,1.5,1.5,10,0)
C     CALL LABL(4.5,5.8,"H",LAB5,BSQ,1.5,1.5,10,0)
      CALL LABL(4.5,5.8,"H",LAB6,BL,1.5,1.5,10,0)
      NP="YES";NG="YES"
      CALL TINPUT(KK)
      TYPE 400
400   FORMAT(1X/1X"ENTER 1 TO GRAPH AGAIN:"$)
      ACCEPT *, GRAG
      IF(GRAG.EQ.1) GO TO 250
      TYPE 500
500   FORMAT(1X/1X"NAME OF OUTPUT FILE:"$)
      ACCEPT 41, FINAME
41    FORMAT(A10)
      OPEN(UNIT=21,FILE=FINAME)
      WRITE(21,*) N
      WRITE(21,*) (X(I),YBSUM(I),YB(I),I=1,N)
      CLOSE(UNIT=21,FILE=FINAME)
      STOP
      END
```

```
      FUNCTION VAVINT(P)
C
C     INPUT IS VAVILOV LAMBDA
C     OUTPUT IS EXPRESSION (III.1) IN APPENDIX III

      DIMENSION F1F(1010),F2F(1010),FAC1(1010),FAC2(1010),
     1 FAC3(1010),G(3),SI(1010),Y(1010)
      COMMON/STUFF/NCOMP,COMP,DY,NMAX,MAXB,MAXT,MAXY
      COMMON/BETKAP/BSQ,D,PV,PMIN
      Y(1)=0.0
      DL=ALOG(D)
      PV=D*(P + DL)
      PVMIN=D*(PMIN + DL)
      GORG=EXP(-D*(1.0 + 0.5772157*BSQ))
      C=DY/(3.0*3.141593*GORG)
      S=0.0
      NCOUNT=0
      G(1)=GORG*(PV - PVMIN)
      DO 260 L=2,NMAX
      IF (MAXY-L) 190,200,200
190   Y(L)=Y(L-1) + DY
      CALL TRIGEX(Y(L),SI(L),CI)
      FAC1(L)=ALOG(Y(L)) - CI
      FAC2(L)=COS(Y(L)) + Y(L)*SI(L)
      FAC3(L)=Y(L)*FAC1(L) + SIN(Y(L))
200   IF (MAXB-L) 210,220,220
210   F1F(L)=EXP(D*(BSQ*FAC1(L) - FAC2(L)))
      F2F(L)=D*(FAC3(L) + BSQ*SI(L))
220   ND=L - 2*(L/2) +2
      SIN1=SIN(Y(L)*PV + F2F(L))
      SIN2=SIN(Y(L)*PVMIN + F2F(L))
      G(ND)=F1F(L)*(SIN1 - SIN2)/Y(L)
      GO TO (260,260,230) ,ND
230   ADD=G(1) + 4.0*G(2) + G(3)
      G(1)=G(3)
      S=S + ADD
      IF (ABS(ADD/S)-COMP) 240,250,250
240   NCOUNT=NCOUNT + 1
      IF (NCOUNT-NCOMP) 260,270,270
250   NCOUNT=0
260   CONTINUE
      MAXT=NMAX
      GO TO 280
270   MAXT=L
280   IF (MAXT-MAXY) 300,300,290
290   MAXY=MAXT
300   IF (MAXT-MAXB) 320,320,310
310   MAXB=MAXT
320   SUM=C*S
      VAVINT=SUM
      RETURN
      END
```

```
C
      FUNCTION VAVDIF(P)
C
C     INPUT IS VAVILOV LAMBDA
C     OUTPUT IS EXPRESSION DEFINED IN APPENDIX II
C
      DIMENSION F1F(1010),F2F(1010),FAC1(1010),FAC2(1010),
     1 FAC3(1010),G(3),SI(1010),Y(1010)
      COMMON/STUFF/NCOMP,COMP,DY,NMAX,MAXB,MAXT,MAXY
      COMMON/BETKAP/BSQ,D,PV,PMIN
      Y(1)=0.0
      DL=ALOG(D)
      PV=D*(P + DL)
      GORG=EXP(-D*(1.0 + 0.5772157*BSQ))
      C=D*DY/(3.0*3.141593*GORG)
      S=0.0
      NCOUNT=0
      G(1)=GORG
      DO 260 L=2,NMAX
      IF (MAXY-L) 190,200,200
190   Y(L)=Y(L-1) + DY
      CALL TRIGEX(Y(L),SI(L),CI)
      FAC1(L)=ALOG(Y(L)) - CI
      FAC2(L)=COS(Y(L)) + Y(L)*SI(L)
      FAC3(L)=Y(L)*FAC1(L) + SIN(Y(L))
200   IF (MAXB-L) 210,220,220
210   F1F(L)=EXP(D*(BSQ*FAC1(L) - FAC2(L)))
      F2F(L)=D*(FAC3(L) + BSQ*SI(L))
220   ND=L - 2*(L/2) +2
      G(ND)=F1F(L)*COS(Y(L)*PV + F2F(L))
      GO TO (260,260,230) ,ND
230   ADD=G(1) + 4.0*G(2) + G(3)
      G(1)=G(3)
      S=S + ADD
      IF (ABS(ADD/S)-COMP) 240,250,250
240   NCOUNT=NCOUNT + 1
      IF (NCOUNT-NCOMP) 260,270,270
250   NCOUNT=0
260   CONTINUE
      MAXT=NMAX
      GO TO 280
270   MAXT=L
280   IF (MAXT-MAXY) 300,300,290
290   MAXY=MAXT
300   IF (MAXT-MAXB) 320,320,310
310   MAXP=MAXT
320   SUM=C*S
      VAVDIF=SUM
      RETURN
      END
C
C
C
      SUBROUTINE TRIGEX(X,SI,CI)
      X2=X*X
      IF (X2 -100.0) 10,40,40
10    SI=0.0
      CI=0.57721566 + 0.5*ALOG(X2)
      T=X
      A=1.0
```

```
      SI=SI + T
      A=A + 1.0
      T=-T*(X*(A-1.0)/(A**2))
      IF (ABS(T)-(1.0E-09)) 100,30,30
30    CI=CI + T
      A=A + 1.0
      T=T*(X*(A-1.0)/(A**2))
      IF (ABS(T)-(1.0E-09)) 100,20,20
40    AMAX=0.5*(X + 1.0)
      P=1.0
      Q=0.0
      S=1.0/X
      A=1.0
50    Q=Q + S
      A=A + 1.0
      IF (A-AMAX) 60,60,90
60    S=-S*(A/X)
      P=P+S
      IF (ABS(S)-(1.0E-12)) 90,70,70
70    A=A + 1.0
      IF (A-AMAX) 80,80,90
80    S=S*(A/X)
      GO TO 50
90    CX=COS(X)/X
      SX=SIN(X)/X
      SI=1.5707963 - P*CX - Q*SX
      CI=P*SX - Q*CX
100   RETURN
      END
```

```
      FUNCTION BLDIF(P,B2)
      DIMENSION C(9),RLMBDA(9),GAMMA(9)
      DATA C/.368,.1843,.0882,.0647,.0359,..164,.0064,.0021,.0006/
      DATA RLMBDA/-1.46,-.738,.17,1.33,2.95,5.39,9.4,16.8,30.6/
      DATA GAMMA/.737,.947,1.23,1.68,2.4,3.66,6.18,12.3,39.7/
      SUM=0.0
      DO 10 I=1,9
      FAC1=C(I)*GAMMA(I)
      FAC2=GAMMA(I)**2 + B2
      FAC3=P - RLMBDA(I)
      SUM=SUM + FAC1*EXP(-FAC3**2/FAC2)/SQRT(FAC2)
10    CONTINUE
      BLDIF=SUM
      RETURN
      END
```

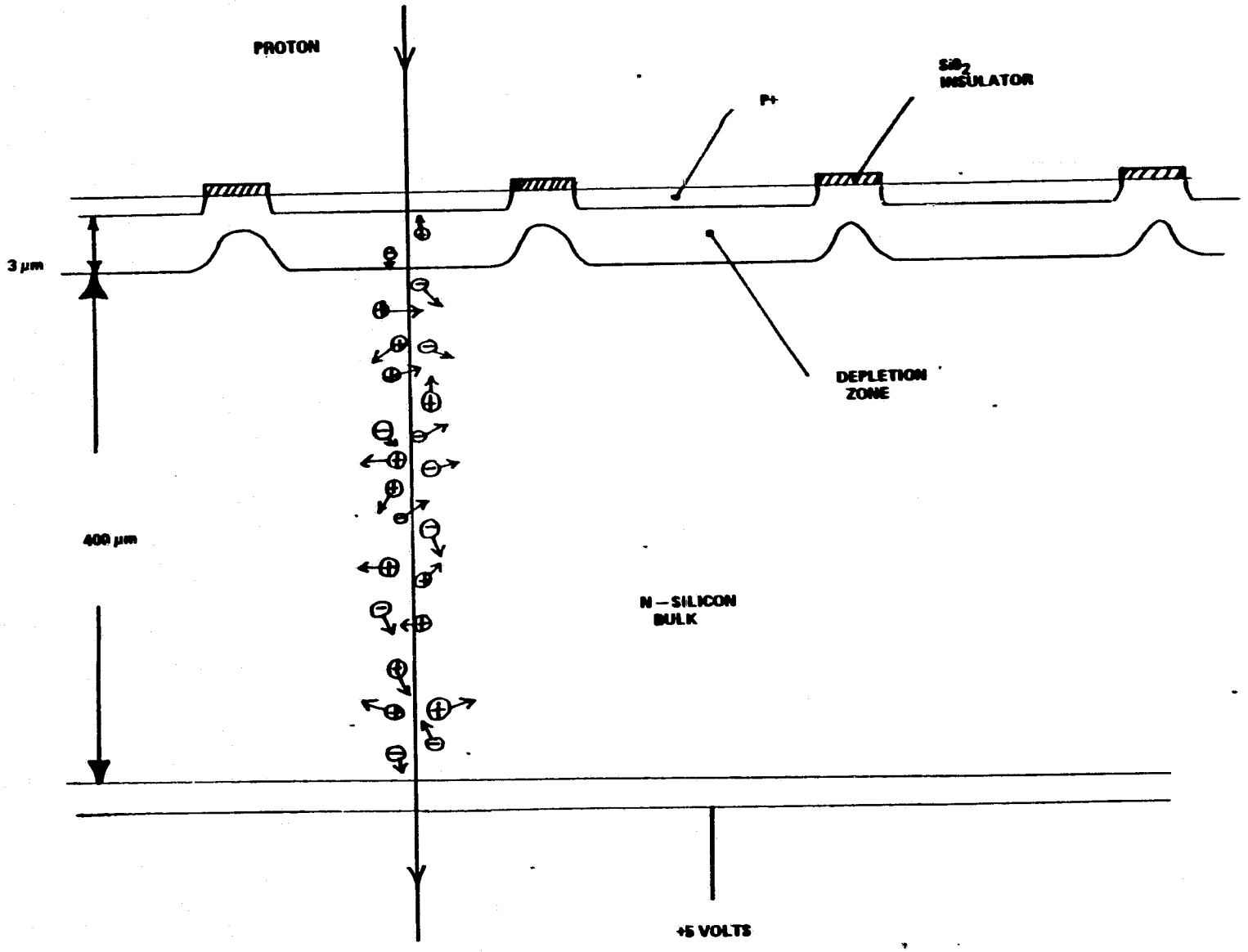

Figure 1. Cutaway view of diodes. P+ layer is about 0.7 μ. Vertical scale is exaggerated.

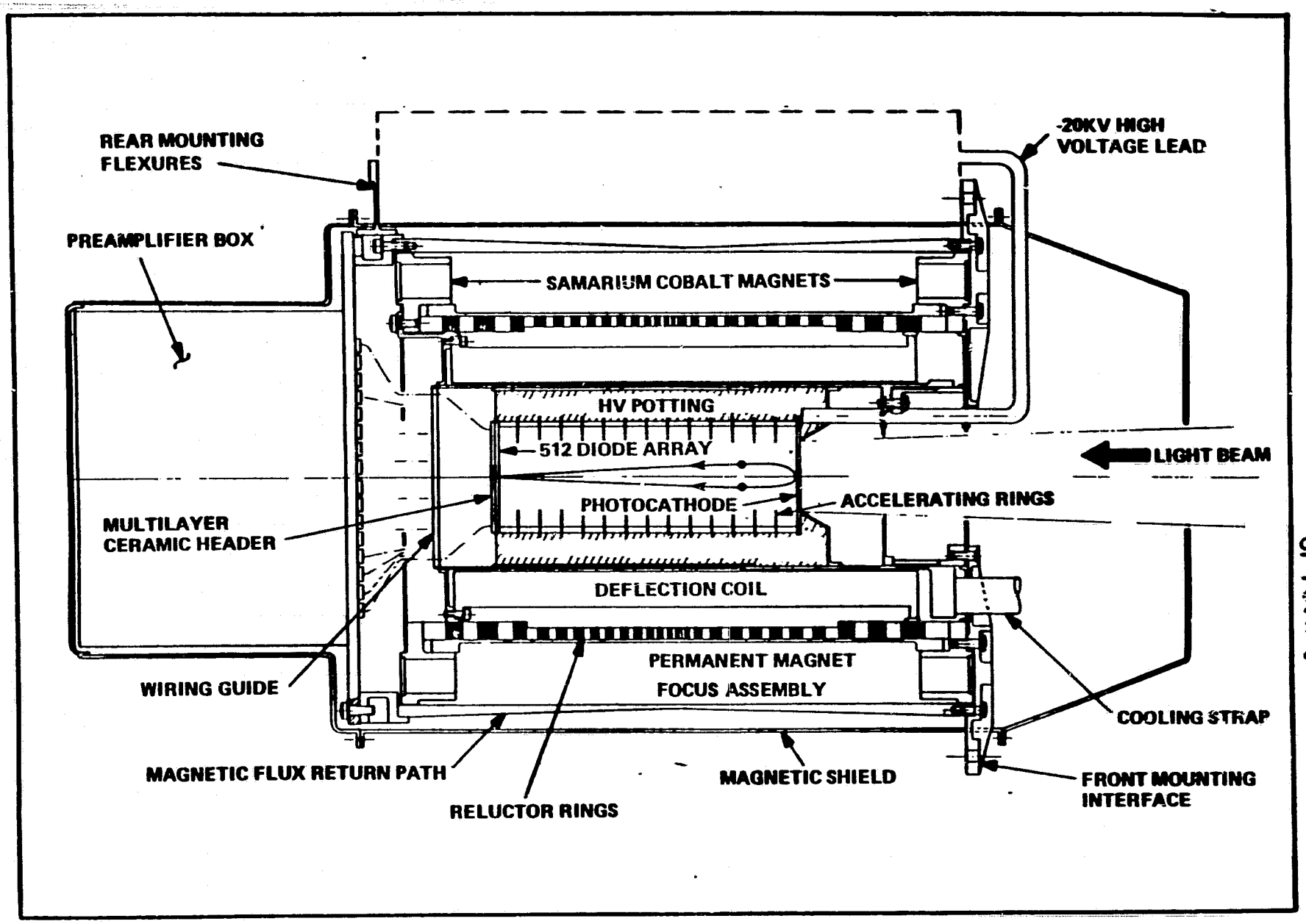

Figure 2. Cross-sectional view of HRS Digicon detector assembly.

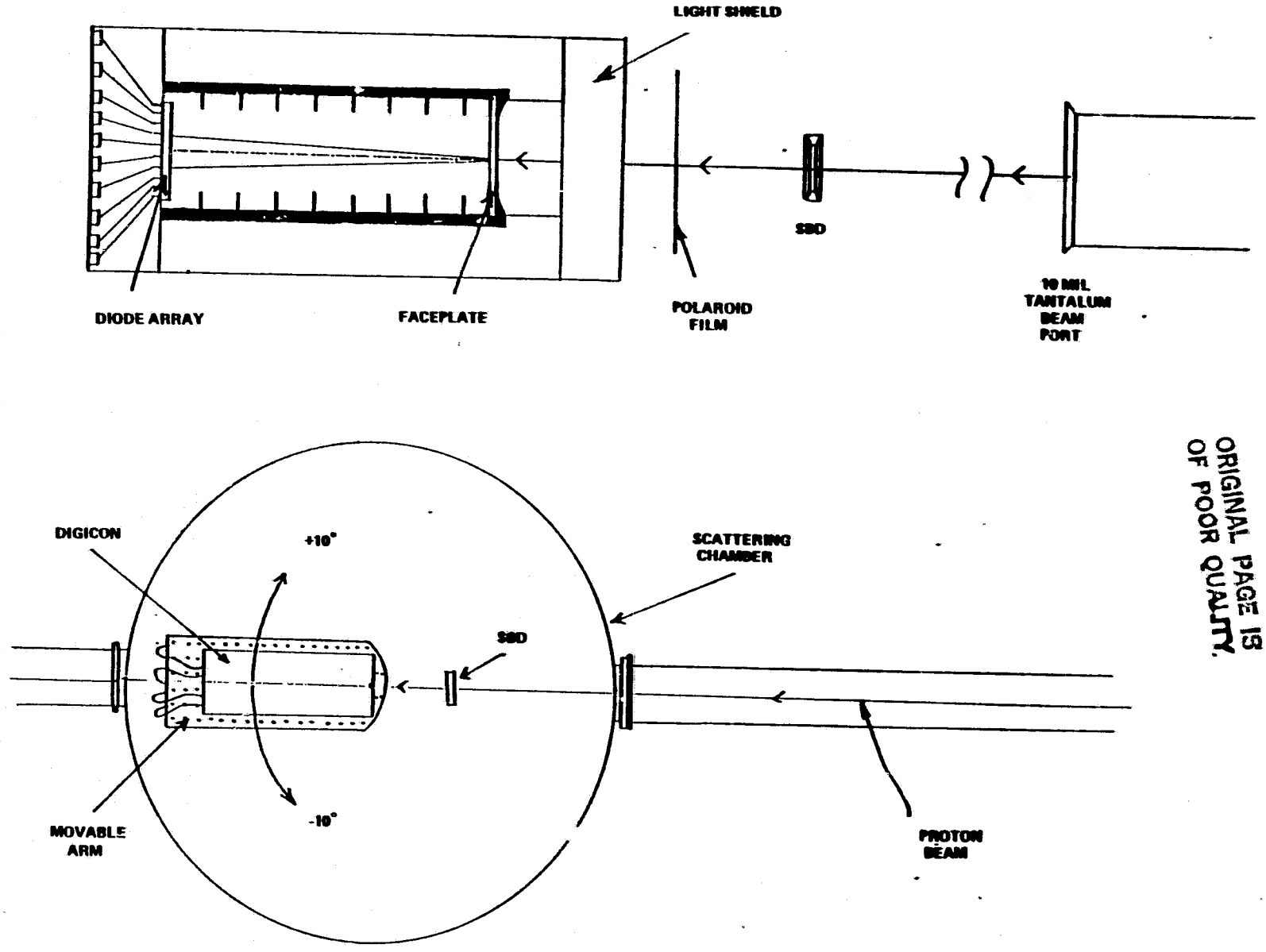

Figure 3. Test configuration used during proton irradiation of HRS Digicon. The tube could be rotated in 0.1° increments up to ±5°, thus allowing the diode array to be swung into or out of the proton beam.

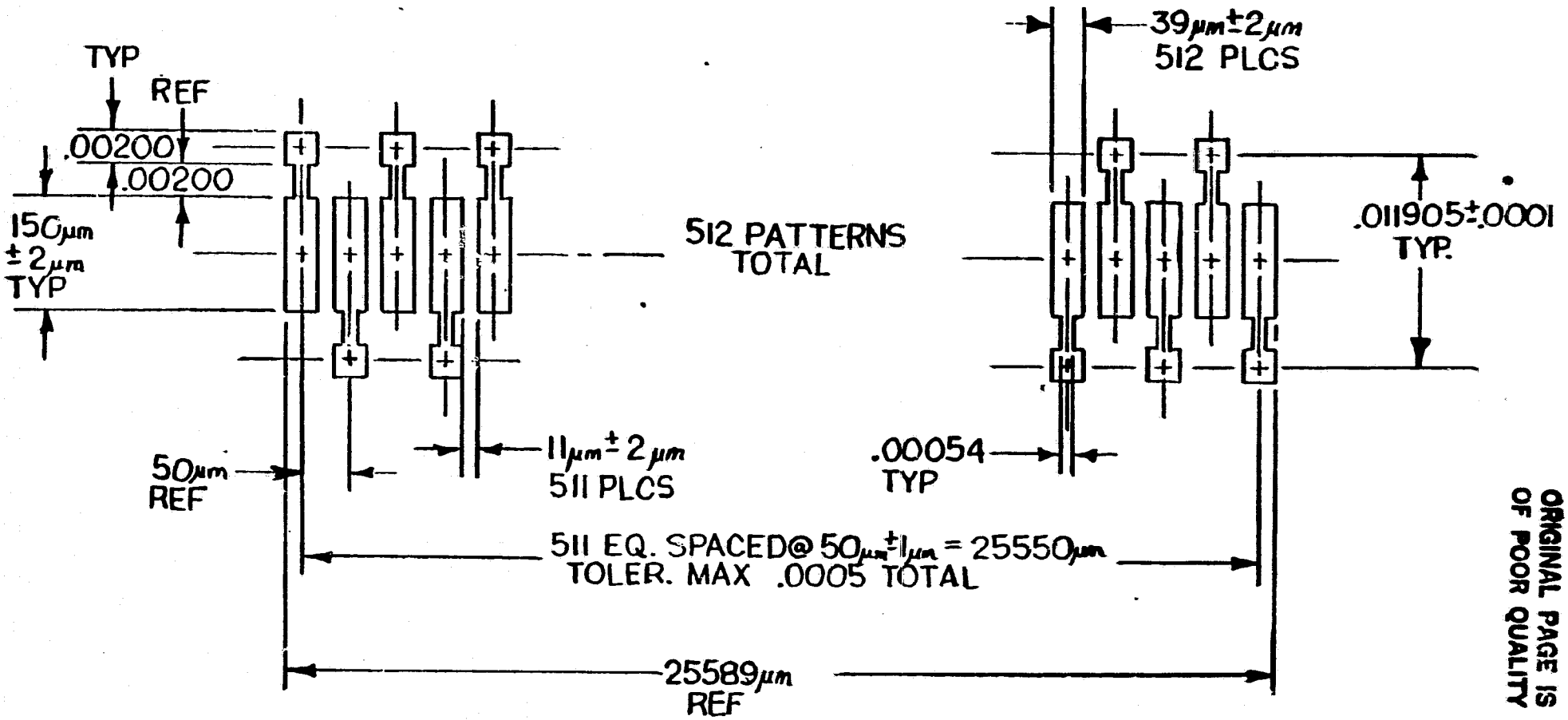

ORGINAL PAGE IS
OF POOR QUALITY

Figure 4. Geometrical arrangement of diodes on the array.

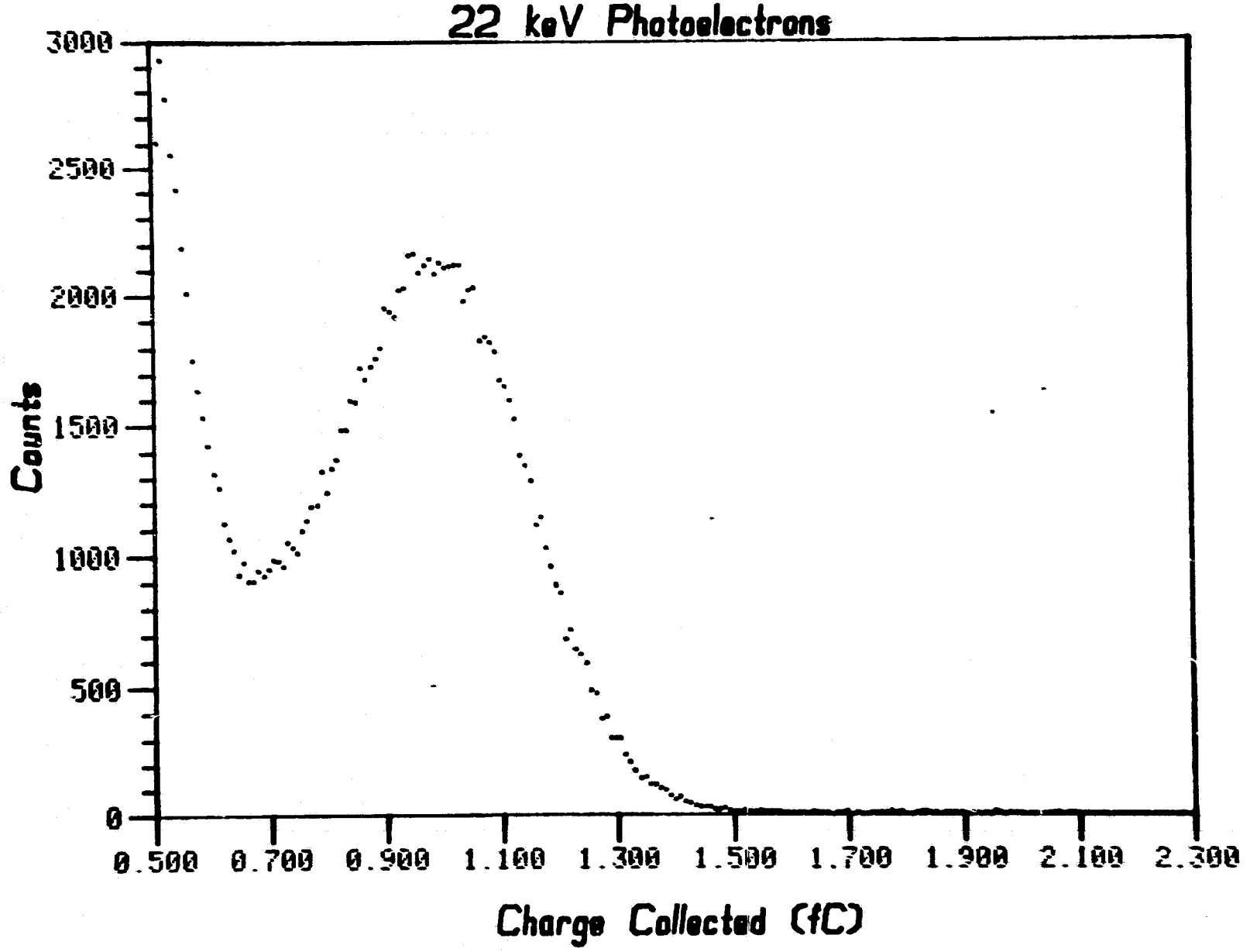

Figure 5. Pulse-height distribution of charge produced in Digicon Diode by 22 keV photoelectrons. Horizontal axis calibrated assuming one electron-hole pair/3.62 eV absorbed energy.

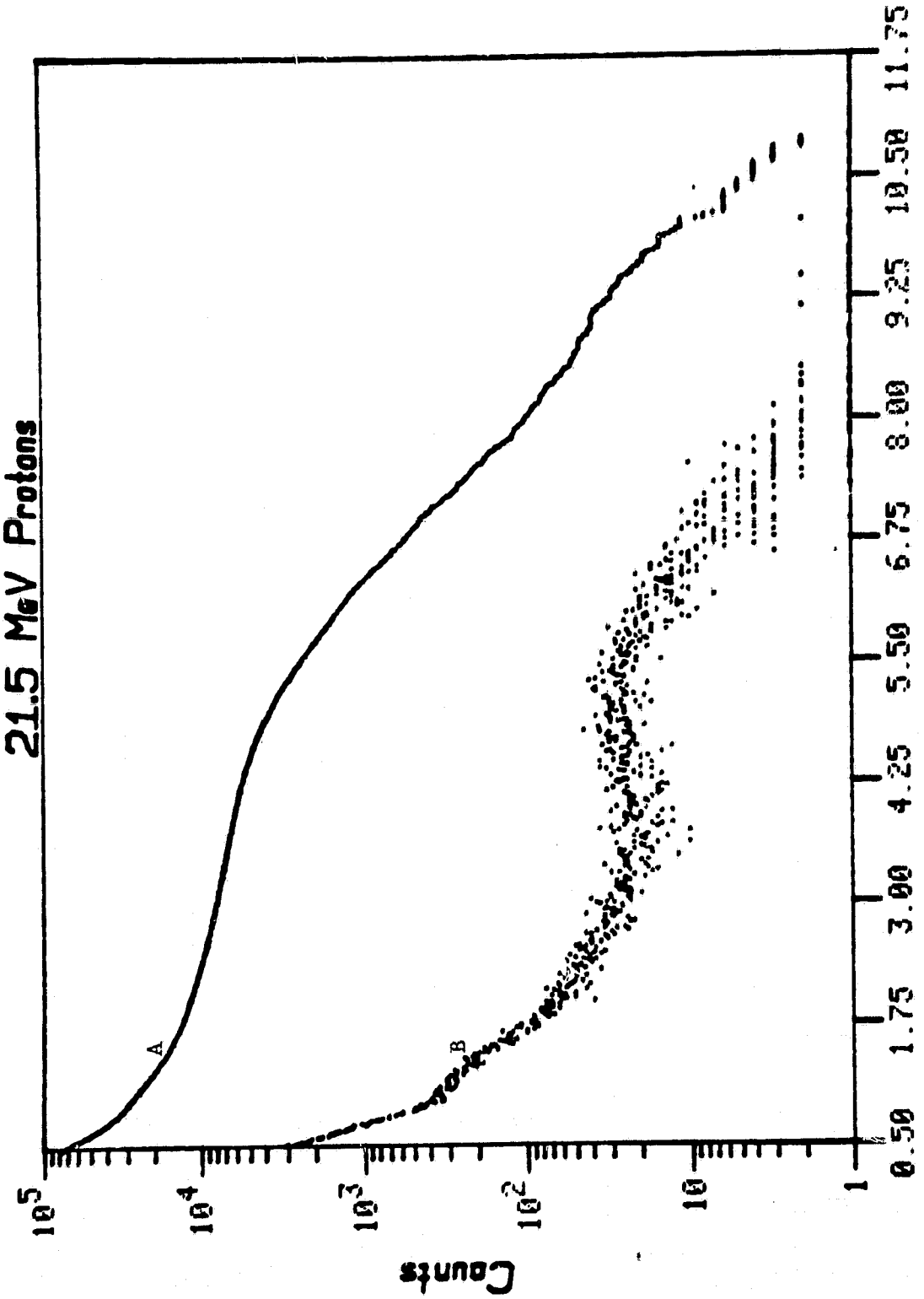

Figure 6. Integral (top curve) and differential pulse-height distributions of noise charge collected by Digicon Diode during irradiation with 21.5 MeV protons.

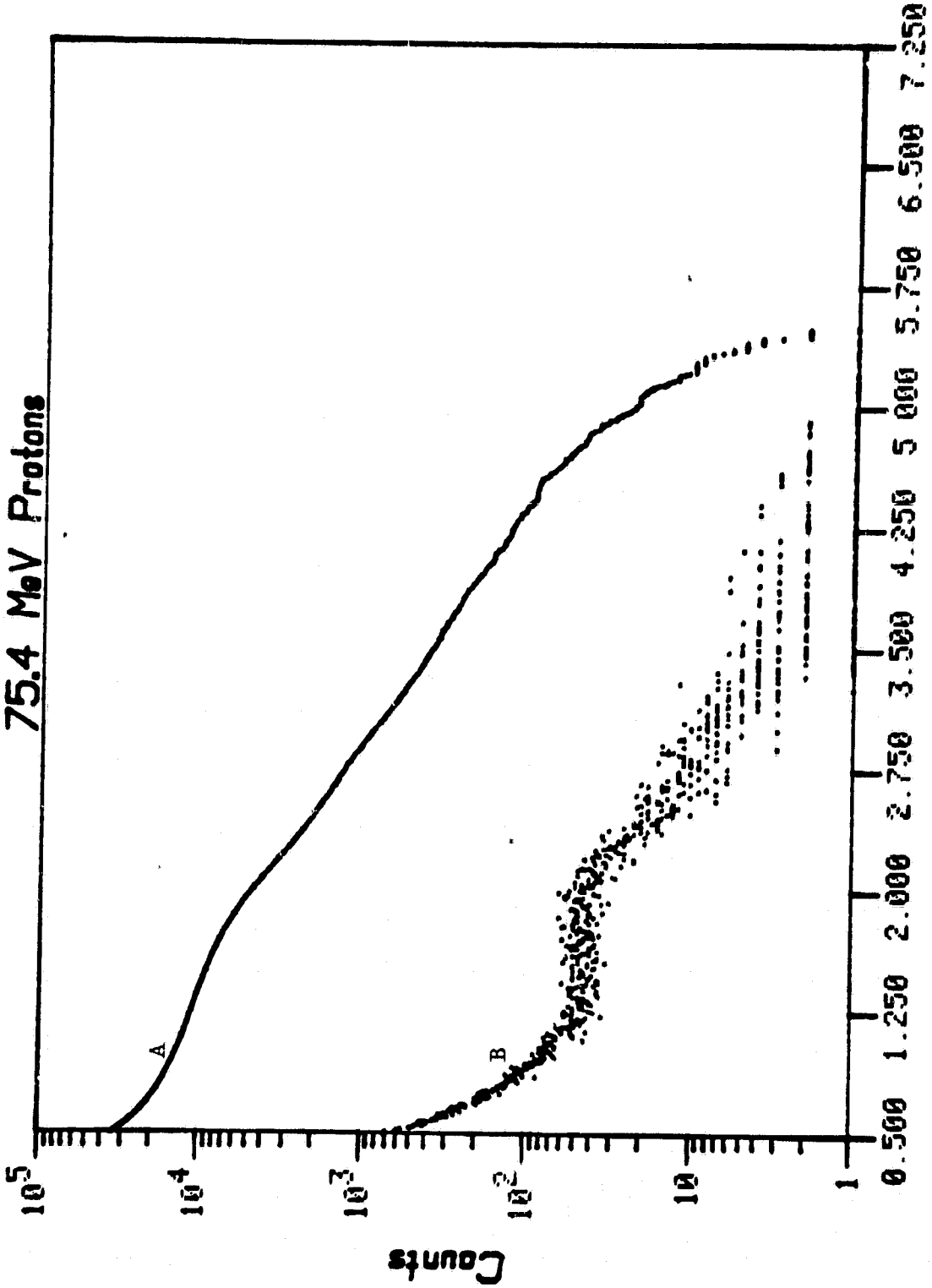

Figure 7. Integral (top curve) and differential pulse-height distributions of noise charge collected by Digicon Diode during irradiation with 75.4 MeV protons.

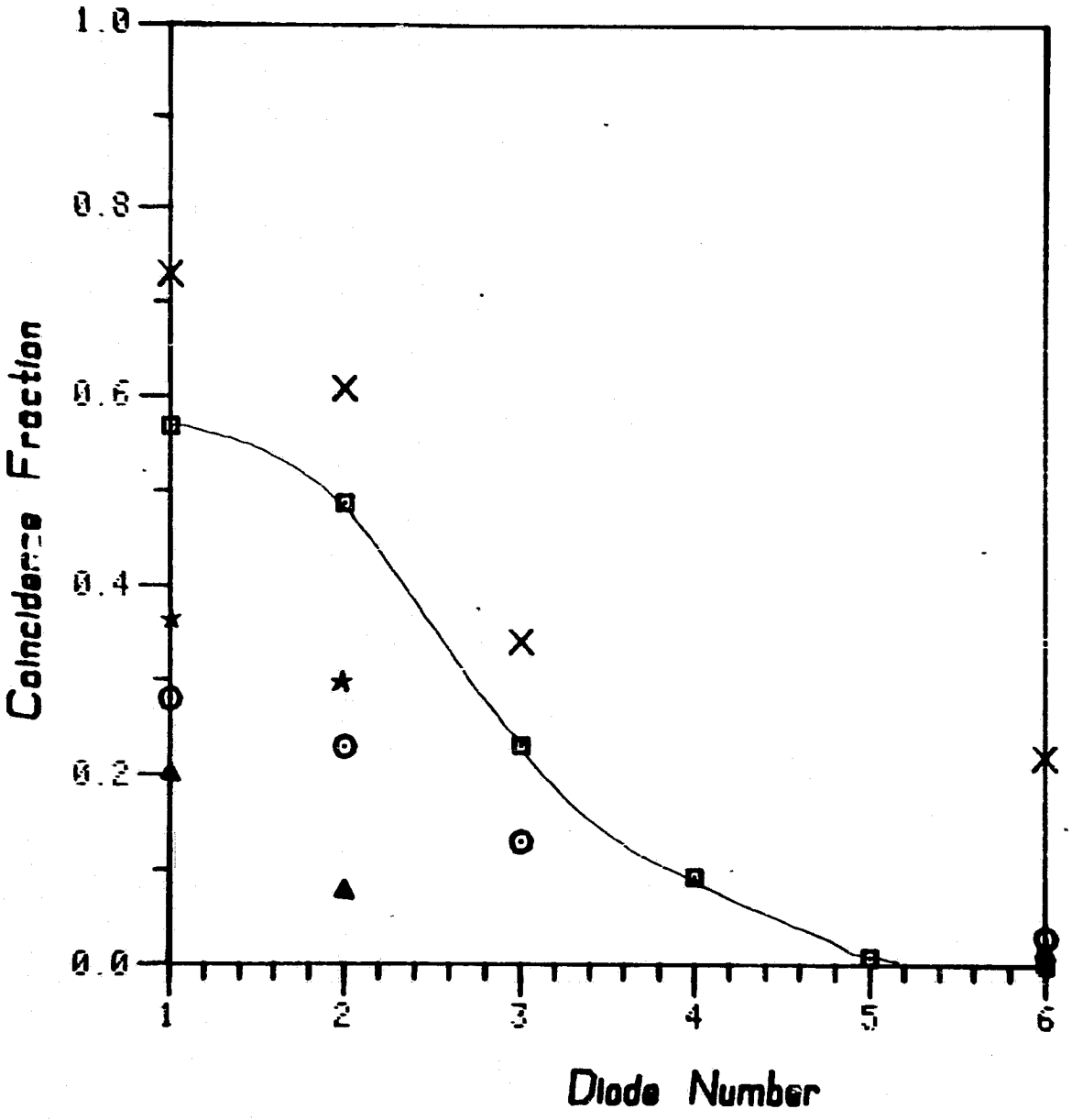

x = 40 μsec 21 MeV

⊙ = 1 μsec 21 MeV

▲ = 1 μ 76 MeV

✱ = 40 μsec 76 MeV

⊡ = THEORY

Figure 8. Coincidence fraction vs. Diode position.

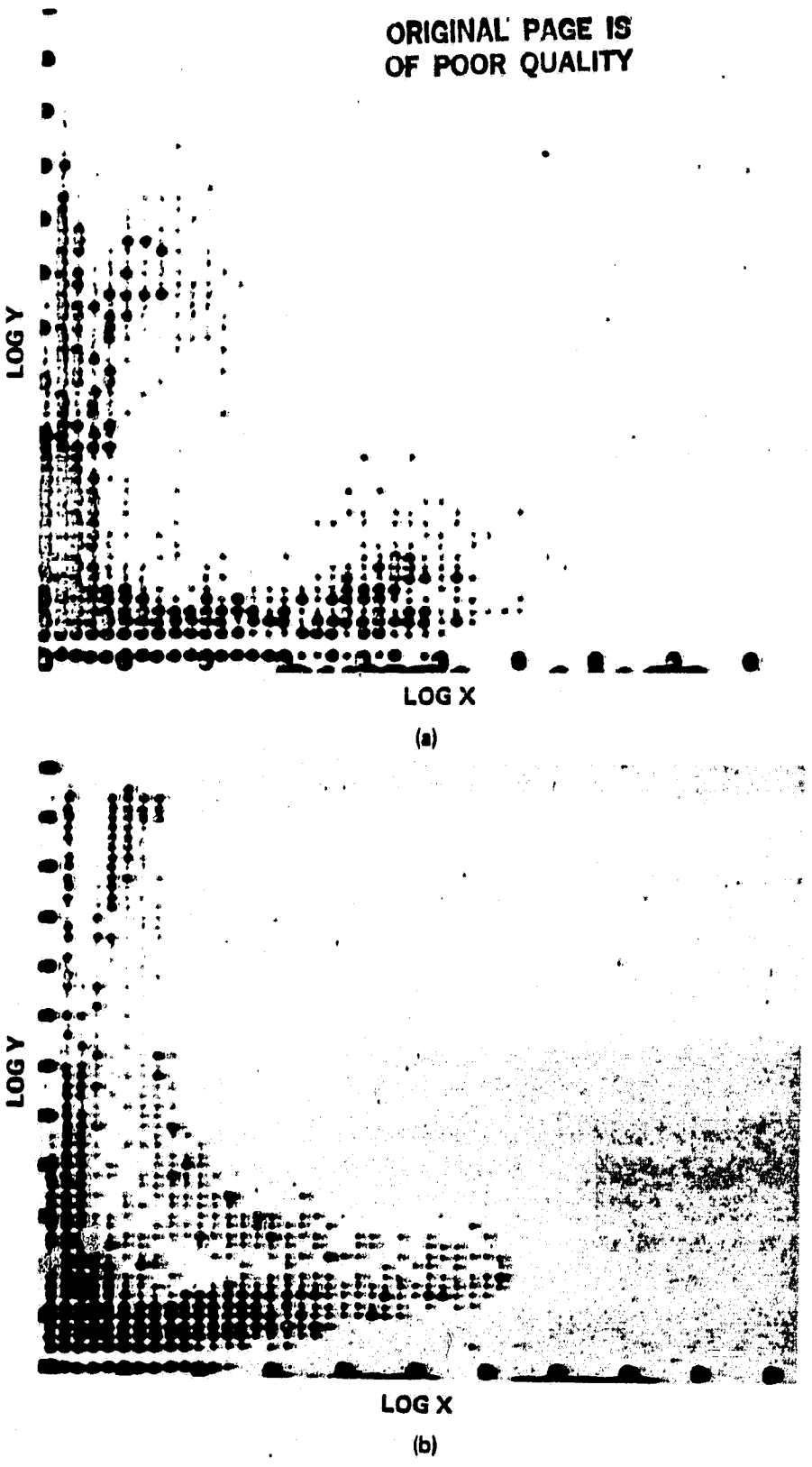

Figure 9. A Z-intensified contour of pulse height of coincident pulses in one diode versus pulse height of coincident pulses in a second diode. 9(a) is for a pair of diodes separated by an even number of diodes while 9(b) is for a pair separated by an odd number of diodes.

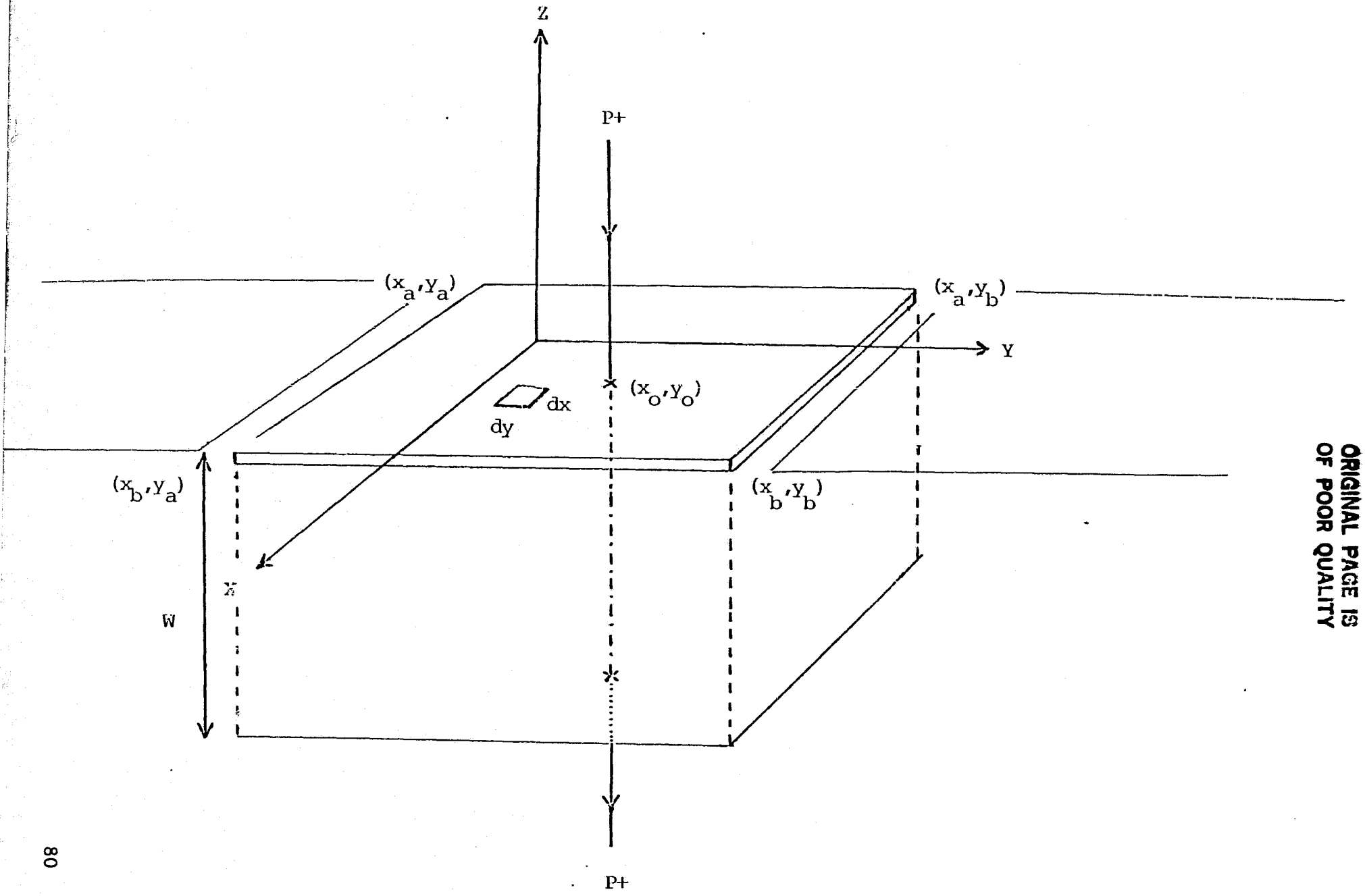

Figure 10. Coordinate system and geometry used in diffusion model.

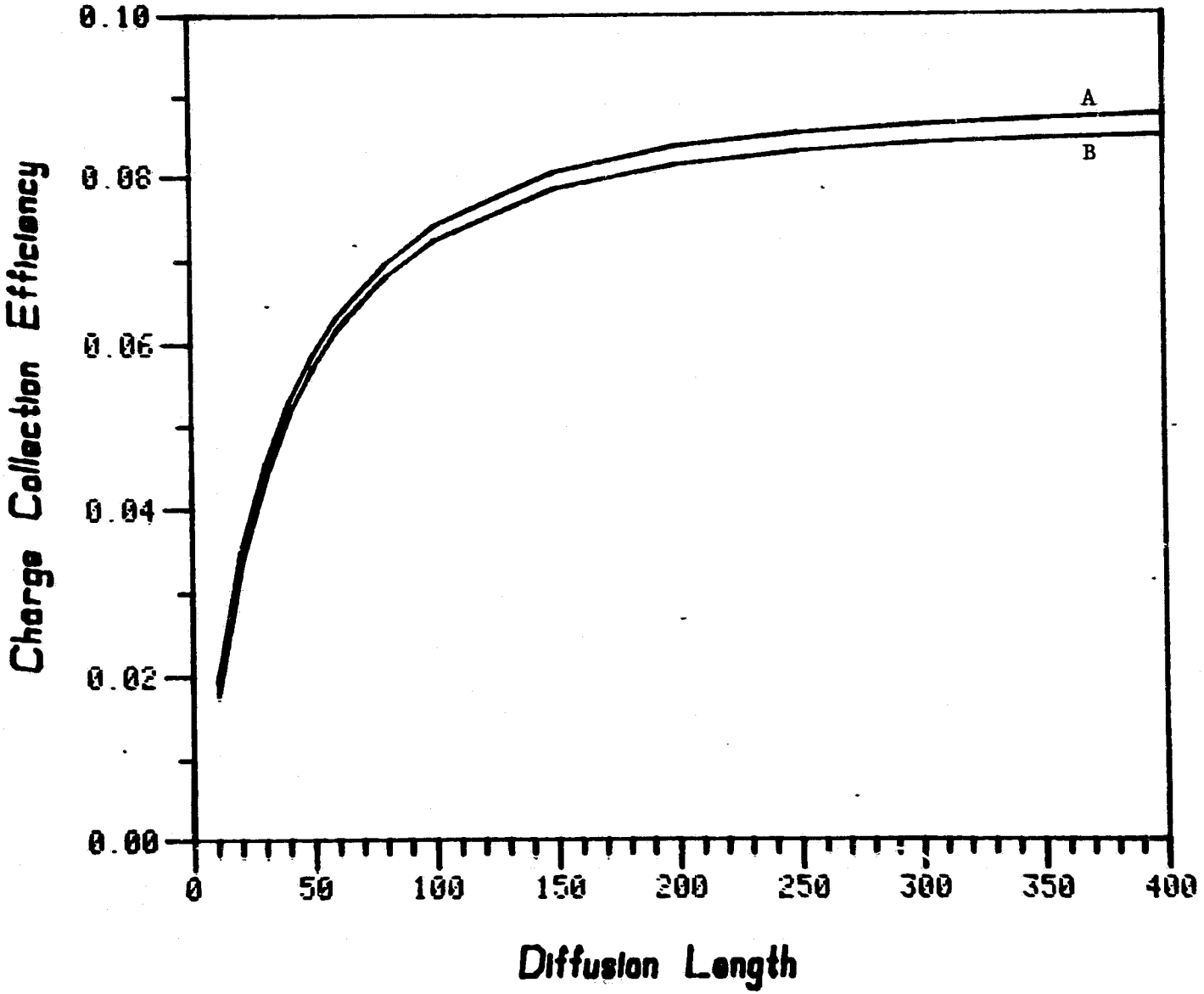

Figure 11. Change collection efficiency vs. diffusion lenght for 400 μ track entering at $x_o = y_o = 0$ wafer thickness 400 μ. (a) $v_w = 0$ (b) $v_w = \infty$.

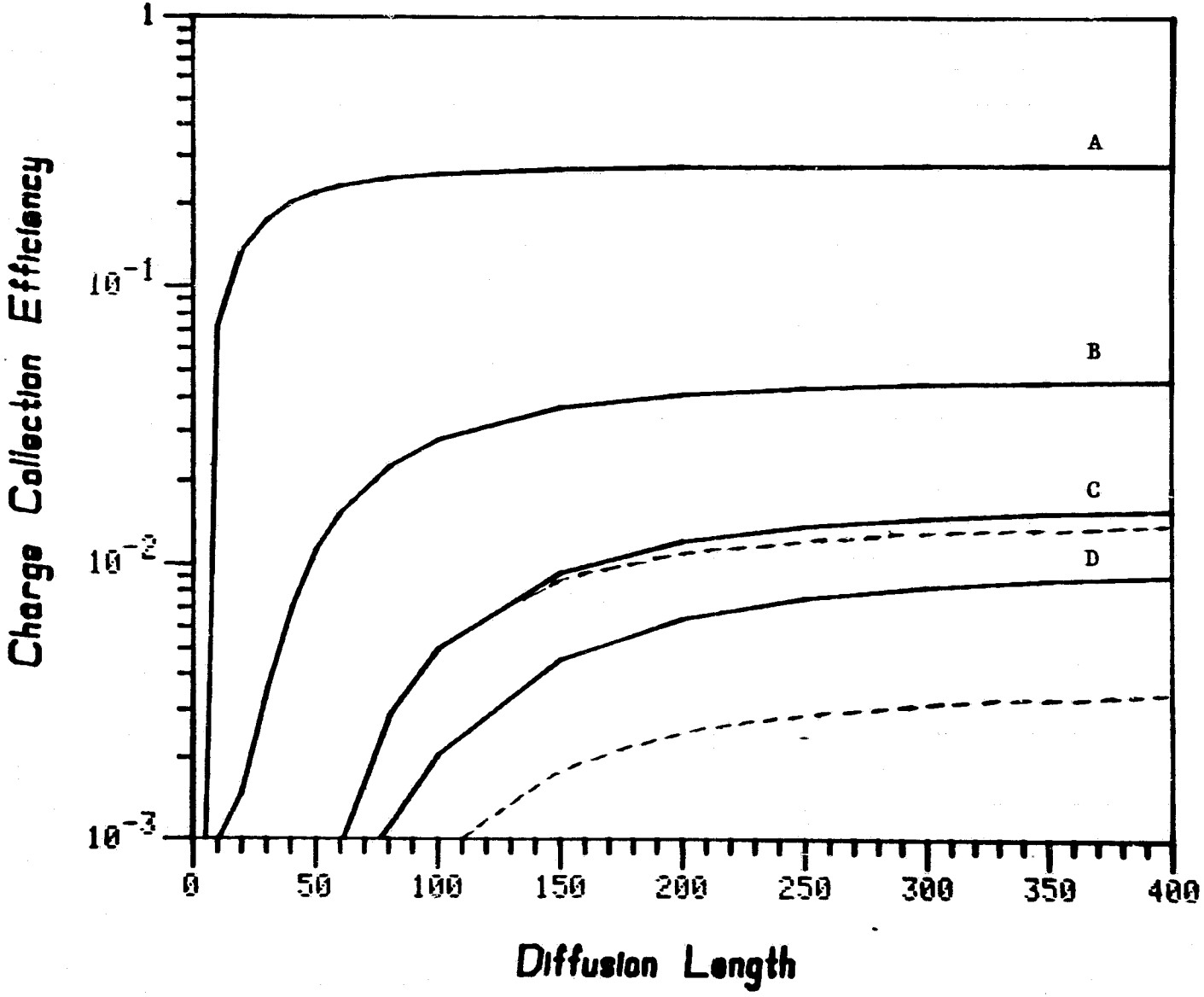

Figure 12. Charge collection efficiency vs. diffusion length for 400 μ track entering at $x_o = y_o = 0$. Wafer thickness 400 μ. (a) 0-100 μ (b) 100-200 μ (c) 200-300 μ (d) 300-400 μ. Solid line - $v_w = 0$. Dashed line - $v_w = \infty$.

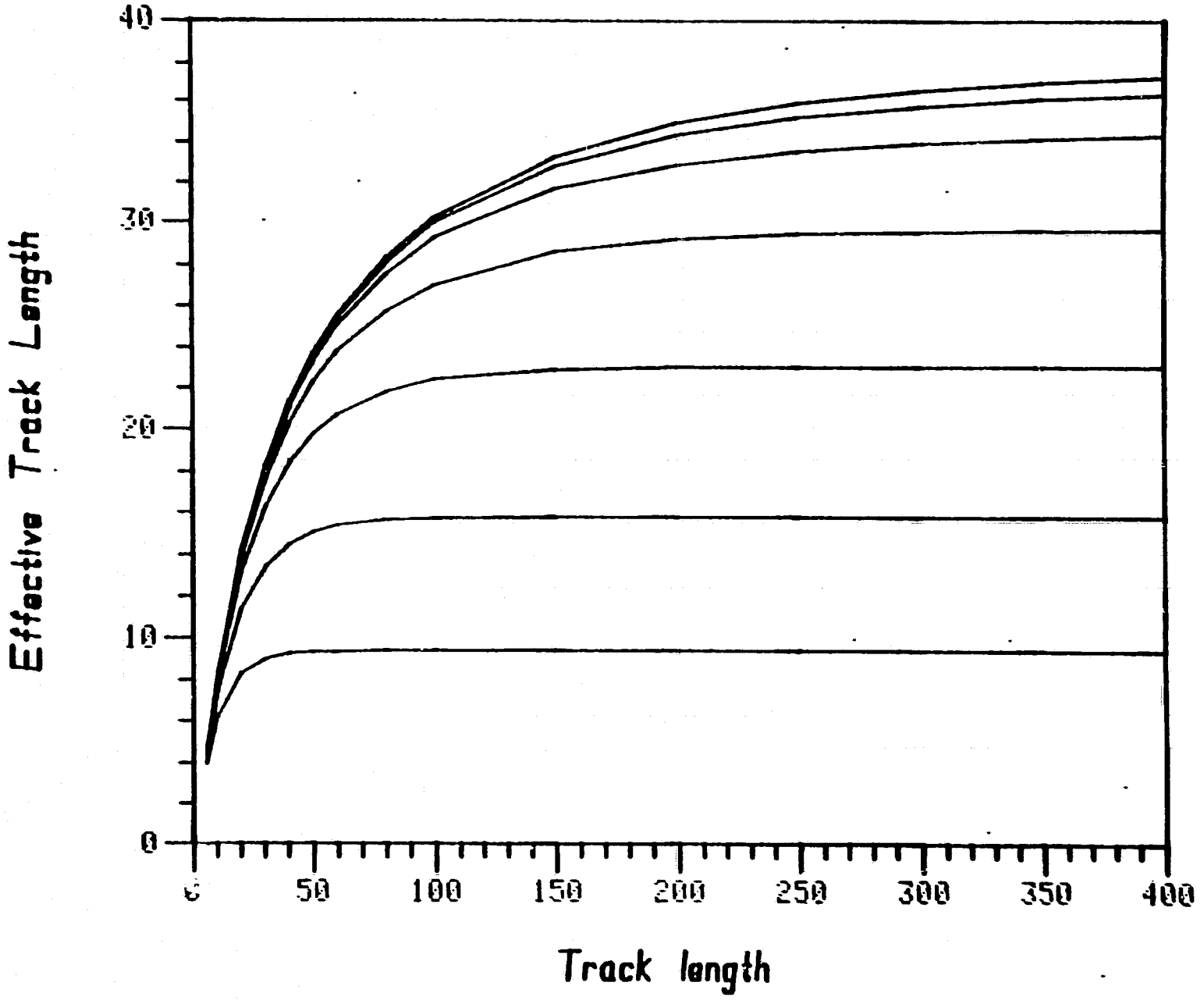

Figure 13. Effective track length W vs. actual track length L. $x_o = y_o = 0$. Semi-infinite approximation. From bottom to top values for L_d are 10, 20, 30, 40, 80, 160, 300 and 1000 μ.

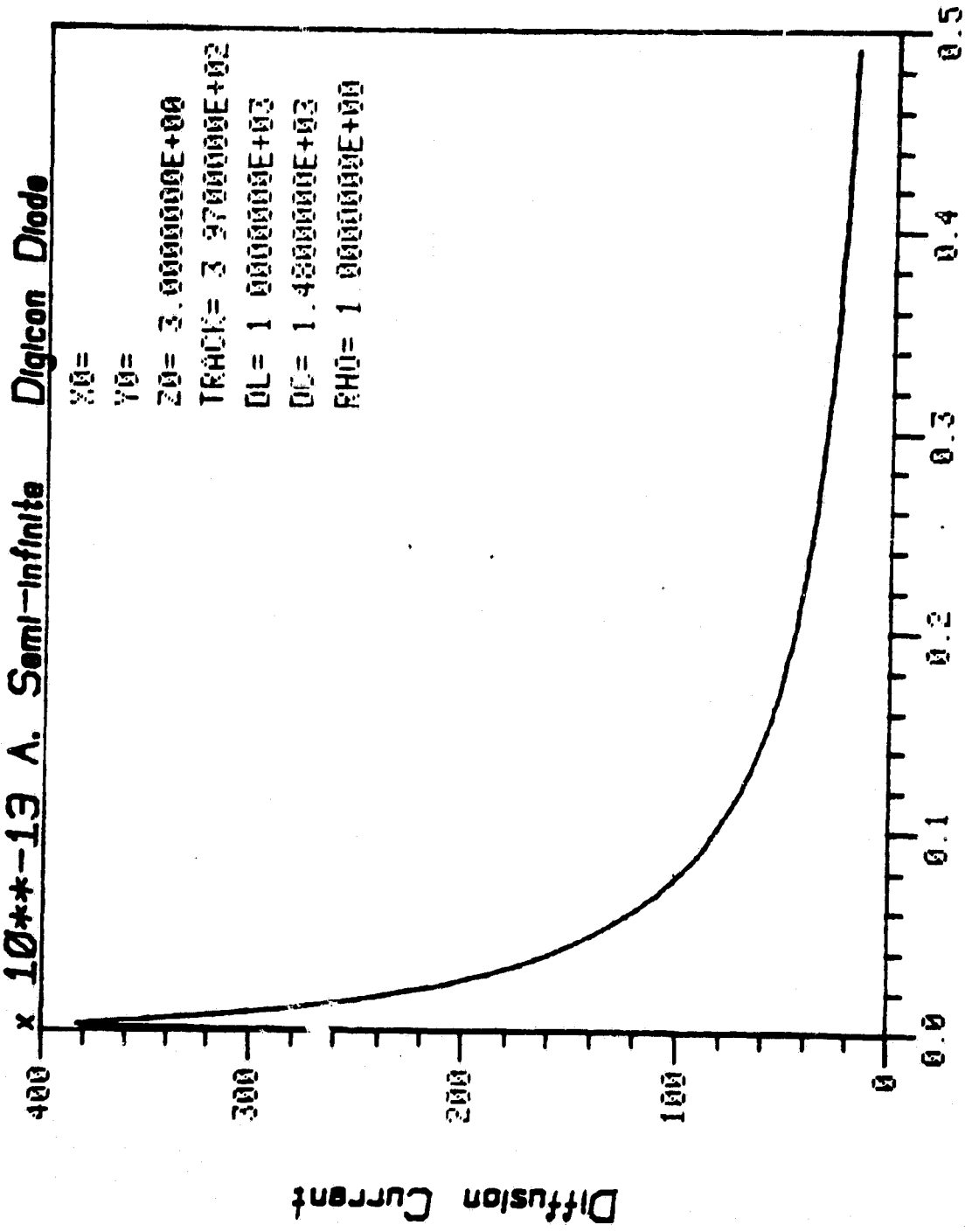

Figure 14. Diffusion current with $x_o = 0$ μ.

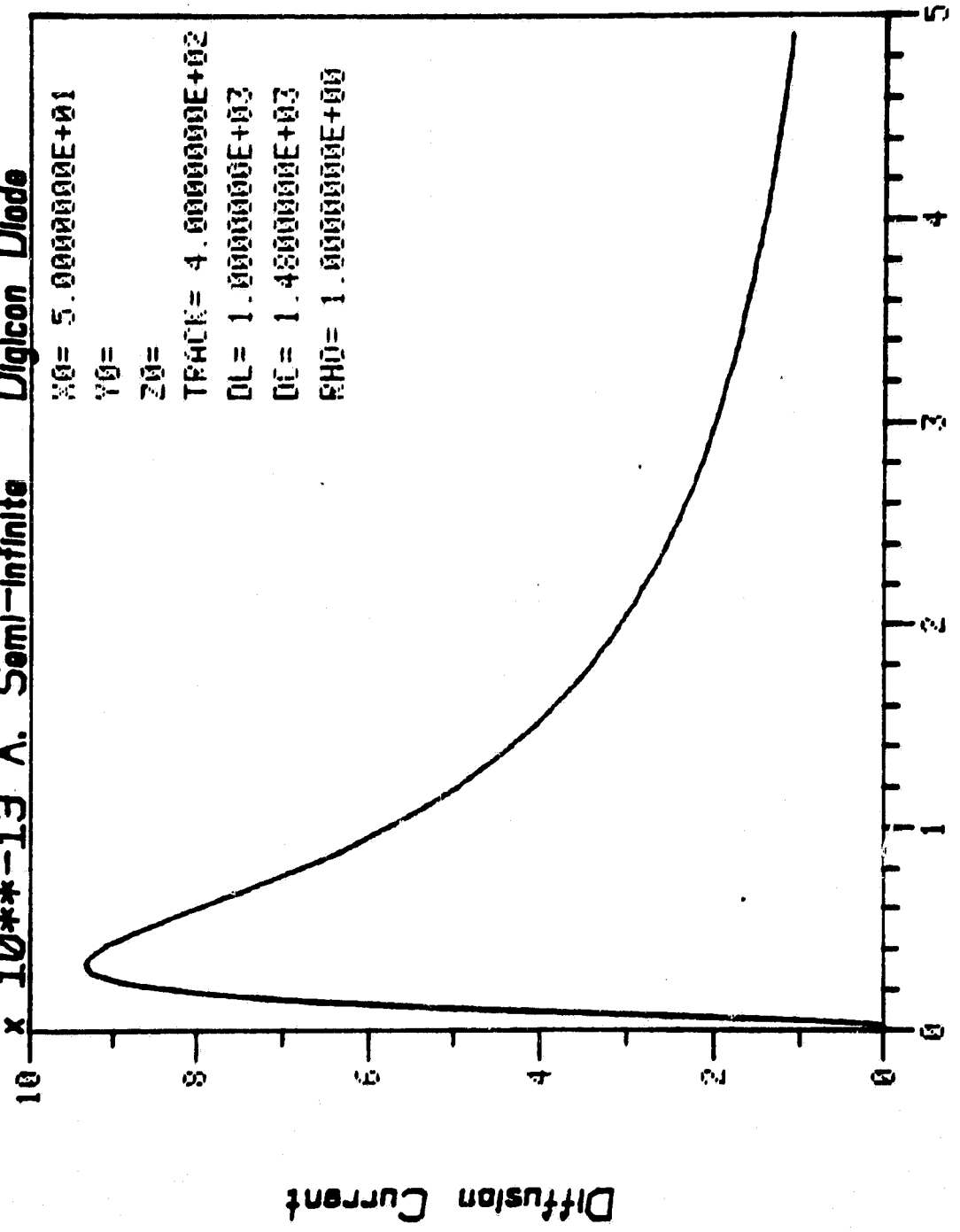

Figure 15. Diffusion current with x_o = 50 μ.

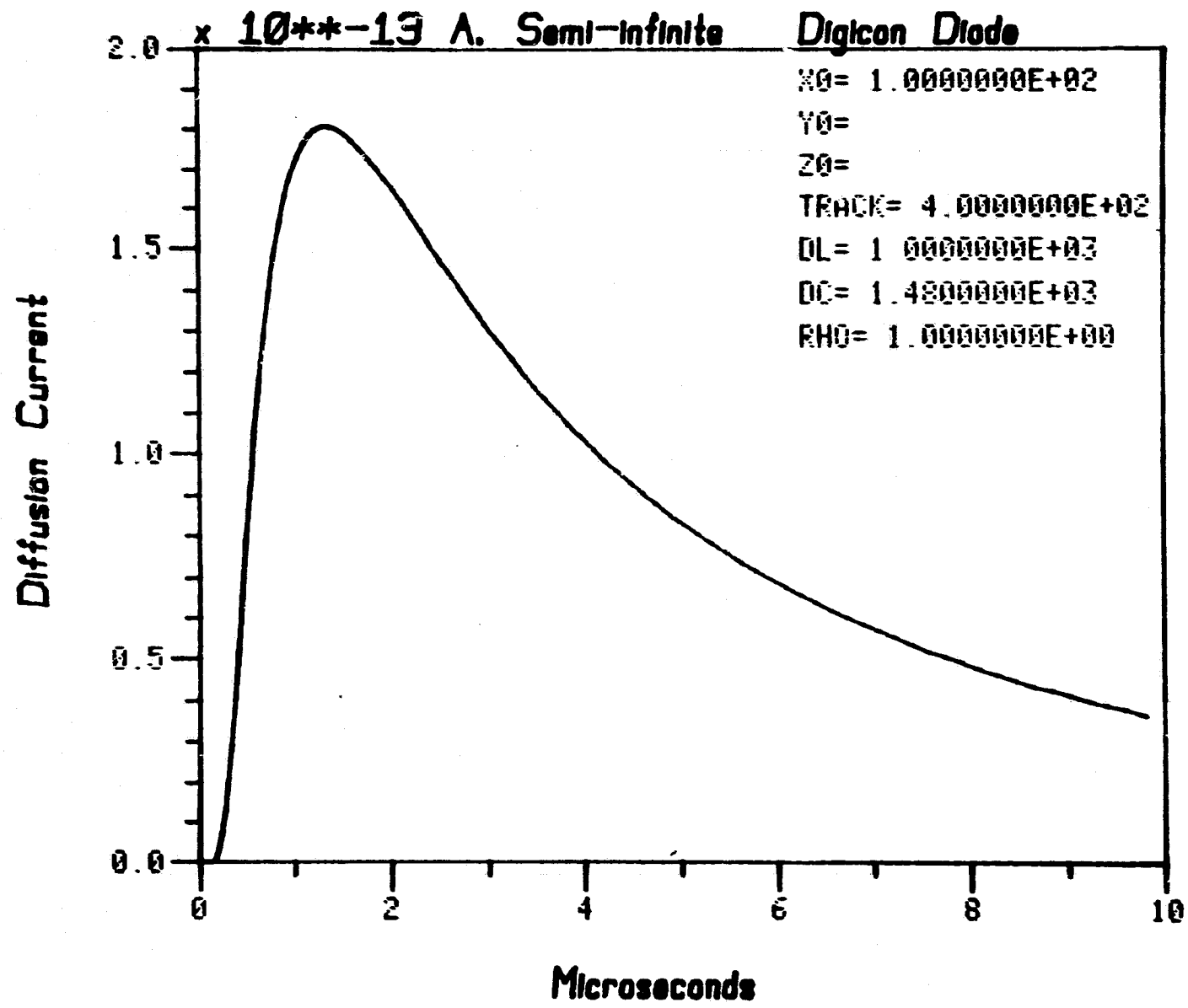

Figure 16. Diffusion current with x_o = 100 μ.

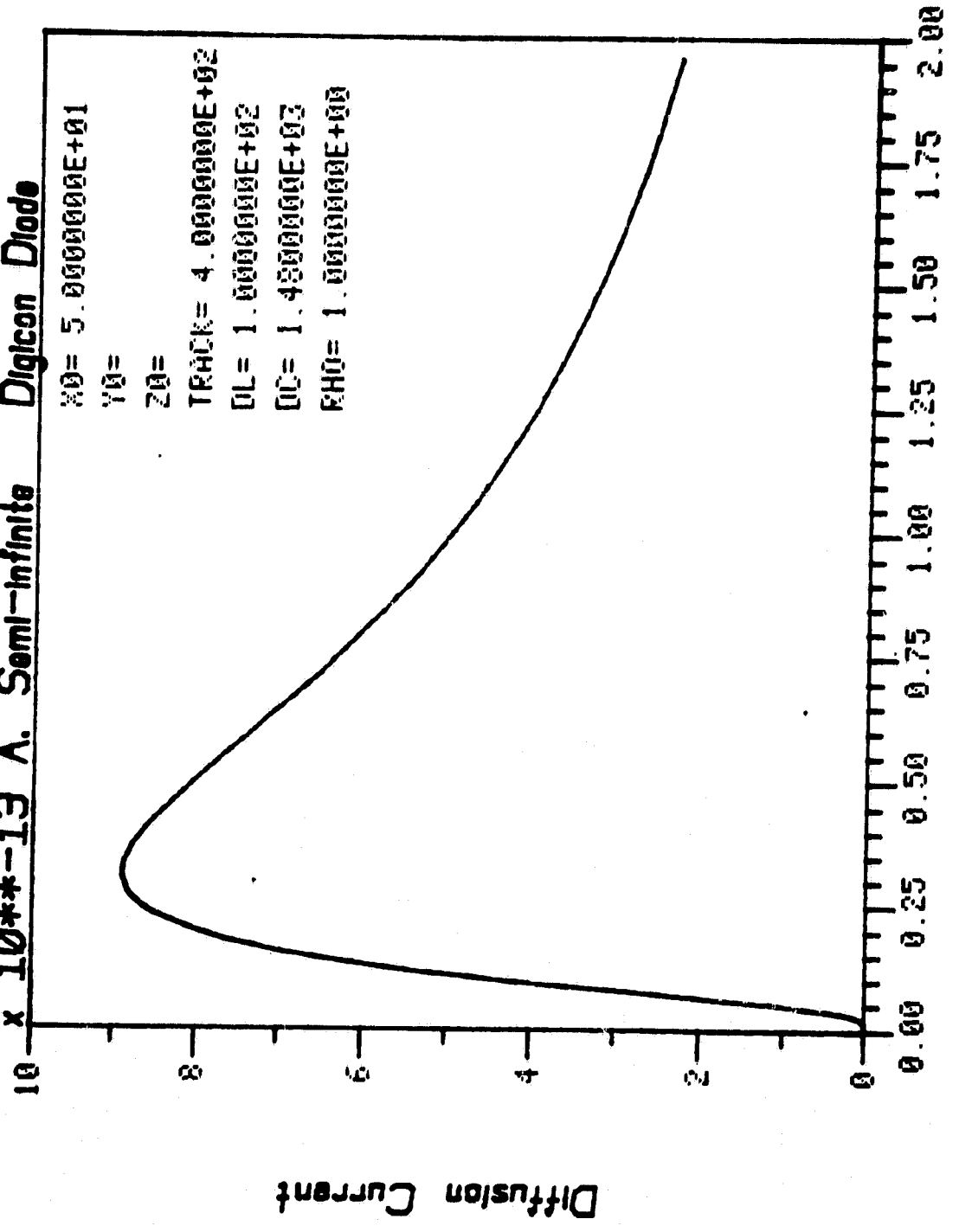

Figure 17. Diffusion current with L_d = 100 μ.

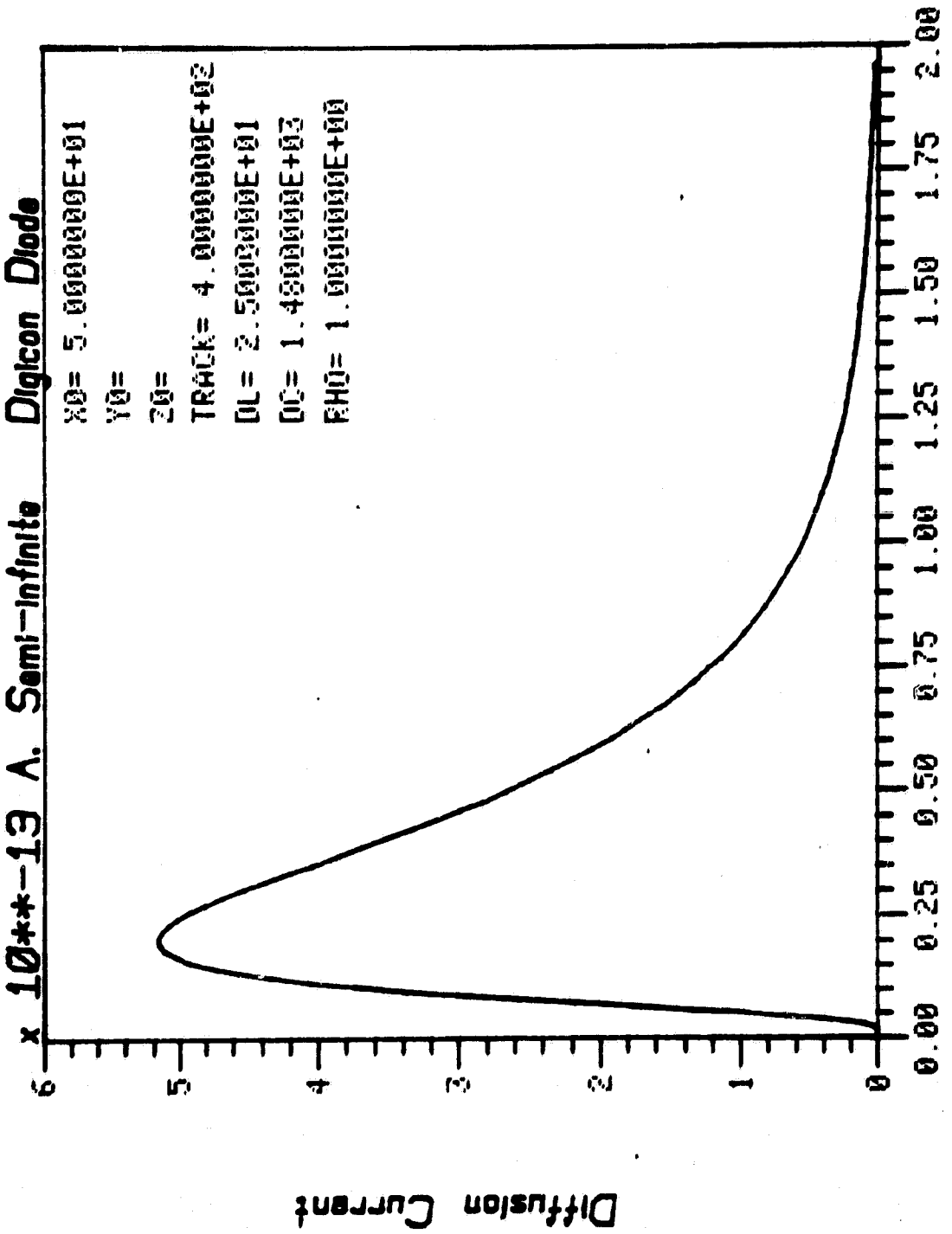

Figure 18. Diffusion current with L_d = 25 μ.

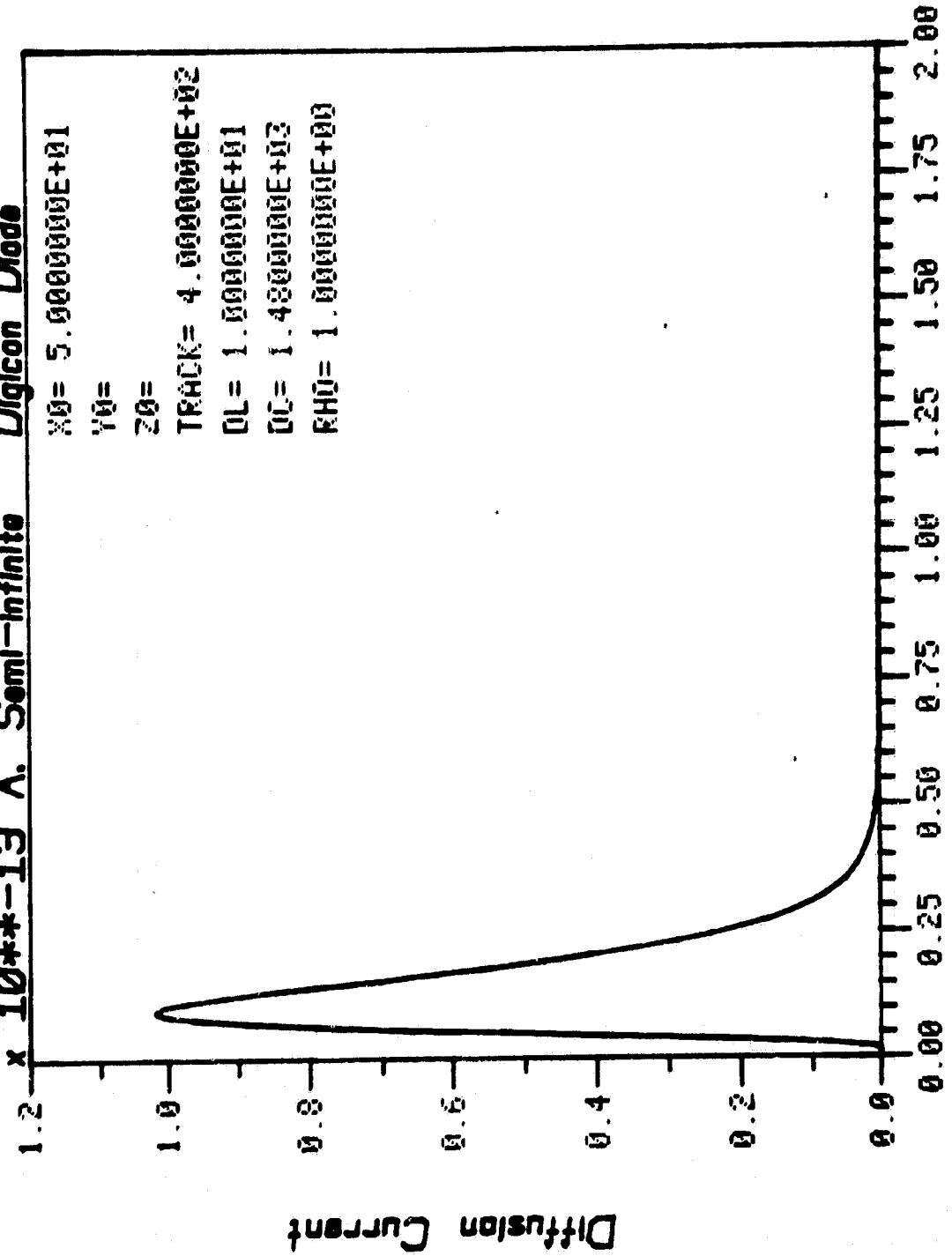

Figure 19. Diffusion current with L_d = 10 μ.

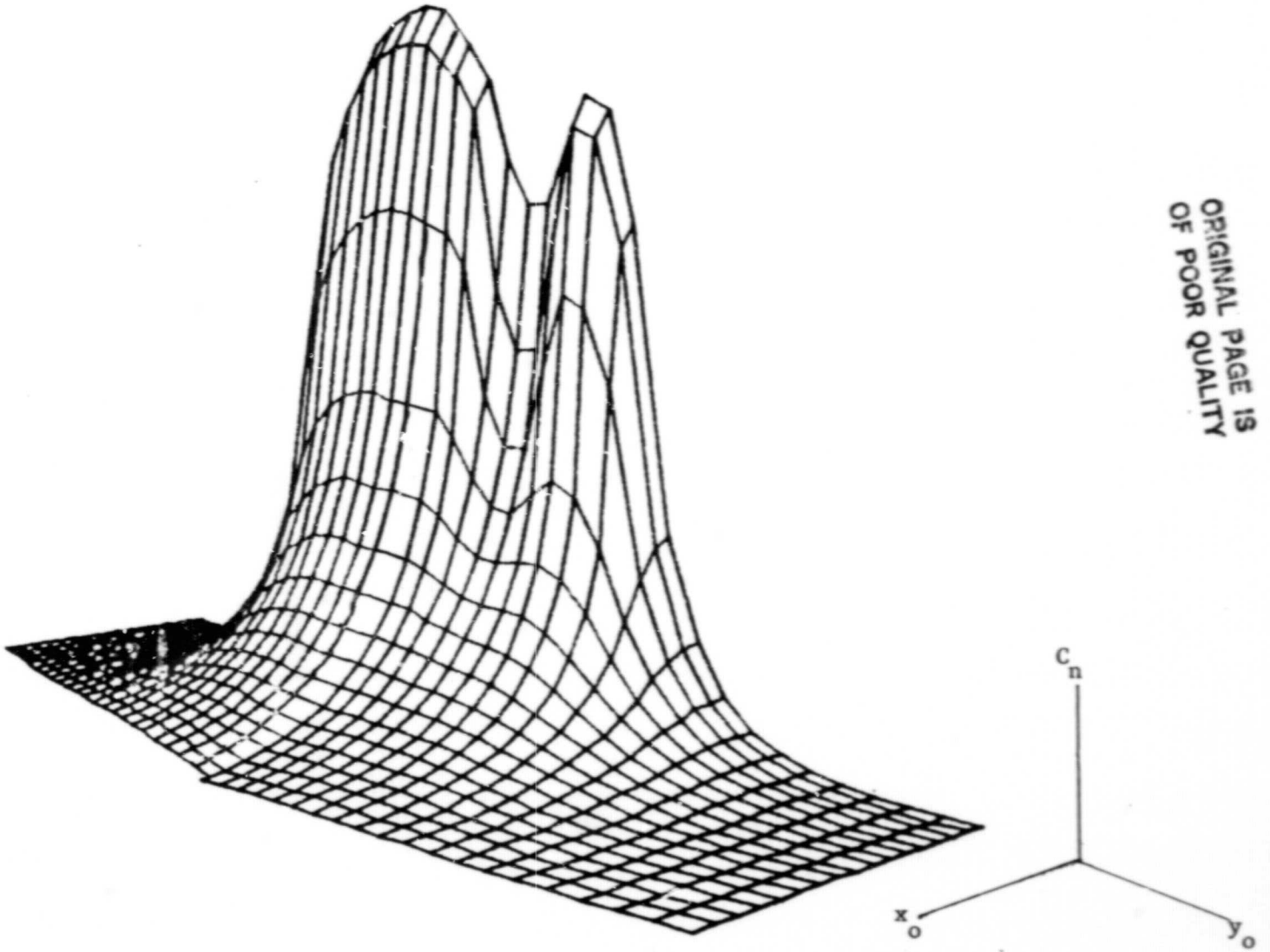

Figure 20. Charge collection efficiency vs. x_o and y_o. Only positive valves of x_o are shown. Track length = 400 μ. Semi-infinite approximation.

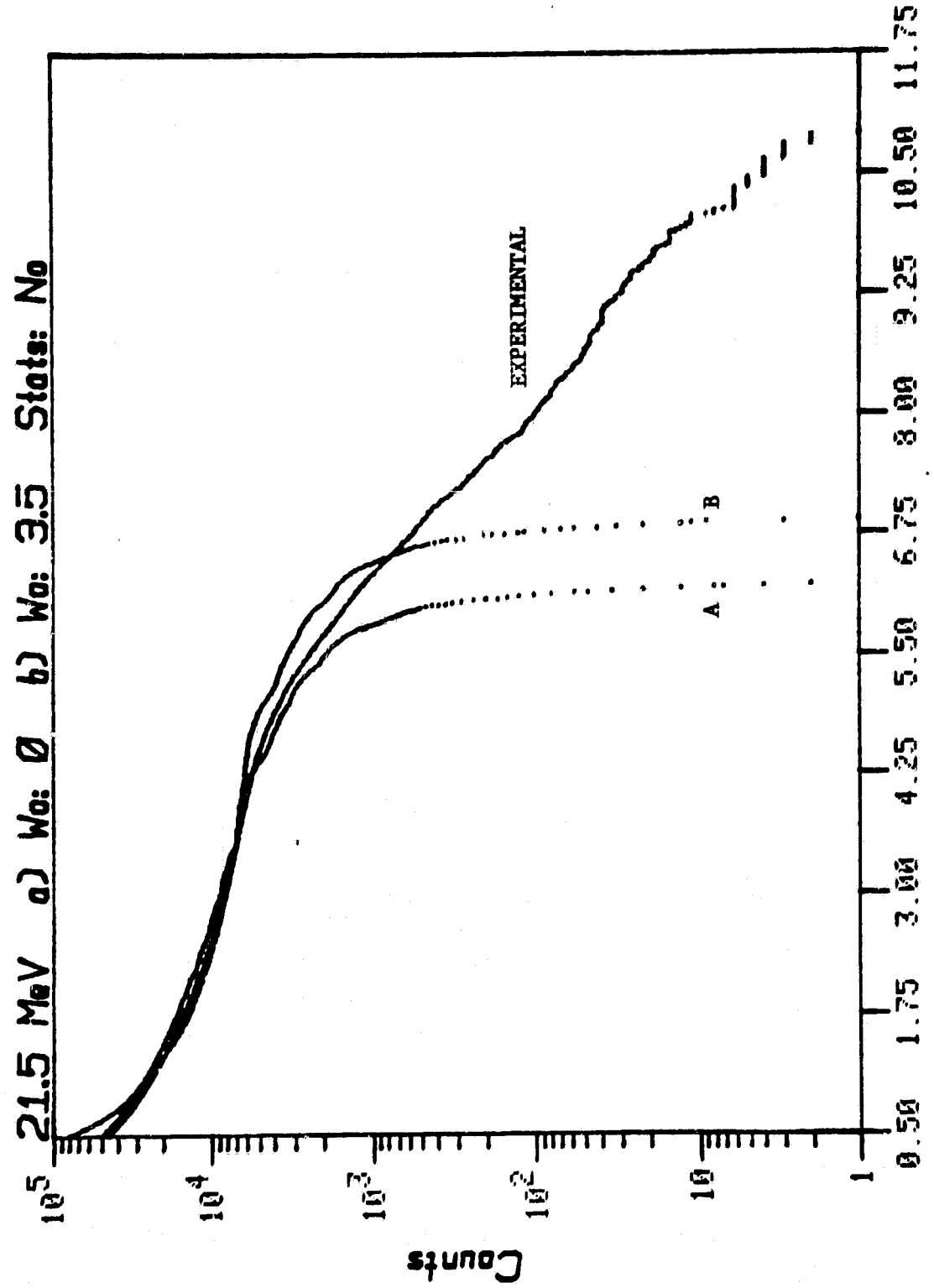

Figure 21. Computed integral pulse height spectrum for 21.5 MeV protons assuming no energy loss fluctuations.

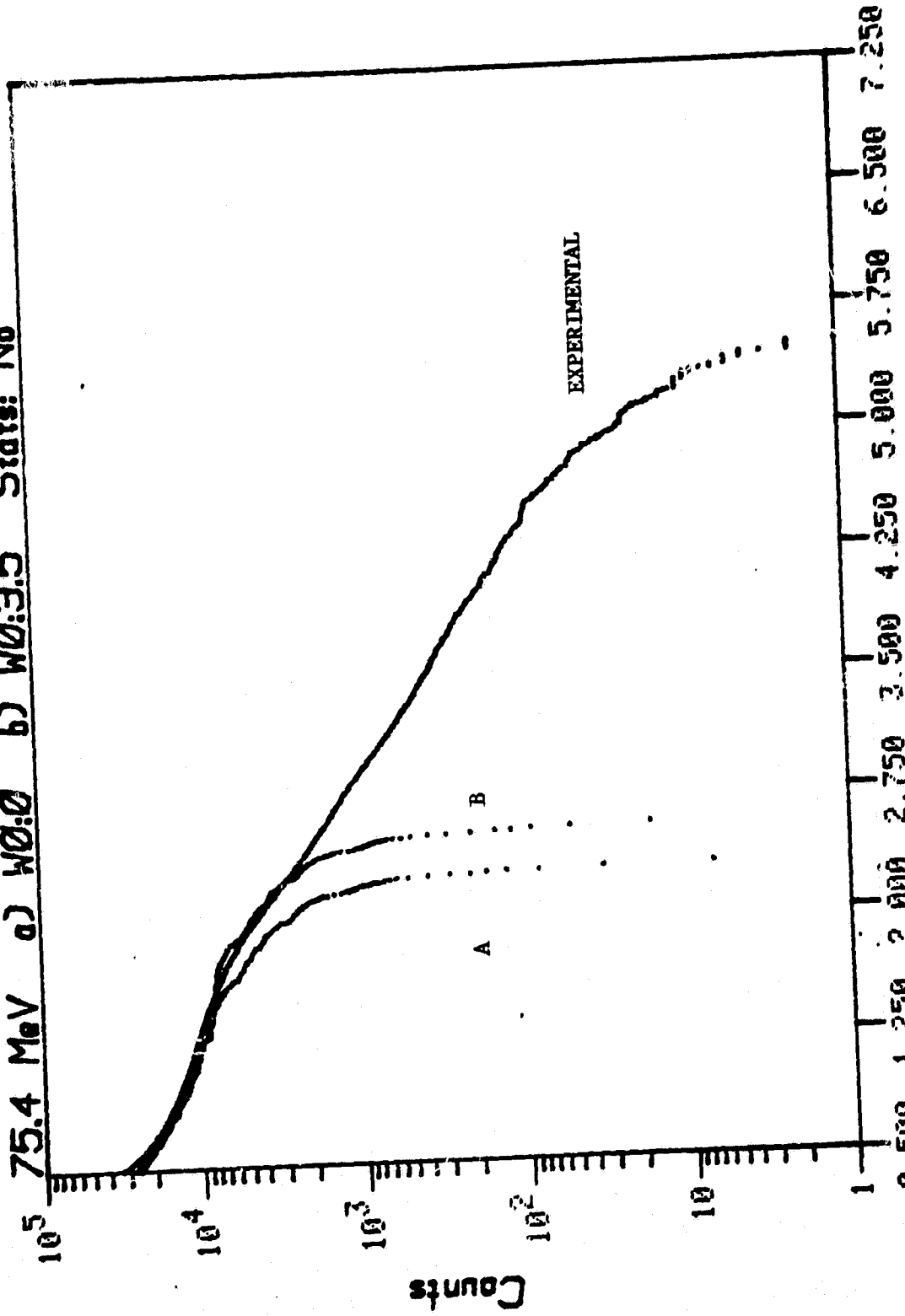

Figure 22. Computed integral pulse height spectrum for 75.4 MeV protons assuming no energy loss fluctuations.

C-2

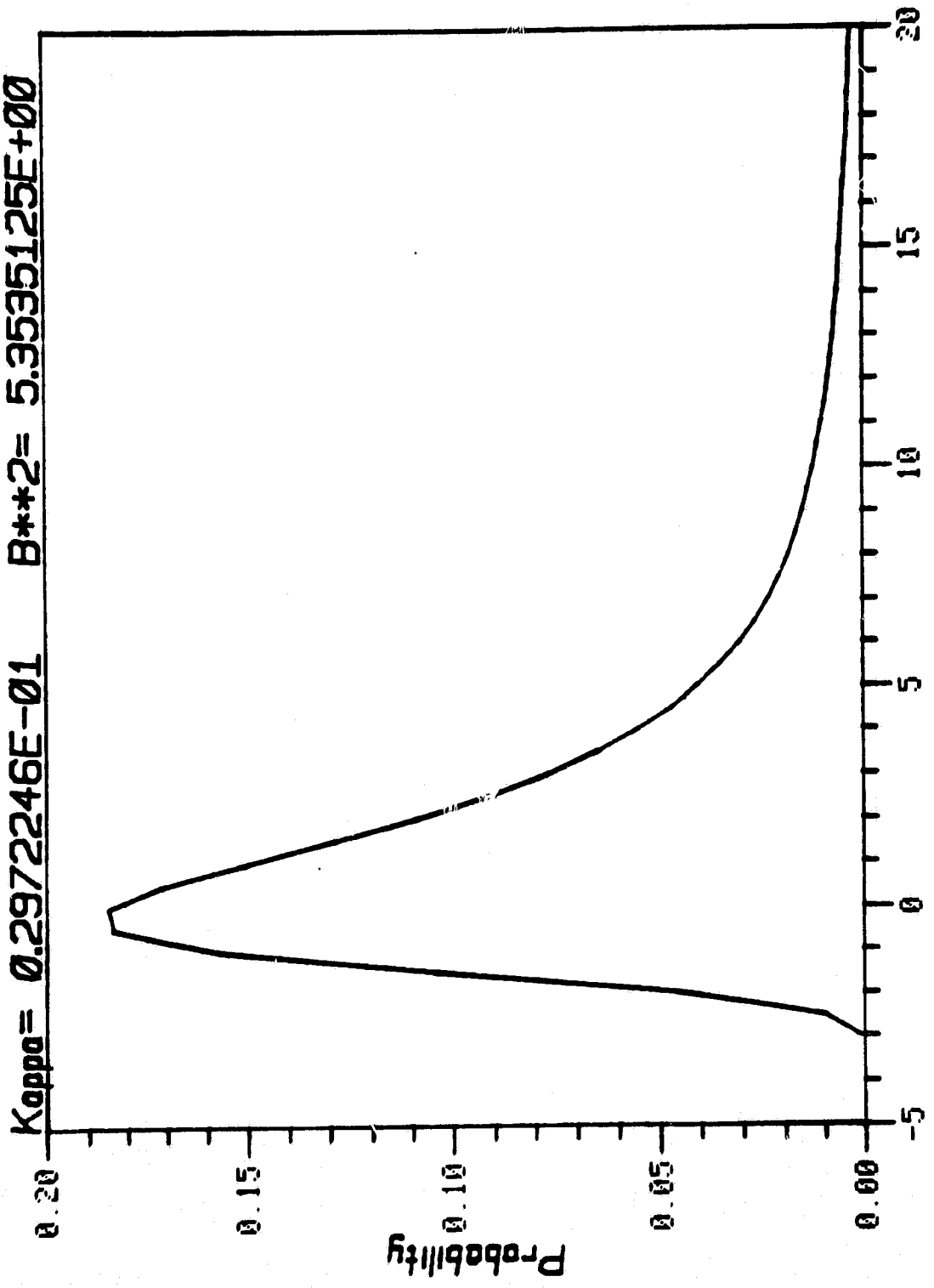

Figure 23. Landau distribution of energy losses.

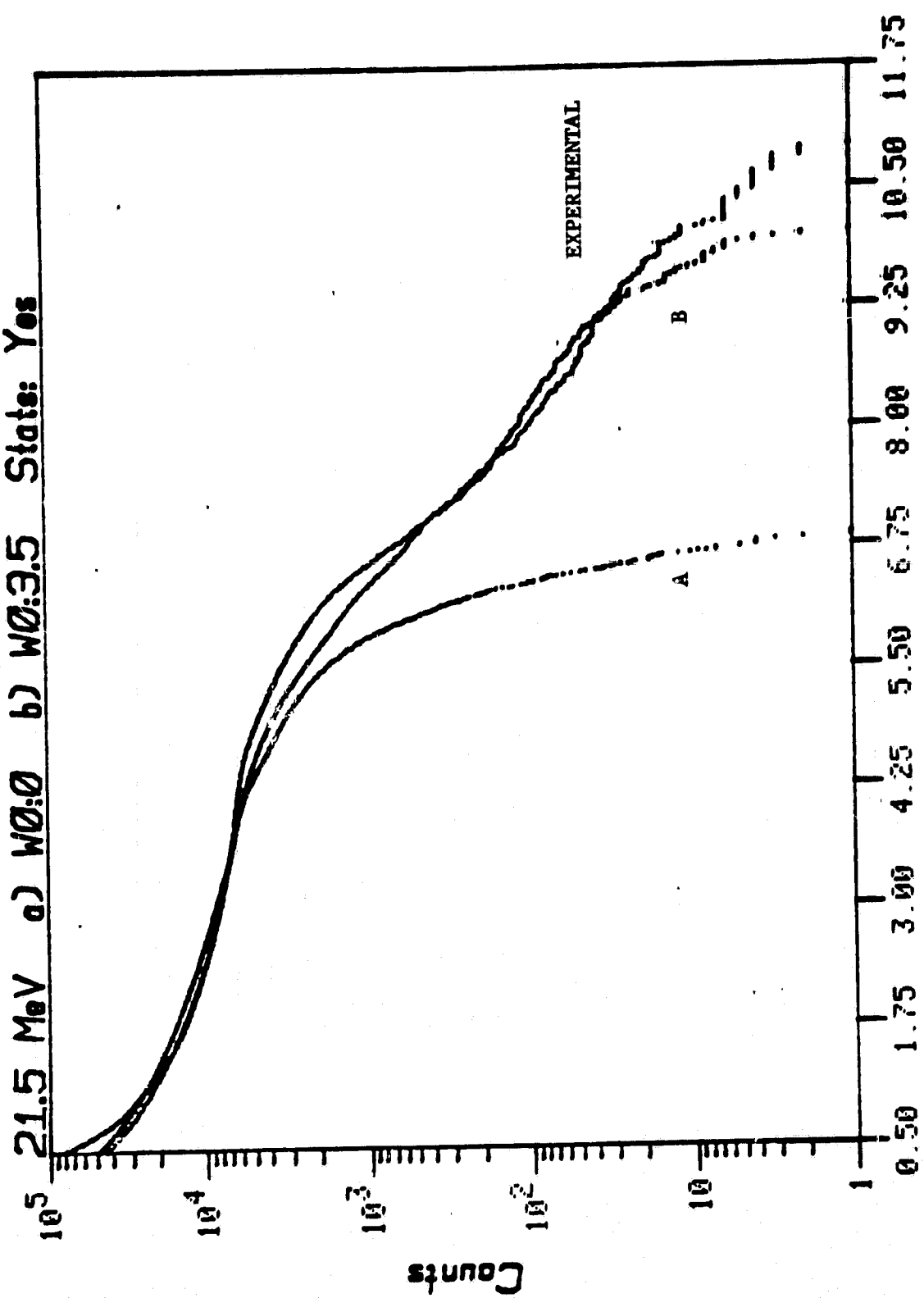

Figure 24. Computed integral pulse height spectrum for 21.5 MeV protons using Gaussian $f(\Delta,s)$ along 400 μ track.

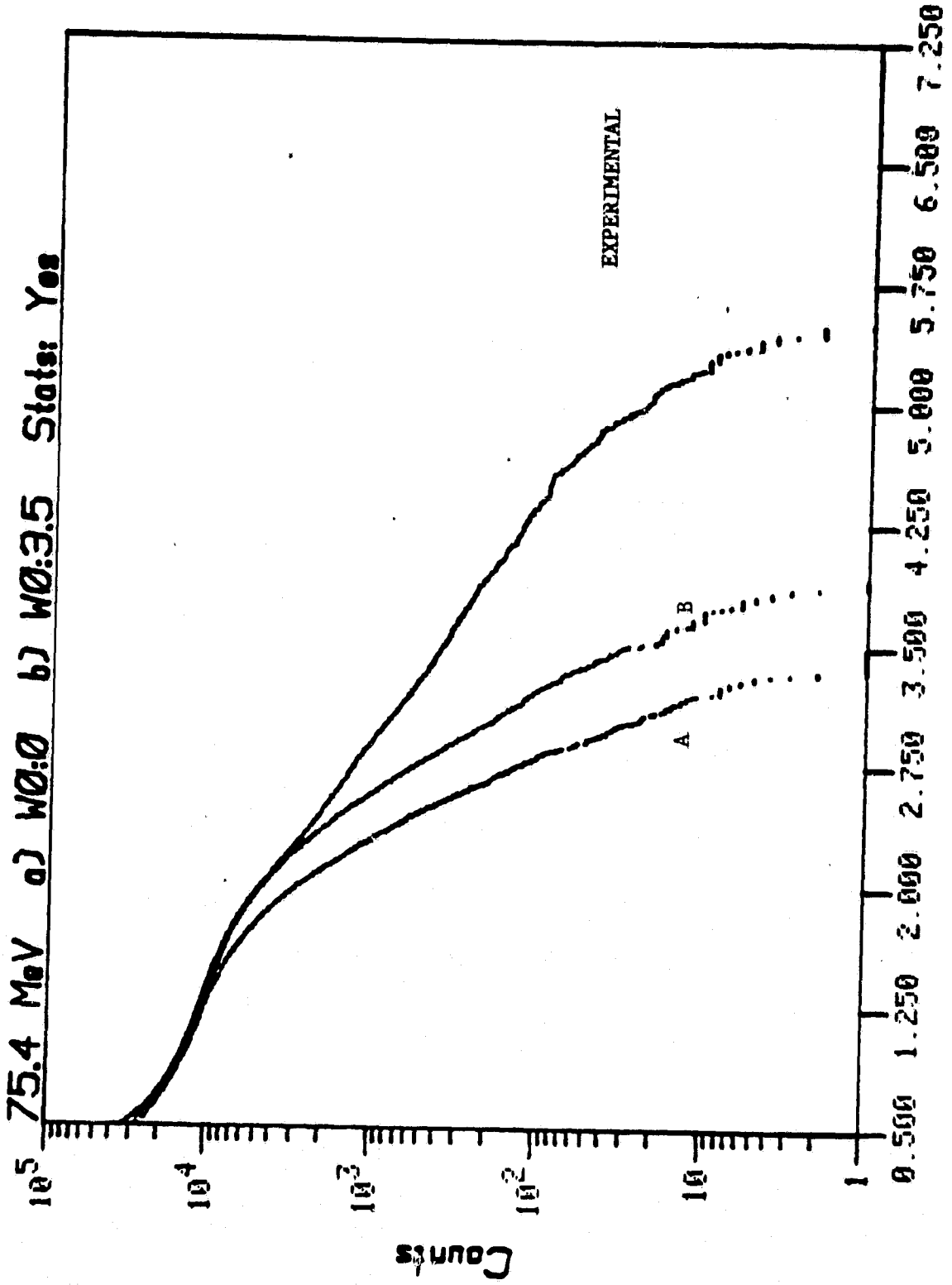

Figure 25. Computed integral pulse height spectrum for 75.4 MeV protons using Gaussian $f(\Delta,s)$ along 400 μ track.

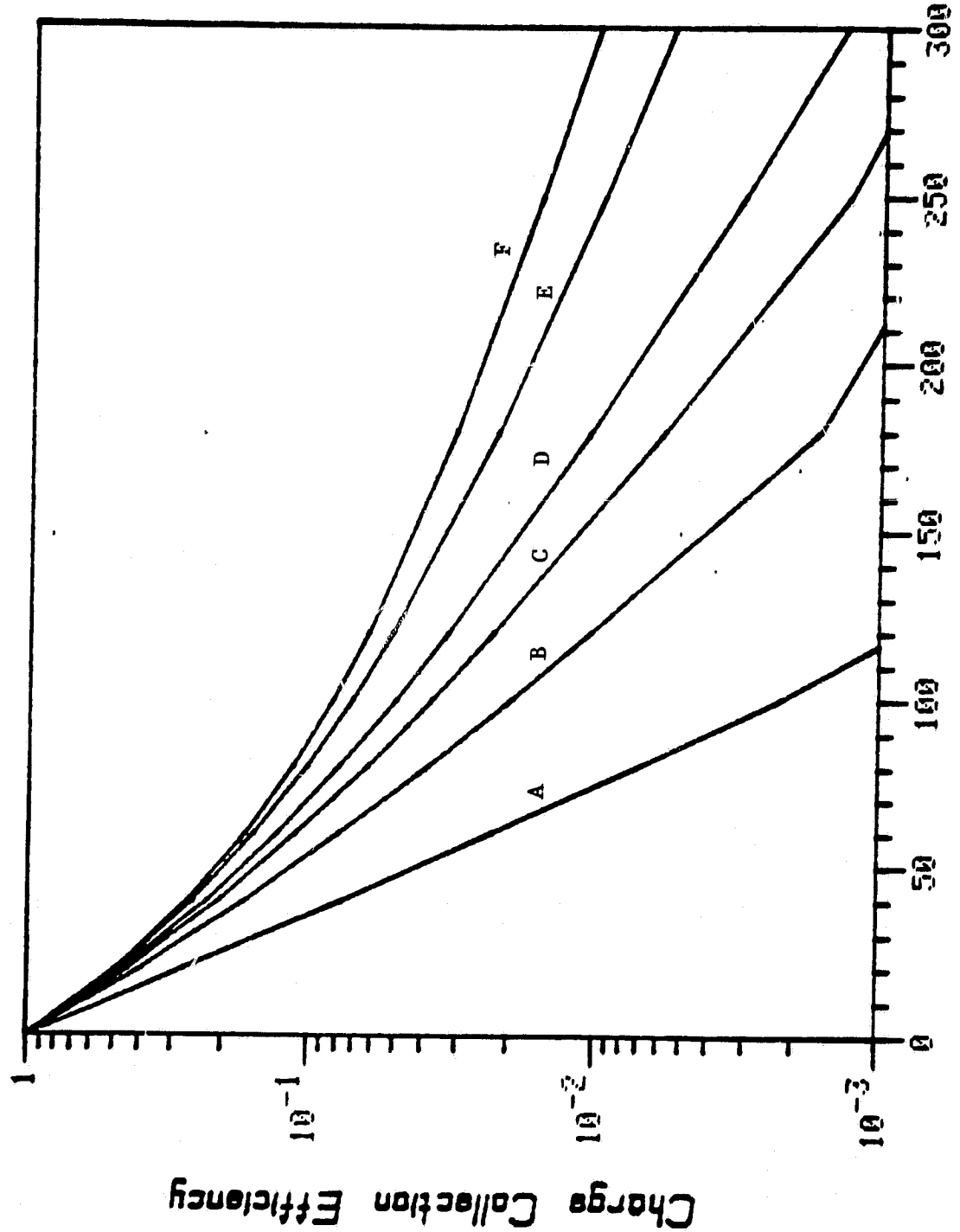

Figure 26. Charge collection efficiency vs. z_o for $x_o = 0$ μ, $y_o = 0$. L_d = 10, 20, 40, 80, 160, 1,000 μ (A - F).

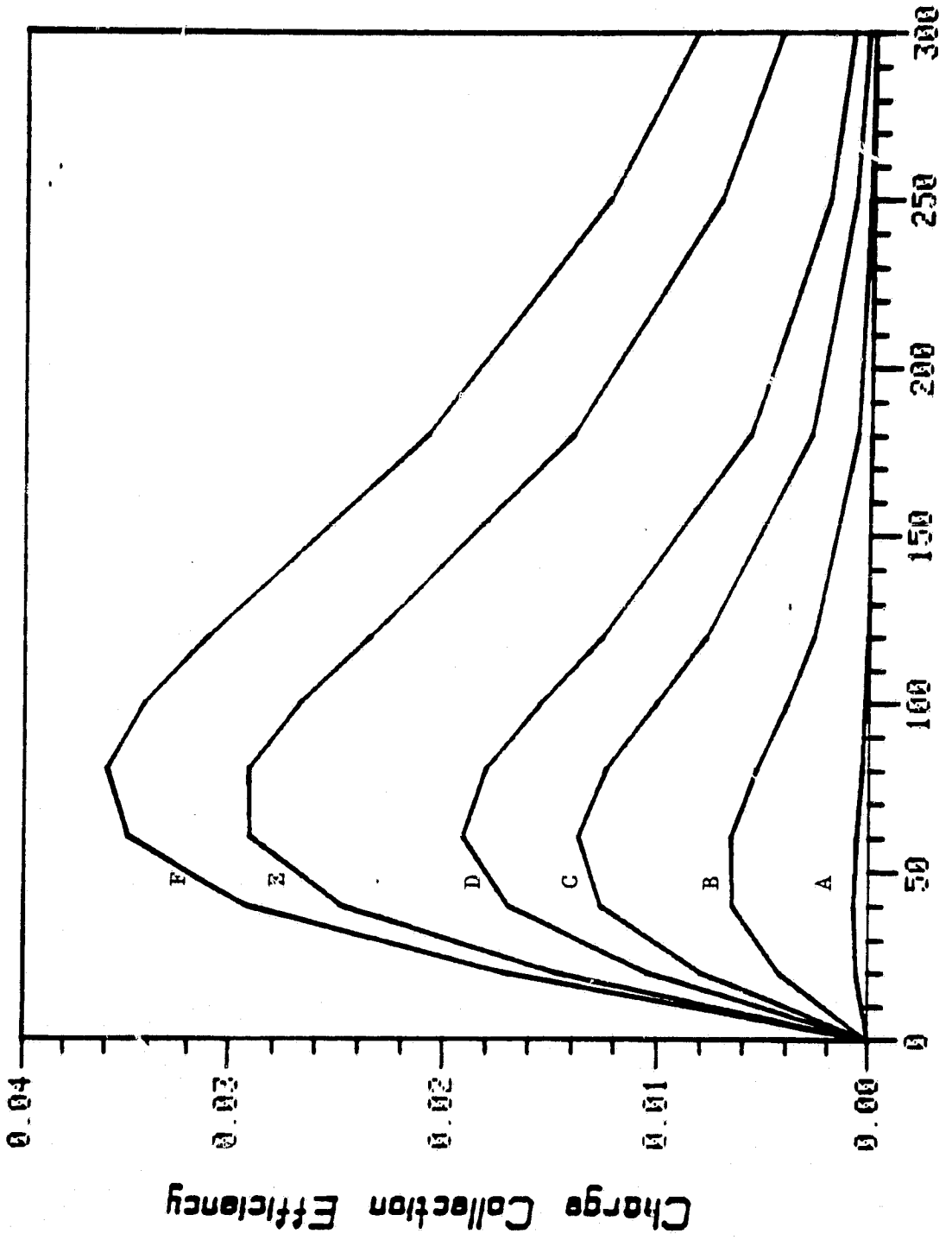

Figure 27. Charge collection efficiency vs. z_o for x_o = 100 μ, y_o = 0. L_d = 10, 20, 40, 80, 160, 1,000 μ.

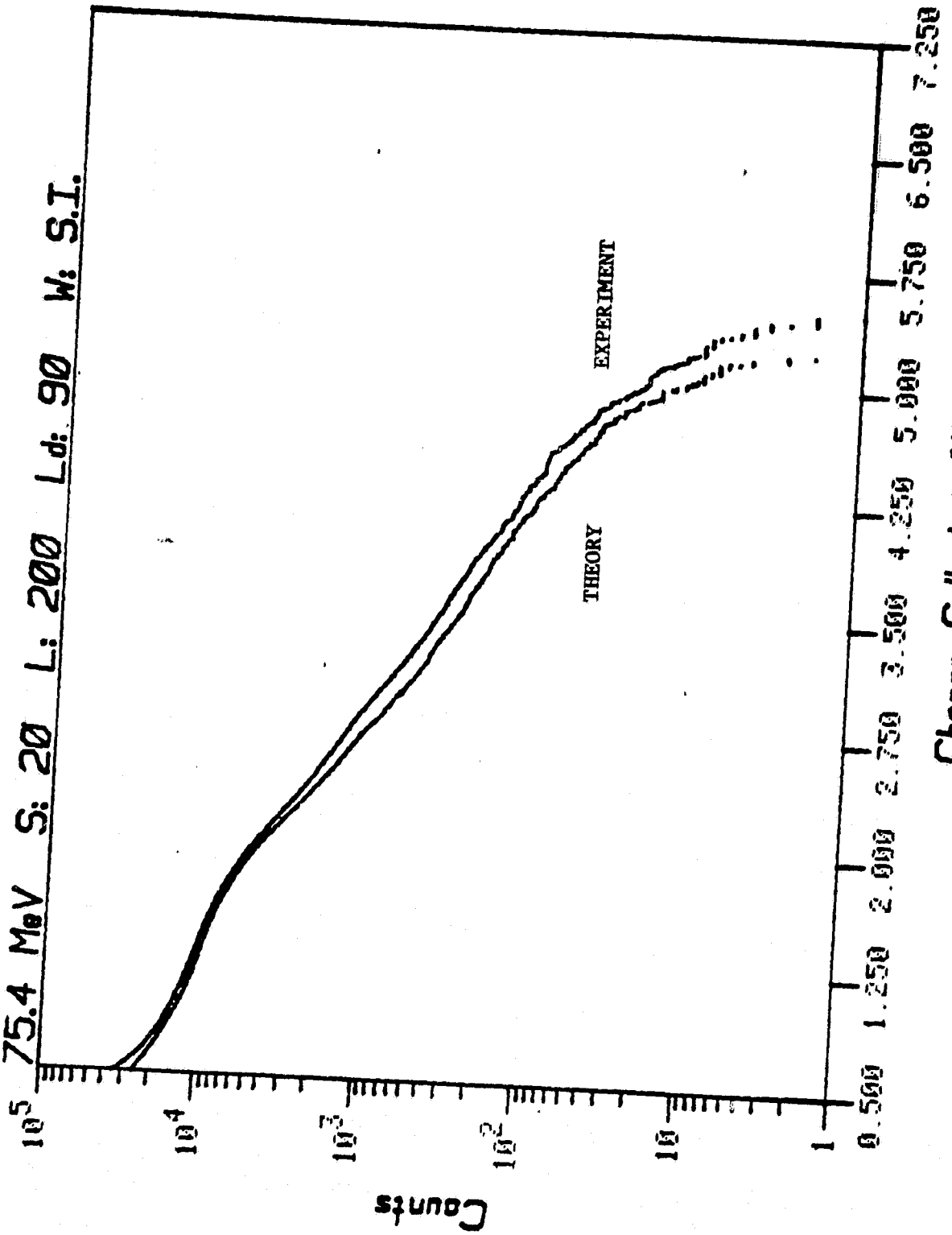

Figure 28. Computed integral pulse height spectrum for 75.4 MeV protons using Vavilov f(Δ,s) along 20 μ segments of 200 μ track.

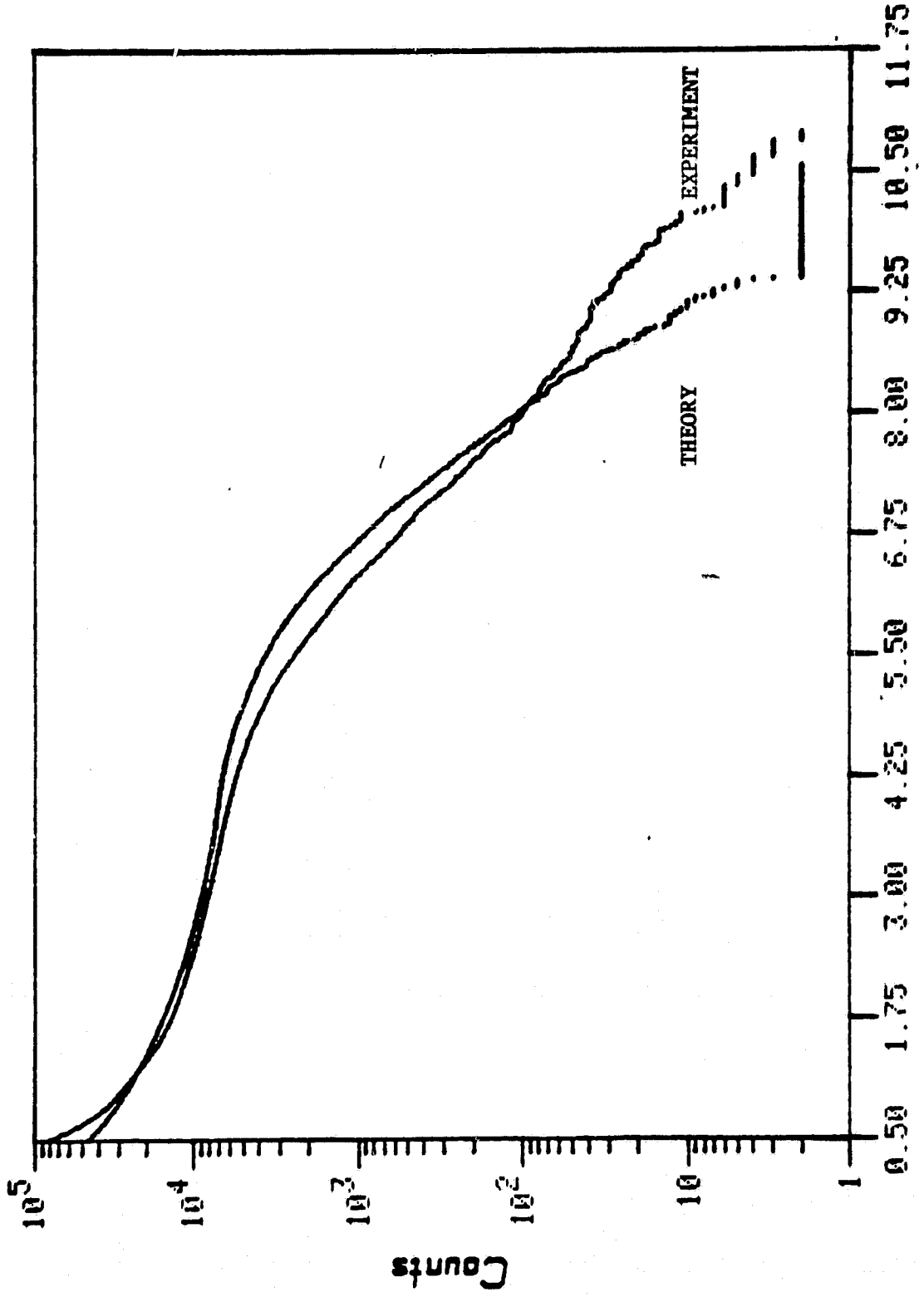

Figure 29. Computed integral pulse height spectrum for 21.5 MeV protons using Vavilov f(Δ, s) along 20 μ segments of 200 μ track.

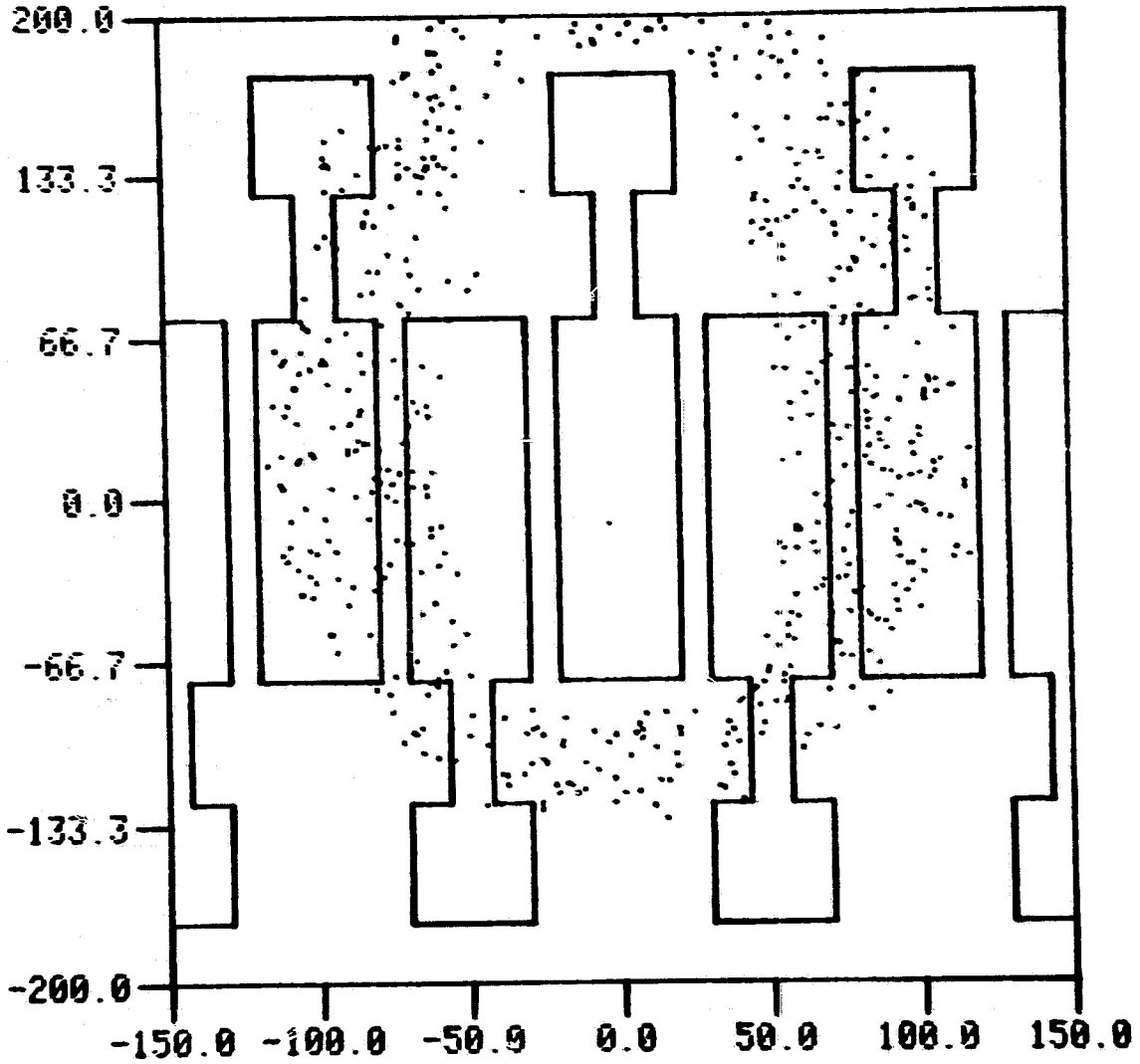

Figure 30. Proton entry points corresponding to charge 3.2 fC collected by Diode at 21.5 MeV.

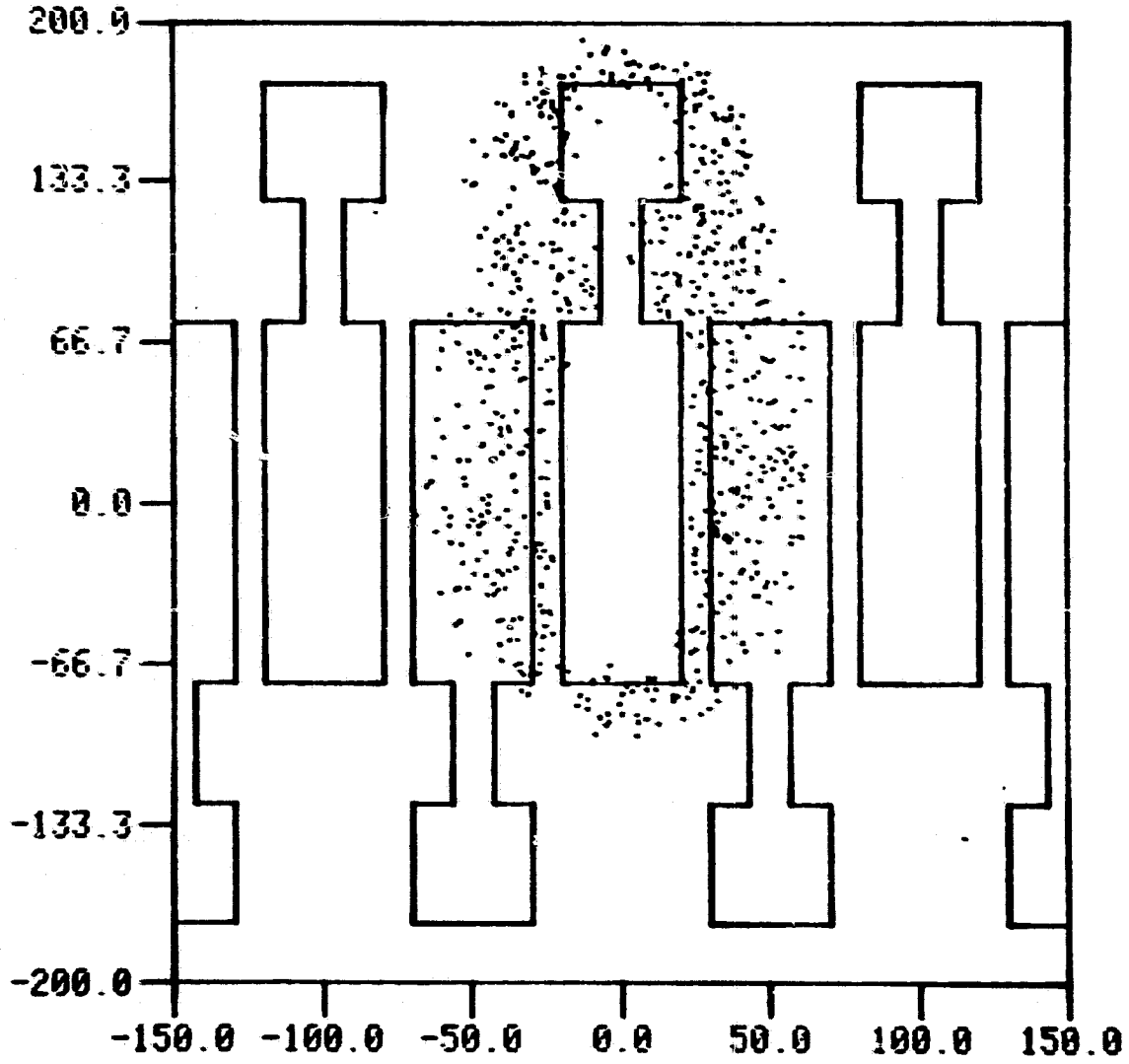

Figure 31. Proton entry points corresponding to charge 3.2 fC collected by Diode at 75.4 MeV.

REFERENCES

1. May, T.C. and Woods, M.H.: "Alpha-Particle-Induced Soft Errors in Dynamic Memories." IEEE Trans. Electron Devices, ED-26, p. 2 (1979).

2. Pickel, J.C. and Blandford, J.T.: "Cosmic-Ray Induced Errors in MOS Memory Cells." IEEE Trans. Nucl. Sci. NS-25, p. 1166 (1978).

3. Yaney, D.S., Nelson, J.T. and Vanskike, L.L.: "Alpha Particle Tracks in Silicon and their Effects on Dynamic MOS RAM Reliability." IEEE Trans. Electron Devices ED-26, p. 10 (1979).

4. Brodsky, Mark: Electronics, 53, p. 117 (1980).

5. Ziegler, S.F. and Lanford, W.A.: Science, p. 206, p. 776 (1979).

6. Ko, Shang-Bin: "Observations of Alpha Particle Effects in the Charge-Coupled Image Sensor." IEEE Trans. Nucl. Sci. NS-27, p. 1500 (1980).

7. Peterson, E.L.: "Nuclear Reactions in Semiconductors." IEEE Trans. Nucl. Sci. NS-27, p. 1494 (1980).

8. Peterson, E.L.: "Soft Errors Due to Protons in the Radiation Belt." IEEE Trans. Nuc. Sci. NS-28, p. 3981 Dec. 1981.

9. Binder, D., Smith, E.C., and Holman, A.B.: "Satellite Anomalies from Galactic Cosmic Rays." IEEE Trans. Nuc. Sci., NS-22, 6, p. 2675 (Dec. 1975).

10. Hier, R.G., Beaver, E.A. and Schmidt, G.W.: "Photon Detection Experiments with Thinned CCD's." Advances in Electronics and Electron Physics, Vol. 52, pp. 463-480, (1979).

11. Marcus, S., Nelson, R. and Lynds, R.: "Preliminary Evaluation of a Fairchild CCD-211 and a New Camera System." Proceedings SPIE Instrumentation in Astronomy III, Vol. 172, pp 207 218, January 1979.

12. Kirkpatrick, Scott: "Modeling Diffusion and Collection of Charge from Ionizing Radiation in Silicon Devices." IEEE Trans. Electron Devices ED-26, p. 1742 (1979).

13. Sai-Halasz, G.A. and Wordeman, M.R.: "Monte Carlo Modeling of the Transport of Ionizing Radiation Created Carriers in Integrated Ciruits." IEEE Electron Device Letters, EDL-1, 10, pp. 211-213, October (1980).

14. Sai-Halasz, et al.: "Alpha-Particle-Induced Soft Error Rate in VLSI Circuits." IEEE Transactions on Electron Devices, ED-29, 4, pp. 725-731, April (1982).

15. Toyable, Toru: "A Soft Error Model for MOS Dynamic RAM's." IEEE Trans. Electron Devices, ED-29 4, pp. 732-737.

16. Choisser, J.P.: "Detecting Photoelectron Images with Semiconductor Arrays for Multichannel Photon Counting." Optical Engineering, Vol. 16, No. 3, p. 262, May/June 1977.

17. Lowrance, J.L., Zucchino, P., Renda, and Long, D.C.: "ICCD Development at Princeton." Advances in Elecronics and Electron Physics, Vol. 52, p. 441-452, (1979)

18. Beaver, LE.A., McIlwain, C.E.: "A Digital Multichannel Photometer," Review of Scientific Instruments, Vol. 42, p. 9, (1971).

19. Becher, J., Kernell, R., Reft, S. and Smith, L.C.: "Radiation Effects Studies for the High Resolution Spectrograph." Technical Report PTR-80-2, Old Dominion University, Norfolk, Virginia, (1980).

20. Smith, L.C. and Becher, J.: "Proton-Induced Noise in Space Telescope Digicon." SPIE Proceedings on UV and Vacuum UV Systems, Vol. 279, p. 156, (1981).

21. Smith, L.C., Becher, J., Fowler, W.B. and Flemming, K.: "Proton-Induced Noise in Digicons." NASA Technical Paper 1852, August 1981.

22. Brandt, J.C., Boggess, A., Heap, R., Maran, S.P., and Smith, A.M.: "High Resolution Spectrograph for the Space Telescope." Proceedings SPIE Applications of Electronic Imaging Systems Vol. 143, p. 27, (1978).

23. Kelsall, T.: "Detectors for the Space Telescope." Proceedings SPIE Applications of Electronic Imaging Systems, Vol. 143, p. 27, (1978).

24. Brandt, J.C.: "High Resolution Spectrograph for the Space Telescope." HRS-680-77-01, NASA, (1977).

25. Walter, F.J. and Boshart, R.R.: "Low Background Counting of Betas and Alphas with Silicon Detectors." Nuclear Instrumentation and Methods, Vol. 42, No. 1, pp. 1-14, (1966).

26. Hseih, C.M., Murley, P.C., and O'Brien, R.R.: "A Field-funneling Effect on the Collection of Alpha-Particle-Generated Carriers in Silicon Devices,." IEEE Electron Device Letters, EDL-2, 4, p. 103 (April 1981).

27. Hu, C.: "Alpha-Particle-Induced Field and Enhanced Collection of Carriers,." IEEE Electron Device Letters, EDL-3, 2, p. 31 (February 1982).

28. Von Roos, Oldwig: "The Determination of Transport Parameters of Minority Carriers in n-p Junctions by Means of an Electron Microscope. Critiques of Recent Developments." Solid State Electronics, Vol. 23, p. 177-182, (1980).

29. Von Roos, Oldwig: "Analysis of the Interaction of an Electron Beam with a Solar Cell." Solid State Electronics, Vol. 21, pp. 1063-1067, (1978).

30. Kamm, J.D. and Bernt, H.: "Theory of Diffusion Constant, Lifetime and Surface Recombination Velocity Measurements with the Scanning Electron Microscope." Solid State Electronics, Vol. 21, pp. 957-964, (1978).

31. Landau, L., USSR J. Phys. 8, p. 201 (1944).

32. Vavilov, P.V., Zh. Experim. i Teor. Fiz. 32, 320 (1957). [English transl.: Soviet Phys.-JETP 5, 749 (1957)].

33. Jackson, J.D.: Classical Electrodynamics, Chap. 13, p. 631, 2nd edition, Wiley, New York (1975).

34. Blunck, O. and Leisegang, S.Z.: Physik 128, p. 500 (1950).

35. Inspirian, K.A., Margarian, A.T. and Zverev, A.M.: "A Monte-Carlo Method for Calculation of the Distribution of Ionization Losses" Nuclear Instruments and Methods, p. 117, 125, (1974).

36. Berger, M.J. and Seltzer, S.M.: Natl. Acad. Sci.-Natl. Res. Council, Publ. 1133; U.S. At. Energy Comm. NAS-NS 39, p. 188 (1964).

37. Seltzer, S.M. and Berger, M.J.: "Energy-Loss Straggling of Protons and Mesons: Computer Code for the Calculation of the Vavilov Distribution National Bureau of Standards Report 9498, NBS Project 23101-11-2310430, March 8, 1967.

38. Bailey, N.B., Steigerwalt, J.E. and Hilbert, J.W.: "Frequency Distributions of Energy Deposition by Fast Charged Particles in Very Small Pathlengths" Phys. Rev., Vol. 2, No. 3, p. 557, (1970).

39. Chechin, V.A. and Ermilovva, V.C.: "The Ionization-Loss Distribution at Very Small Absorber Thickness" Nuc. Inst. and Meth., 136, pp. 551-558, (1976).

40. Kolata, J.J., Amos, T.M. and Bichsel, H.: "Energy-Loss Straggling of Protons in Silicon" Phys. Rev., 176, 2, 484, (1968).

41. Maccabee, H.D., Raju, M.R. and Tobias, C.A.: "Fluctuations of Energy Loss by Heavy Charged Particles in Thin Absorbers." Phys. Rev., 165, 2, 469, (1968).

42. Hilbert, J.H., Baily, N.A., and Lane, R.G.: "Statistical Fluctuations of Energy Deposited in Low-Atomic-Number Materials by 43.7-MeV Protons.". Rev., 168, 2, 290, (1968).

43. Ozisik, M.N.: Boundary Value Problems of Heat Conduction, International Textbook Company, Scranton, Penn. (1968).

44. Rossi, B.: High Energy Particles, Prentice-Hall, New York, (1952).

45. Bevington, P.R.: "Data Reduction and Error Analysis for the Physical Sciences." New York: McGraw-Hill Book Company, (1969).